Aspects of Non-Gaussian Signature Generation in Scalar Field Inflation

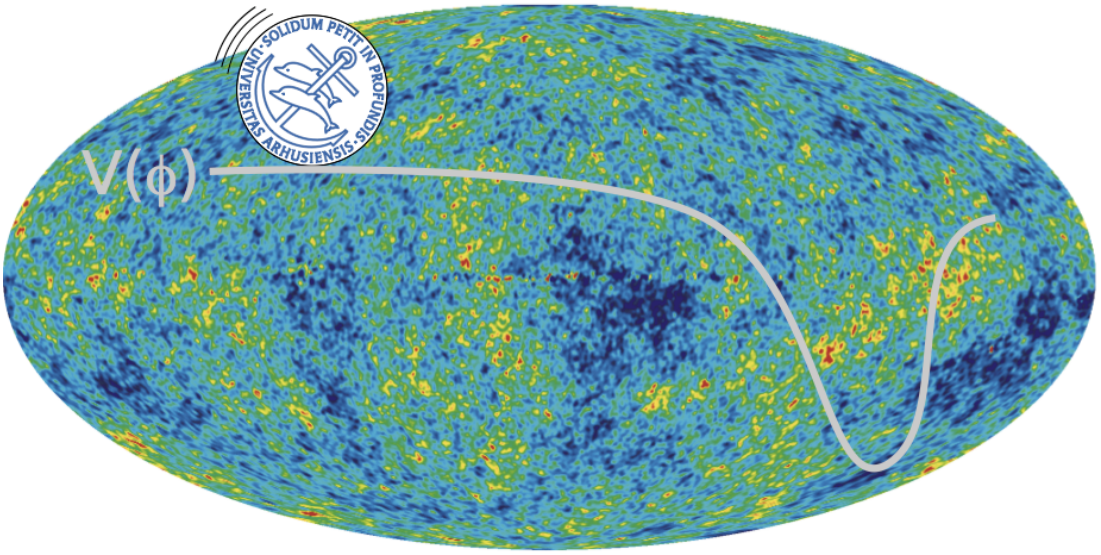

Ph.D. Dissertation

Philip Roland Jarnhus

Supervisor: Steen Hannestad

Co-Supervisor: Martin S. Sloth

DEPARTMENT OF PHYSICS
AND ASTRONOMY
FACULTY OF SCIENCE
AARHUS UNIVERSITY

Aspects of Non-Gaussian Signature Generation in Scalar Field Inflation

A Dissertation
Presented to the Faculty of Science
of Aarhus University
in Partial Fulfilment of the Requirements for the
Ph.D. Degree

by
Philip Roland Jarnhus
July 30, 2010

Abstract

This thesis compiles the results of three works on the subject of non-Gaussianities in scalar field inflation, as well as an introduction to the needed background knowledge.

We present a numerical study of the axion monodromy model. We find several allowed parameter sets that produce $f_{NL} \sim \mathcal{O}(5)$ which should be detectable with the Planck satellite.

Furthermore the fourth order action of scalar perturbations in the uniform density gauge is derived, along with the related gauge transformations. A discussion on the slow roll dependence of the higher order actions is also included.

Finally a work in progress is included. This work is on the determination of an observed bispectrum from a primordial one. A recursive scheme for calculating the integral over the product of the three spherical Bessel functions is written down and analysed for squeezed and folded triangles, giving limits that do not diverge.

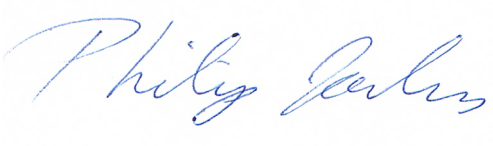

Philip Roland Jarnhus
July 30, 2010
Department of Physics and Astronomy, Aarhus University

Table of Contents

Notations and Conventions iii

Summary v

Dansk resumé vii

1 – Cosmological Background 1
- 1.1 Content of the Universe . . . 1
- 1.2 Cosmological Principle and the FRW Metric . . . 3
- 1.3 Basics of Measurements . . . 6
- 1.4 Measuring the Geometry of the Universe . . . 7
- 1.5 Measuring the Expansion of the Universe . . . 8
- 1.6 Recapping the Universe . . . 10

2 – Issues with the Big Bang Scenario 13
- 2.1 The Flatness Problem . . . 13
- 2.2 The Horizon Problem . . . 13
- 2.3 A Possible Solution to Both Problems . . . 14
- 2.4 Inflation at a Glance . . . 16

3 – Statistics and Perturbation Theory 21
- 3.1 Metric Perturbations . . . 21
- 3.2 Perturbing the FRW Metric . . . 22
- 3.3 Perturbations in Single Field Inflation . . . 23
- 3.4 Statistics in Expanding Spacetime . . . 25

4 – Single Field Inflation 31
- 4.1 Basic Properties of Single Field Inflation . . . 31
- 4.2 Power Spectrum of the Field Fluctuations . . . 32
- 4.3 First Order Perturbations . . . 33
- 4.4 Non-Gaussian Signals . . . 36

5 – Axion Monodromy Model 39
- 5.1 Axion Monodromy Potential . . . 39
- 5.2 Isosceles Limit Estimates of the Bispectrum . . . 40
- 5.3 Semiclassical Estimates of the Trispectrum . . . 43

5.4 Numerical Computations 44
5.5 Numerical Results 47

6 – Observing CMB Power Spectra **53**
6.1 Angular Power Spectrum 53
6.2 Polarisation 55
6.3 Observational Bounds and Future Potential 58

7 – The Observational Bispectrum **61**
7.1 Bispectra in the CMB 61
7.2 Delta Function Integral 62
7.3 Spherical Coordinates in the 1-norm and the Shape Function 68

8 – Beyond the Bispectrum **71**
8.1 The Action to Fourth Order in Uniform Density Gauge 71
8.2 Gauge Transformation 73
8.3 The de Sitter Limit 76
8.4 Challenges of Numerical Computation 79

9 – Concluding Remarks **81**

Acknowledgements **85**

Bibliography **87**

A – Appendix **95**

NOTATIONS AND CONVENTIONS

The sign convention of the metric is throughout this work chosen to be $(-+++)$. Lowered indices represent covariant quantities, while raised indices represent contravariant quantities. Greek indices run from 0 to 3 with 0 being the time coordinate, while roman indices only run over the spatial components (1 to 3). Summation over repeated indices is implied.

Every equation is presented in natural units, i.e. $c = \hbar = 1$. To further ease notation the reduced Planck mass $M_{pl}^{-2} = 8\pi G$ is set to 1. The partial derivative ∂_μ is defined as

$$\partial_\mu \equiv \frac{\partial}{\partial x^\mu} \ .$$

From this the LaPlacian is defined as

$$\partial^2 = \partial_\mu \partial^\mu = g^{\mu\nu} \frac{\partial}{\partial x^\mu} \frac{\partial}{\partial x^\nu}$$

and along with it, the inverse LaPlacian (∂^{-2}) is defined as

$$\partial^{-2} \partial^2 = \mathbf{1} \ .$$

A dot ($\dot{x}$) indicates as derivative with respect to physical time, while a prime x' is context specific and can mean one of three things:

1. A prime on the potential means a derivative with respect to the field: $V'(\phi) = \frac{\partial V}{\partial \phi}$
2. A prime on a conformal time variable τ simply indicates a new variable τ'. This is primarily used as an integration variable.
3. A prime on all other quantities is a derivative with respect to conformal time (τ): $z' = \frac{\partial z}{\partial \tau}$

The Fourier transform is defined as

$$f(\boldsymbol{x}) = \int \mathrm{d}^3\boldsymbol{k} f(\boldsymbol{k}) e^{-i\boldsymbol{k}\cdot\boldsymbol{x}} \ ,$$

with the inverse transformation

$$f(\boldsymbol{k}) = \int \frac{\mathrm{d}^3\boldsymbol{x}}{(2\pi)^3} f(\boldsymbol{x}) e^{i\boldsymbol{k}\cdot\boldsymbol{x}} \ .$$

SUMMARY

This thesis presents my work on single field inflation theory.

The current standard model of cosmology, the ΛCDM model, provides a good fit to data, but is, on its own, insufficient as it lacks an explanation for the flat, homogeneous and isotropic universe we observe. At present cosmological inflation seems to be the best candidate for a dynamical scenario, that provides the needed initial conditions. Though inflation is understood on a basic level, one still needs to work out the details and determine the exact mechanism that creates the near exponential expansion of the Universe.

By studying the statistical properties of the perturbations arising during inflation, one can discriminate between the proposed models through prediction of observations from theory and inference from data. Such measurements give a unique opportunity to study physics at the Planck scale.

This work reviews single field inflation (chapter 4) and cosmological perturbation theory (chapter 3). The present constraints from observations are discussed in chapter 6, where mention is also given to why present observations favour inflation over other scenarios.

Chapter 5 is focussed on calculating the bispectrum for a specific model. The axion monodromy model is derived from string theory and have a very distinct bispectrum. Furthermore this model is especially interesting as it produces a signal in the bispectrum, that is strong enough to be detected within the next few years. The trispectrum is estimated theoretically in special limits.

Based on the result of chapter 5, it is described how one computes the observed bispectrum in chapter 7. One of this chapter's main results is a recursive scheme for calculating a numerically difficult integral over a product of three spherical Bessel function. Finally a triple integral is written down, that can be computed numerically. This still needs to be done and is, at the time of writing, a work in progress.

Finally the fourth order action in the uniform density gauge is calculated in chapter 8, along with the third order gauge transformation. The chapter includes a discussion of the slow roll properties of higher order actions in the isocurvature gauge and the uniform density gauge. Concluding the chapter is a discussion of the challenges involved in calculating the trispectrum numerically

Concluding remarks are found in chapter 9.

Dansk resumé

Denne afhandling er en præsentation af mit arbejde med enkeltfeltsinflation.

Den nuværende beskrivelse af universet, kaldet ΛCDM modellen, giver i sig selv en glimrende beskrivelse af de observerede data, men den har dog stadig mangler. Modellen kan ikke redegøre for, hvorfor universet skal være geometrisk fladt, homogent og isotropt. Med vores nuværende viden om universet tyder alt på, at kosmologisk inflation er det bedste bud på et dynamisk scenarie, der kan producere de begyndelsesbetingelser, der skal til for at kunne reproducere det univers, som vi ser i dag. Selv om inflation er rimelig godt forstået på det mest basale niveau, er det stadig nødvendigt at udarbejde detaljerne og bestemme præcist hvilken mekanisme, der ligger til grund for den nærmest eksponentielle udvidelse af universet.

Ved at studere de statistiske egenskaber for de perturbationer, der opstår under inflation, er det muligt at skelne mellem modellerne ud fra teoretiske forudsigelser af observationer, samt ved at bruge observationer til at sætte generelle begrænsninger på de parametre, der beskriver den statistik, som perturbationerne adlyder. Sådanne målinger vil give en helt unik mulighed for at studere fysikken, som den tager sig ud ved Planckskalaen.

Dette værk indeholder en opsummering af enkeltfeltsinflation (kapitel 4) og kosmologisk perturbationsteori (kapitel 3), samt en diskussion af hvad vi kan udlede fra observationer (kapitel 6). Diskussionen berører desuden hvorfor inflation er det foretrukne scenarie frem for andre modeller for the tidlige univers.

I kapitel 5 fokuseres der på at udregne bispektret for en bestemt model. Axion monodromy modellen er udledt fra strengteori og producerer et let genkendeligt bispektrum. Modellen er især interessant i og med, at den kan resultere i signaturer i bispektret, der kan observeres inden for de næste par år. Ud over bispektret estimeres trispektret i bestemte grænsetilfælde.

På baggrund af resultaterne i kapitel 5 beskriver kapitel 7 hvordan det observerede bispektrum beregnes. Et af hovedresultaterne i kapitlet er et sæt af rekursive ligninger, der gør det muligt at beregne et numerisk svært integral over et produkt af tre sfæriske Besselfunktioner. Slutteligt opstilles et tredobbelt integral, der kan beregnes numerisk. Dette er, i skrivende stund, endnu ikke fuldført.

Endelig beregnes det fjerde ordens virkningsintegral og den tredje ordens gaugetransformation for *uniform density gauge*. Kapitlet afsluttes med en diskussion af de udfordringer, som skal løses for at kunne udregne trispektret numerisk.

Et konkluderende sammendrag findes i kapitel 9.

1 Cosmological Background

Astronomy has undergone an amazing development through the ages. Starting from a merely descriptive science, which involved observing and cataloguing the celestial objects visible to the naked eye, probing ever deeper as telescopes became more advanced, until the field emerged as the multi branched science of modern astrophysics it is today.

One branch that has gained increasing attention over the last decades is cosmology; the study of the Universe on large scales of time and distance. Concerning itself with the structure, content and evolution of the Universe, cosmology draws inspiration and knowledge from many branches of physics, ranging from particle physics and statistical physics to large scale gravitational physics.

The new developments of methods and instruments have provided an improved precision of the data, that forms the basis of all cosmological theory. This makes cosmology an excellent test bed for physics beyond the standard model and possible expansions of the fundamental theories, which form the basis of most of our current knowledge of nature.

In order to truly understand the scenario that provides the background for most of the work done in astrophysics and cosmology, one needs to revisit the initial observations and assumptions that lead to the currently accepted model, the ΛCDM-universe. This chapter presents a summary of the standard textbook material on the ΛCDM-model, see e.g. [1, 2].

1.1 Content of the Universe

When one attempts to unravel the properties of the Universe, one encounters problems in situations which, in everyday life, seem trivial. A first complication is the lack of depth perception. This comes mainly from the inability to accurately determine distance in a way that is completely free of assumption. This is, in fact, only possible on very short length scales, i.e., at most the scale of our galaxy, where the determination is done using parallax techniques.

The second complication, which often give theorists considerable free rein, is that very few fundamental parameters can be observed directly. That is to say that most of our deductions are derived through model specific assumptions, impeding certainty in our conclusions. We will therefore begin our description based firmly on what can be observed.

Finally we are limited by having only one universe, which we view from only one point. This complicates matters as we analyse data, as the statistics are often limited to very few data points.

BARYONIC MATTER AND RADIATION

When we first observe, we see the world around us. A good measure of baryonic matter lumped together in greater or smaller masses, ranging from interstellar dust of molecular size to planets and stars. Though we see a vast difference between a mote of dust, a human being and a star, they can, on a cosmological scale, be considered as a low density gas of non-relativistic massive particles. We can therefore describe the baryonic content as an ideal gas with pressure

$$P = \frac{\rho}{\mu} k_B T \ , \tag{1.1}$$

where μ is the mean mass of the particles. As the gas is non-relativistic, ρ is roughly the energy density (in $c = 1$ units). Expressing the temperature in terms of the mean square of the thermal velocity ($3k_B T = \mu \langle v^2 \rangle$), one can write the pressure as

$$P = \frac{\langle v^2 \rangle}{3} \rho \ . \tag{1.2}$$

From this one can conclude that normal baryonic matter can, in cosmological contexts, be described as being dominated by its energy density and having almost zero pressure.

From observing the world around us we can deduce one additional fact; as we are able to see things around us, the Universe must contain photons. They have a pressure of one-third the energy density:

$$P = \frac{\rho}{3} \ . \tag{1.3}$$

COLD DARK MATTER

To discover the next component of the Universe one has to look beyond the immediate surroundings. Dark matter is a species of matter that does not interact with standard model particles to any strong degree, but only affects the visible universe through gravitational interactions. This makes direct detection of dark matter extremely difficult and so far most of our knowledge about dark matter is inferred from observations of galactic dynamics.

Dark matter was original hypothesised after observing the rotation of galaxies. Since the observed surface brightness of galaxies drops exponentially as one moves further away from the centre, one would expect the orbital speed of the stars in the galaxy to decrease as $v \propto R^{-1/2}$. This is the line labelled disc in figure 1.1

As can be seen in figure 1.1 the orbital speed stagnates instead of decreasing for large radii (data points in figure 1.1), implying that there must be more matter within the galaxy than that which can be observed directly. Further indications of dark matter have recently been observed in colliding galaxy clusters [3].

Though there are many realisations of dark matter, the class that seems to be of cosmological significance is the cold dark matter, which has an equation of state like baryonic matter, i.e., $P \approx 0$. This leaves us with three species of cosmological content with two distinct equations of state. We will defer the determination of their quantities and instead focus on cosmological observations and what we can derive from them.

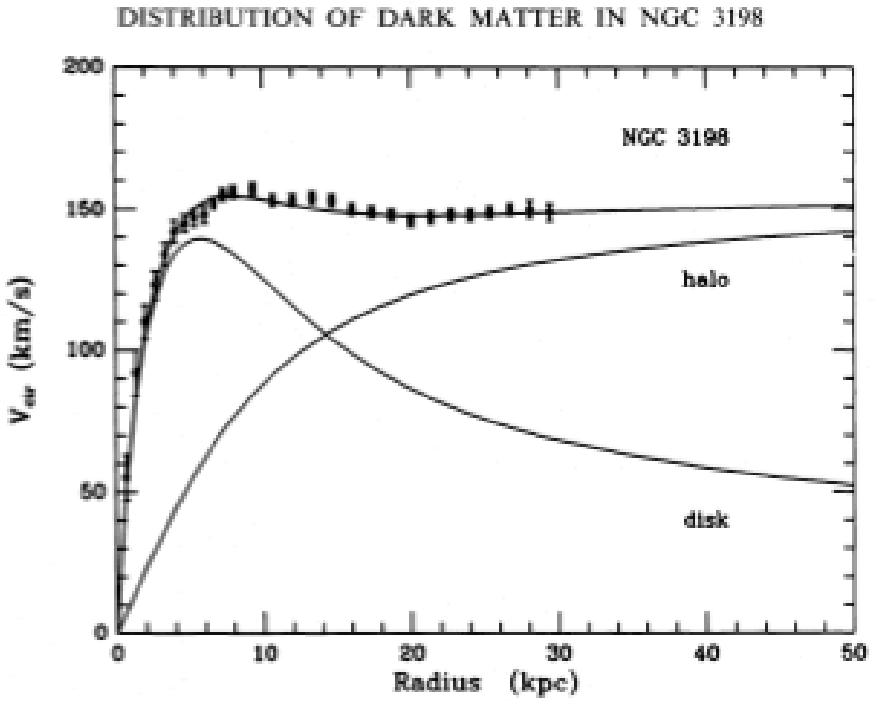

Figure 1.1: Rotation curve data from NGC3198 along with fits for dark matter profile. Taken from [4]

Part of the dark matter comes from neutrinos, which are, in the ΛCDM model, treated as ultra-relativistic particles. They will therefore contribute to the radiation term.

1.2 Cosmological Principle and the FRW Metric

Having observed the matter and radiation of the Universe, we can apply these initial observations to paint the characteristics of the Universe with a broad brush. Doing a full sky survey of the radiation, one finds first of all that there is a microwave background, which exhibits a remarkably perfect black body spectrum with a peak at a temperature of about 2.73K (see figure 1.2 on the following page).

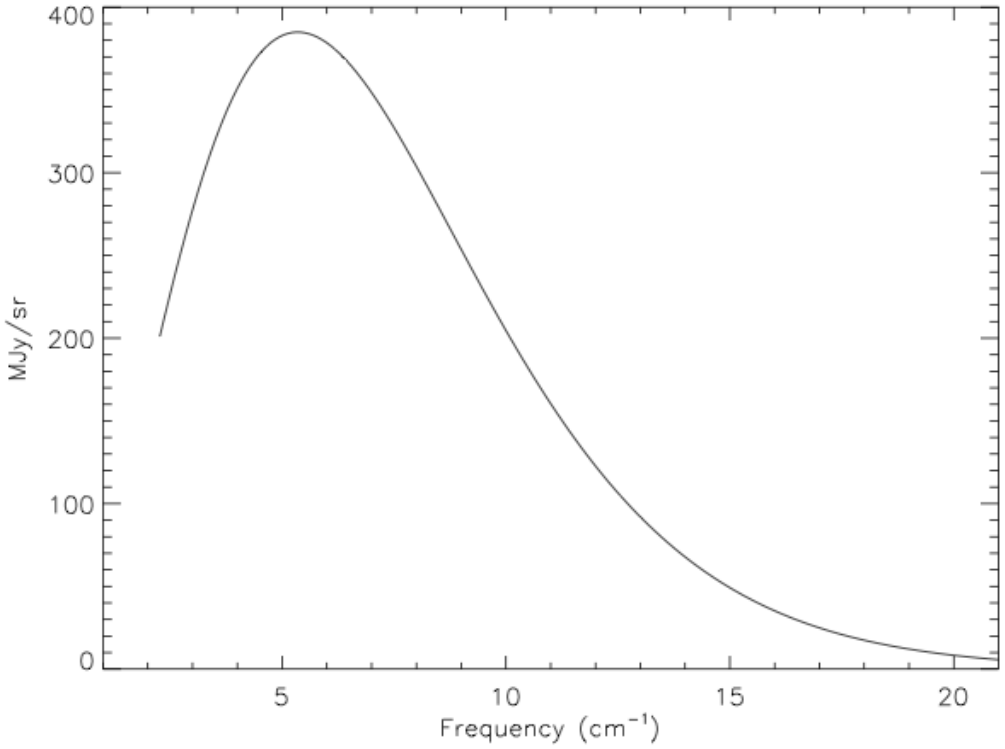

Figure 1.2: Black body spectrum of the CMB by the COBE satellite. From [5]

Comparing this result with a map of how the temperature varies over the sky (see figure 1.3. Note that the variations are of the order of 0.1 mK), one notices that the observed radiation is astoundingly isotropic.

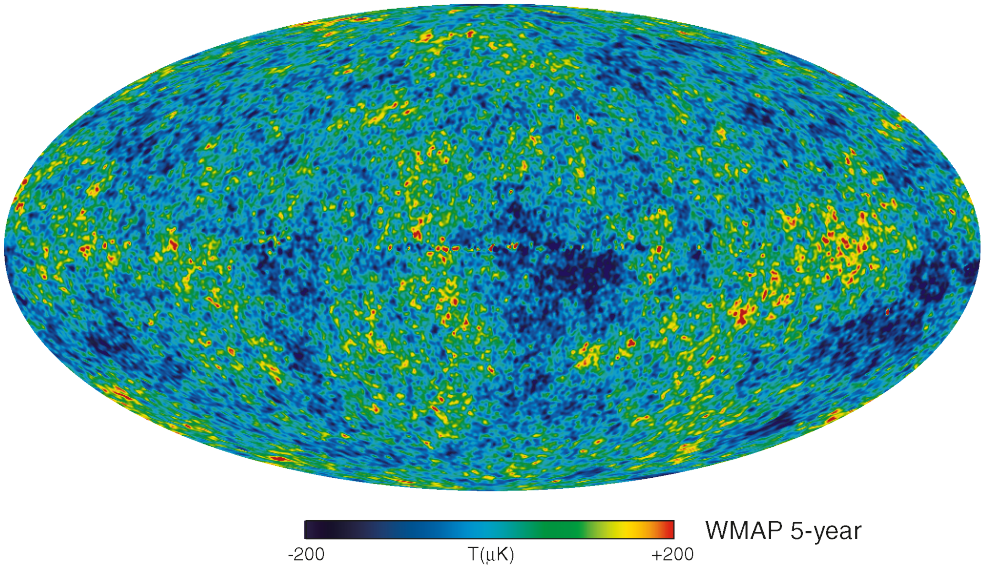

Figure 1.3: Full sky map by the WMAP satellite after subtraction of galactic foreground, mean temperature and dipole contribution. From [6]

If one furthermore maps out the matter distribution on large scales, it emerges that on large scales the distribution of galaxies can be seen to be both isotropic like the Cosmic Microwave Background (CMB), as well as homogeneous. These observations support what is known as the cosmological principle; *that the Universe can, on scales larger than roughly 100 Mpc, be regarded as homogeneous and isotropic.*

COSMOLOGICAL DYNAMICS

At these length scales gravitation dominates the other fundamental forces, making it possible to describe the dynamics of the Universe on cosmological scales by the general theory of relativity. Invoking general relativity one can write down the Friedmann-Robertson-Walker (FRW) metric as the most general metric, which obeys the cosmological principle:

$$ds^2 = -dt^2 + a(t)^2 \left[dr^2 + S_\kappa(r)^2 \left(d\theta^2 + \sin^2(\theta) d\phi^2\right)\right] \tag{1.4}$$

with

$$S_\kappa(r) = \begin{cases} R_0 \sin(r/R_0) & \kappa = 1 \text{ (Closed universe/positive curvature)} \\ r & \kappa = 0 \text{ (Flat universe)} \\ R_0 \sinh(r/R_0) & \kappa = -1 \text{ (Open universe/negative curvature)} \end{cases} . \tag{1.5}$$

Here R_0 is the curvature radius of the Universe. Inserting the FRW metric into the Einstein equation one finds the Friedmann equation from the 00-component, which connects the evolution of the scale factor $a(t)$ to the content of the Universe and its curvature:

$$H^2 \equiv \left(\frac{\dot{a}}{a}\right)^2 = \frac{\rho}{3} - \frac{\kappa}{R_0^2 a(t)^2} . \tag{1.6}$$

This serves as a definition of the Hubble parameter, H, which quantifies the relative expansion rate of the Universe, while ρ denotes the total energy density of the Universe. Solving the Friedmann equation in conjunction with the continuity equation

$$\dot{\rho} + 3H(\rho + P) = 0 , \tag{1.7}$$

one can find the evolution of the scale factor as a function of the physical time. For the two components (we will from now on regard baryonic matter and cold dark matter as parts of the same component, i.e., cold matter which exerts negligible pressure) introduced earlier, one can solve eq. 1.7 to find

$$\rho(a) = \rho(a_0) \begin{cases} \left(\frac{a_0}{a}\right)^3 & \text{cold matter} \\ \left(\frac{a_0}{a}\right)^4 & \text{radiation} \end{cases} . \tag{1.8}$$

One could easily have argued that the energy densities should depend on the scale factor in this fashion. Both components are diluted as the Universe expands giving an a^{-3} dependence. The extra factor a^{-1} for the radiation comes from the red shifting of the photons as they travel through an expanding space.

In addition to the two components already introduced there is a third component, which will play a key role throughout this work. That is a component with a constant energy density. Assuming this, one finds from eq. 1.7 that such a component exerts

negative pressure: $P = -\rho$. Sometimes named a cosmological constant or dark energy, a flat universe dominated by this will have a constant Hubble parameter and will therefore expand exponentially. Such a universe, called a *de Sitter space*, will play an integral role in the following chapters.

Defining the critical density of the Universe ($\rho_{c,0}$) as the one needed for making a flat universe ($\kappa = 0$), one can express the present day value as

$$\rho_{c,0} = 3H_0^2 \ , \tag{1.9}$$

where H_0 is the present value of the Hubble parameter. Collecting the results derived thus far, one can write the Hubble parameter as

$$H^2 = H_0^2 \left[\frac{\Omega_{r,0}}{a^4} + \frac{\Omega_{m,0}}{a^3} + \Omega_{\Lambda,0} + \frac{1 - \Omega_0}{a^2} \right] \ . \tag{1.10}$$

In the above and for the rest we have set $a_0 = 1$ as the present day value of the scale factor and written the energy densities as fractions of the critical energy density today:

$$\Omega_{i,0} \equiv \frac{\rho_{i,0}}{\rho_{c,0}} \ , \ \Omega_0 \equiv \sum_i \Omega_{i,0} \ . \tag{1.11}$$

The four terms in eq. 1.10 are radiation, cold matter, cosmological constant and curvature, respectively. We have anticipated events slightly by adding the cosmological constant term, even though it has not, at this point, been argued to be part of our universe. One should bear in mind that there is so far no physical explanation for this term, and it acts merely as a placeholder needed to describe the observations. One can find many possible realisations that fulfil the observed properties (see [7] and references within).

To determine the evolution of the Universe, one now needs to fix the parameters by observation.

1.3 BASICS OF MEASUREMENTS

Starting from the little we know at present, we utilise the fact that most of the photons in the Universe are part of the CMB, which has a black body spectrum (see figure 1.2 on page 4). One can therefore estimate the energy density of radiation from Stefan-Boltzmann's law and find

$$\Omega_{\gamma,0} = 2.469 \times 10^{-5} h^{-2} \ , \ h \equiv \frac{H_0}{100\text{km/s/Mpc}} \ . \tag{1.12}$$

The notation $\Omega_{\gamma,0}$ denotes purely the photon contribution. The total contribution to the radiation energy density also includes neutrinos, which will not be discussed in detail in this work.

This result is fairly independent of the model assumptions as opposed to the other cosmological parameters. One should therefore start with reviewing the methods of observation and the notion of scales that is employed, when one fixes the cosmological parameters.

As observers of the Universe we are limited by the fact, that we can only observe light and particles that come to us. This results in a set of data that not only has the imprint of the original source, but also holds information about anything that is passed

on the way from the source to the observer. To complicate matters further, one cannot rely on the measurement of a well-defined physical distance (the coordinate distance of the FRW-metric), as this is prohibited by causality in an expanding universe.

To establish a distance measure one defines the *luminosity distance* in terms of the measured flux, f, and luminosity of a source, L, which can usually be inferred by some other methods:

$$d_L \equiv \left(\frac{L}{4\pi f}\right)^{1/2} . \tag{1.13}$$

One should note that this quantity only corresponds to the physical distance in a static, Euclidian, three dimensional space.

In a universe with a FRW metric of general curvature the geometry and expansion manipulates the perceived flux from a source. This is caused by three different effects on the photons emitted from the source. Firstly the area over which the photons are spread, given by

$$A_\kappa(r) = 4\pi S_\kappa(r)^2 \tag{1.14}$$

changes with the curvature of the Universe. Secondly the photons are redshifted, diminishing the energy of the photon by a factor of of $(1+z)^{-1}$, where z is the redshift of the source. Lastly, two photons emitted a time Δt apart will arrive with an interval of $\Delta t(1+z)$ due to the expansion, contributing another factor of $(1+z)^{-1}$ to the flux:

$$f = \frac{L}{4\pi S_\kappa(r)^2(1+z)^2} . \tag{1.15}$$

This leads to a luminosity distance of

$$d_L = (1+z)S_\kappa(r) . \tag{1.16}$$

1.4 MEASURING THE GEOMETRY OF THE UNIVERSE

As the curvature of the Universe plays such an immense role in our perception of distance, it should be one of the first parameters we attempt to determine. Though it cannot be done in a completely model independent way, it can be found almost independent of the other cosmological parameters.

Measuring the anisotropies of the CMB and fitting the measured power spectrum[1] to a theoretical one, will not only allow us to infer Ω_0, but also give us an estimation of the other cosmological parameters. There are, however, still a fairly large solution space allowed from the CMB data alone. One therefore needs further data to pin down the correct values of the cosmological parameters. This will be illuminated in the following section.

Exploiting the information in the CMB anisotropies requires a little knowledge of the history of the Universe. Based on repeated observations of objects on the cosmological scales it is concluded that the Universe is expanding. This implies that the Universe must at some point have started from a hot, dense state. As the Universe expanded, the equilibrium between baryons, leptons and photons shifted until atoms started forming in the *recombination epoch*, making the Universe electrically neutral. This was followed by

[1] A more thorough definition of the power spectrum will be presented in chapter 3 on page 21

the *photon decoupling epoch*, which occurred when the expansion of the Universe came to dominate the photon-electron scattering rate. Shortly after this the mean free path of the photons grew to make them free stream, marking the *last scattering surface* which we now observe as the CMB. One of the more notable things about the last scattering surface, is that the redshift at which it takes place, $1 + z_{ls} \approx 1100$, is nearly independent of the cosmological parameters. This makes it ideal for observing the curvature of Universe.

If one observes two fluctuations in the CMB that were a physical distance l apart on the last scattering surface, one would observe them to have an angular distance of

$$\Delta\phi = \frac{l}{a(t_{ls})S_\kappa(r)} = \frac{l(1+z_{ls})^2}{d_L} \ . \tag{1.17}$$

Whereas the numerator is largely independent of the chosen cosmology, the denominator depends on the geometry of the Universe as d_L becomes smaller in a closed universe and larger in an open. Thus

$$\Delta\phi_{\text{open}} < \Delta\phi_{\text{flat}} < \Delta\phi_{\text{closed}} \ . \tag{1.18}$$

We do, however, not have any knowledge of the actual physical size of the fluctuations in the CMB, but we can construct an angular power spectrum (figure 1.4) from the fluctuation map (figure 1.3 on page 4). As this is a function of the angular distance in the sky, one

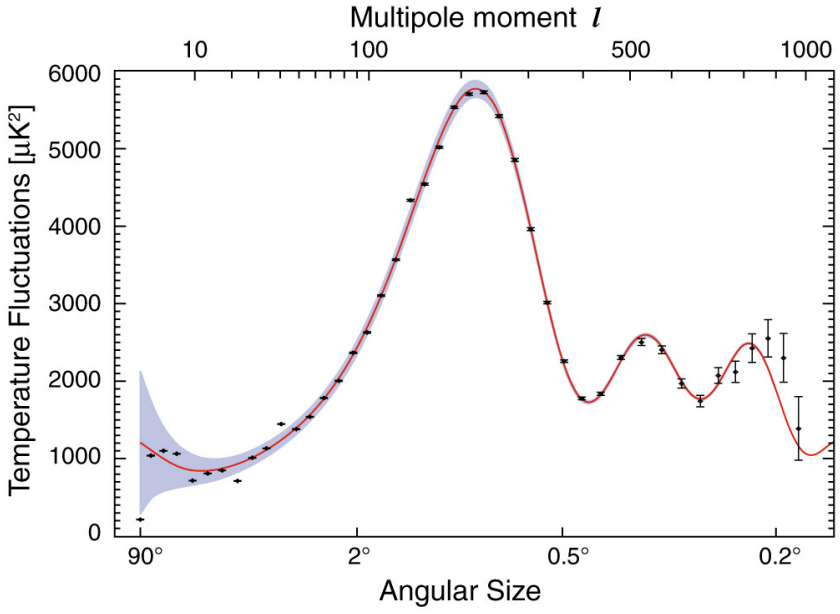

Figure 1.4: Angular CMB power spectrum. From [6]

can fit the curvature to match the peak. Current bounds on the curvature are $-0.0175 < 1 - \Omega_0 < 0.0085$ (95% CL) [8].

1.5 MEASURING THE EXPANSION OF THE UNIVERSE

Even though the observation of a flat universe simplifies matter greatly, we are still limited by having very little knowledge of exact distances and luminosities of the observed objects.

One way to resolve this problem is to look for standard candles. These are objects that all have the same luminosity independent of the redshift at which they are observed.

The preferred standard candle of cosmology is the type Ia supernova, which is extremely luminous and have adequately known properties. Originating from a binary system where a white dwarf accretes matter from a companion star, the white dwarf will collapse when its mass exceeds the Chandrasekhar limit of 1.4 $M_\odot$. Though the luminosities of these supernovae vary slightly (around $(3-5)\times 10^9 L_\odot$), they have been found to obey redder-dimmer and wider-brighter relations, which makes it possible to find the luminosity of the supernova. See figure 1.5 from [9] and further references therein for details. To relate the

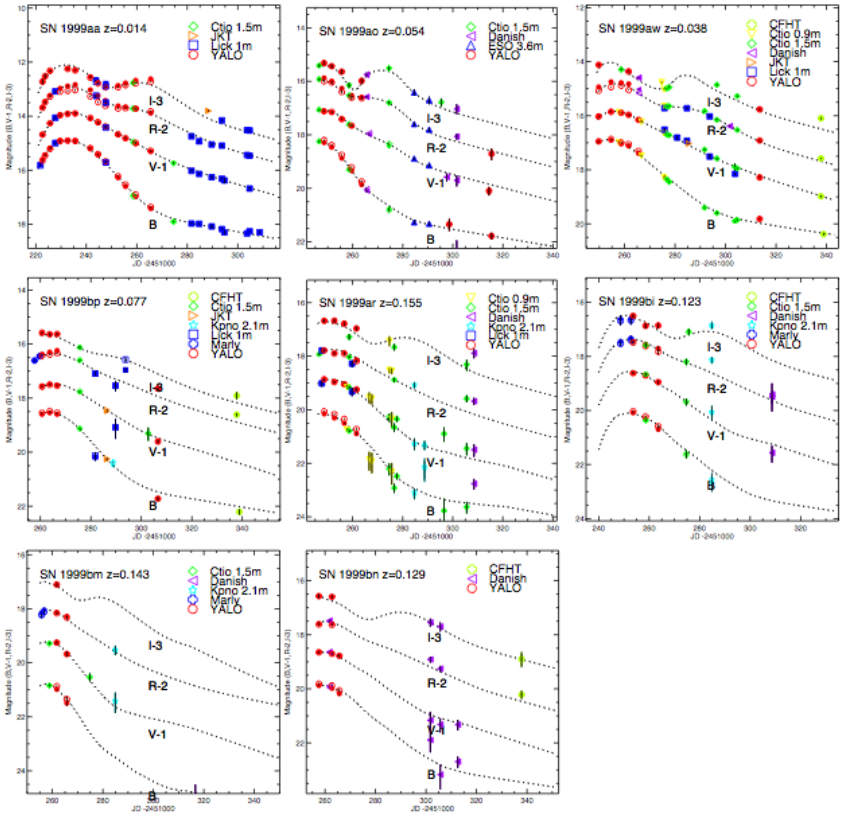

Figure 1.5: Observed magnitudes and model for eight supernovae [9]

luminosities and the measured redshift to the expansion of the Universe, one compares observations to a model universe and perform a complete statistical analysis. We will demonstrate the principles here by limiting the analysis to observations of the recent past, i.e., very low redshifts.

Expanding the scale factor to the second order around present day (t_0), one finds

$$\frac{a(t)}{a(t_0)} \approx 1 + H_0(t-t_0) - \frac{q_0}{2}H_0^2(t-t_0)^2 \tag{1.19}$$

where we have defined the deceleration parameter

$$q_0 = -1 - \left(\frac{\dot{H}}{H^2}\right)_{t=t_0} = \Omega_{r,0} + \frac{\Omega_{m,0}}{2} - \Omega_{\Lambda,0}\ . \tag{1.20}$$

Measuring this parameter gives us the means to determine $\Omega_{m,0}$ and $\Omega_{\Lambda,0}$ in combination with the CMB anisotropy data. In order to couple redshift and luminosity distance, we use the fact that the Universe is approximately flat at the distances we consider, making

$$d_L(t_0) = (1+z)d_p(t_0) = (1+z)\int_{t_e}^{t_0} \frac{\mathrm{d}t}{a(t)} \approx (1+z)\left[(t_0 - t_e) + \frac{H_0}{2}(t_0 - t_e)^2\right] \tag{1.21}$$

to the second order in $t_0 - t_e$. Here $d_p(t_0)$ is the physical distance a photon, emitted at t_e, has travelled at the time t_0. Inverting $\frac{1}{a(t)} = 1 + z$ one finds

$$d_L(z) \approx \frac{z}{H_0}\left(1 + \frac{1-q_0}{2}z\right) \tag{1.22}$$

to the second order in z. Expressing the observations in distance modulus

$$m - M = 5\log_{10}\left(\frac{d_L}{1\mathrm{Mpc}}\right) + 25 \ , \tag{1.23}$$

one finds a simple relation between the distance modulus and the redshift:

$$m - M \approx 45.33 - 5\log_{10}\left(\frac{H_0}{70\mathrm{km/s/Mpc}}\right) + 5\log_{10}(z) + 1.086(1-q_0)z \ , \tag{1.24}$$

under the assumption that $\frac{1-q_0}{2}z \ll 1$. Using this relation in conjunction with the CMB data, one can fit the cosmological parameters. Figure 1.6 on the next page shows the result from a full analysis. The difference in the theoretical curve in the figure and the relation for low redshifts comes from plotting a corrected version of the distance modulus, which takes systematic errors and light absorption from dust between source and observer, and other effects as well into account(see [9] for details).

1.6 RECAPPING THE UNIVERSE

Combining the discussed observations with observation of Baryon Acoustic Oscillations (BAO), one can tightly constrain the cosmological parameters and give a reasonable description of the history of the Universe. The BAO are the result of temperature fluctuations in the primordial plasma, making the photon-baryon gas expand and thus sending an acoustic wave through the plasma. This creates a spherical sound wave through the baryons and photons, leaving the dark matter untouched. This happens at every overdensity resulting in a wave pattern, which can be observed in the distribution of galaxies. The growth of these sound horizons stops at the time of photon decoupling as the interactions between photons and baryons stops, relieving the pressure of the system. As the sound waves imprints themselves on the structure formation, this makes for a standard ruler that is approximately 150 Mpc today [10].

From the three measurements (drawn in figure 1.7 on page 12) one can compile a best fit to the cosmological model of eq. 1.10 on page 6 with [8]:

$$\begin{aligned}
\Omega_{r,0} &= \Omega_\gamma(1 + 0.2271N_{\mathrm{eff}}) = 8.49 \times 10^{-5} \\
\Omega_{m,0} &= \Omega_{b,0} + \Omega_{c,0} \ , \ \Omega_{b,0} = 0.0462 \pm 0.0015 \ , \ \Omega_{c,0} = 0.233 \pm 0.013 \\
\Omega_{\Lambda,0} &= 0.721 \pm 0.015 \\
H_0 &= 70.1 \pm 1.3\mathrm{km/s/Mpc}
\end{aligned} \tag{1.25}$$

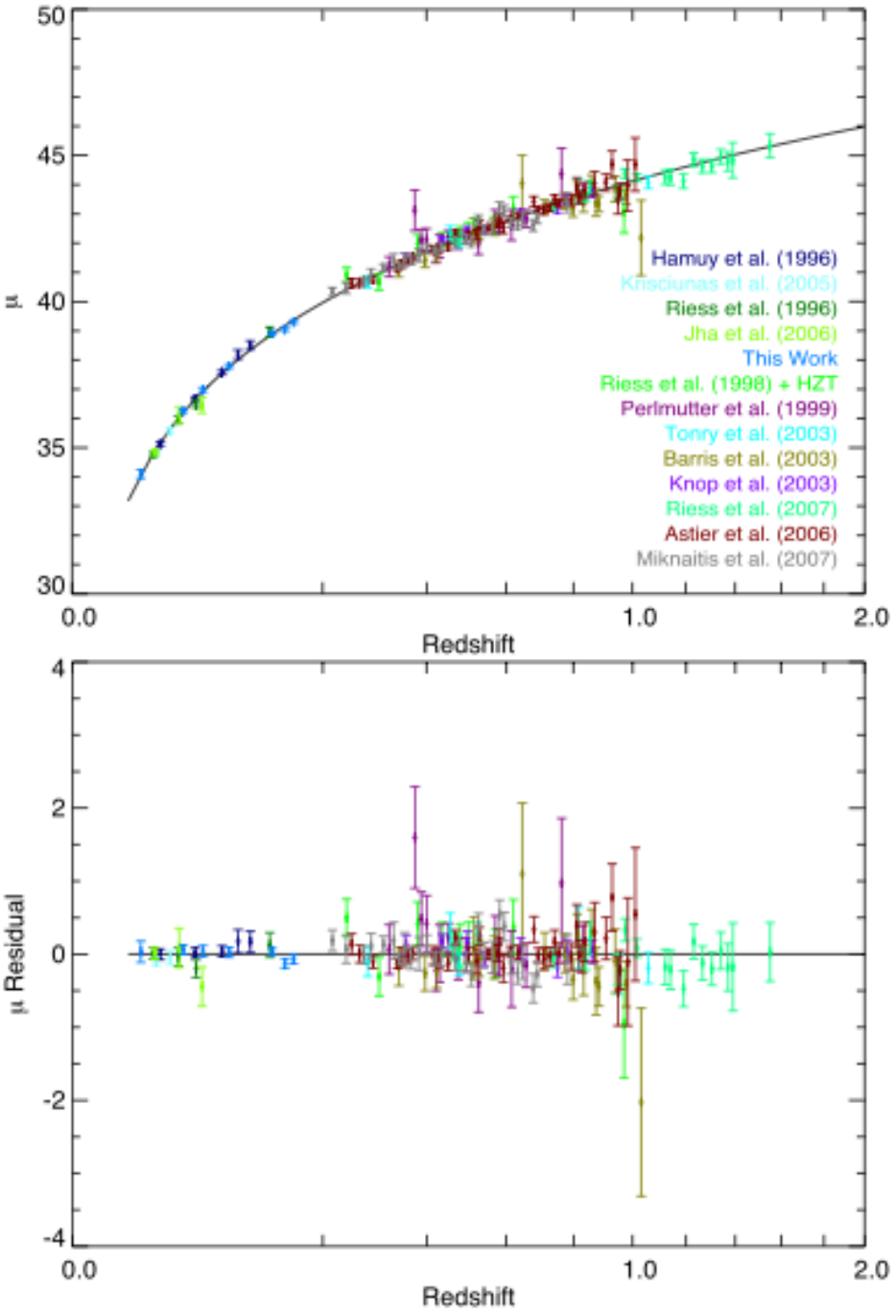

Figure 1.6: Binned Hubble diagram from [9]. Bottom shows residuals from best fit

One should note that the effects of neutrinos are taken into account in the radiation term with $N_{\text{eff}} = 3.04$ as the standard value.

One can thus summarise the history of the Universe: Starting from a hot dense state, the Universe expanded and cooled. After a time the plasma had cooled enough for atoms to form. This *recombination epoch* was followed by the *photon decoupling epoch* when scattering rate for photon-electron scattering becomes lower than the Hubble parameter.

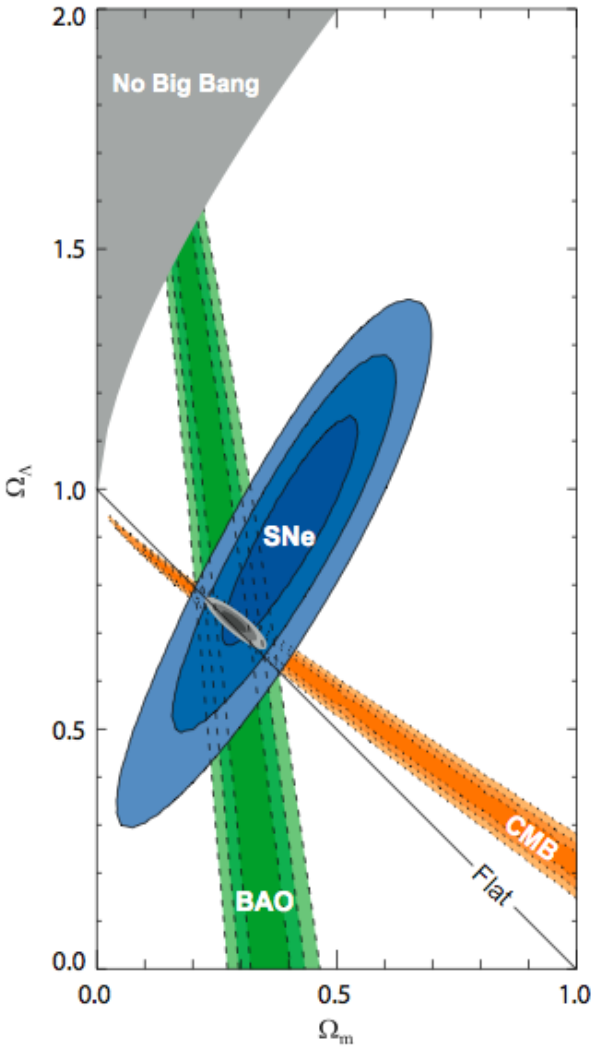

Figure 1.7: Plot of $\Omega_{m,0}$ vs. $\Omega_{\Lambda,0}$ with 1σ, 2σ and 3σ confidence intervals. From [9]

Shortly after this decoupling the mean free path of the photons became so large, that the photons could free stream from the time of the *last scattering surface*. As the expansion continued matter began to cluster and form the structures we observe today in our flat, homogeneous and isotropic Universe.

Though this is a nice scenario, there are still some issues in the hot Big Bang scenario, that needs to be addressed. This will be done in the following chapter.

2 Issues with the Big Bang Scenario

Though the ΛCDM-model provides a good explanation of the data (see figures 1.4 and 1.7), certain aspects of it may be slightly disturbing. These will need to be addressed, if one is to accept the ΛCDM-model. The following paragraphs are based on [1, 2, 11, 12].

2.1 The Flatness Problem

Fits to data show that the Universe is flat ($\Omega_0 = 1$) to within a few per cent. One would not usually take a fine tuning to within a few per cent to be a major concern, but one should bear in mind that the deviation from a flat universe should be extremely small at the time of Big Bang Nucleosynthesis (BBN) in order to give an Ω_0 so close to 1 today.

If one regards the total relative energy density (Ω_0) as a function of the scale factor

$$\Omega_0(a) = \frac{\rho}{3H^2} = 1 + \frac{\kappa}{(aH)^2 R_0^2}, \tag{2.1}$$

one sees that $|\Omega(a) - 1|$ grows through matter ($w = 0$) and radiation ($w = \frac{1}{3}$) dominated epochs as $(aH)^2 \propto a^{-1}$ and $(aH)^2 \propto a^{-2}$, respectively. Taking matter-radiation equality to be around redshift of $1 + z_{eq} \sim 3600$ and BBN around redshift $1 + z_{BBN} \sim 10^{10}$, one finds $\Omega(a_{BBN}) - 1 \sim 10^{-18}$ at the time of BBN in order to meet the observational constraints.

This seems highly unlikely and requires a great deal of fine-tuning of the initial parameters. Hence he Flatness Problem arises as a fine-tuning problem. An illustration of the curvature is provided in figure 2.1 on the following page.

2.2 The Horizon Problem

If one further regards the fundamental assumption for the FRW universe, one encounters a second problem with the hot Big Bang model described previously. This fundamental assumption, the cosmological principle, states that the Universe is, on large scales, homogenous and isotropic, which does indeed seem to be in agreement with the measurements. The observations of the CMB have, in fact, limited the relative variations in the CMB temperature to be of the order 10^{-5}. This is particularly remarkable when one compares the distance a light signal could travel before decoupling to the size of the horizon. Assuming, for the sake of simplicity that recombination and the generation of the last scattering surface coincides, one can find the travelled distance to be

$$L = a_{\mathrm{rec}} \int_0^{t_{\mathrm{rec}}} \frac{\mathrm{d}t}{a(t)} = 2t_{\mathrm{rec}} = H_{\mathrm{rec}}^{-1} = H_0^{-1}(1 + z_{\mathrm{rec}})^{-3/2}, \tag{2.2}$$

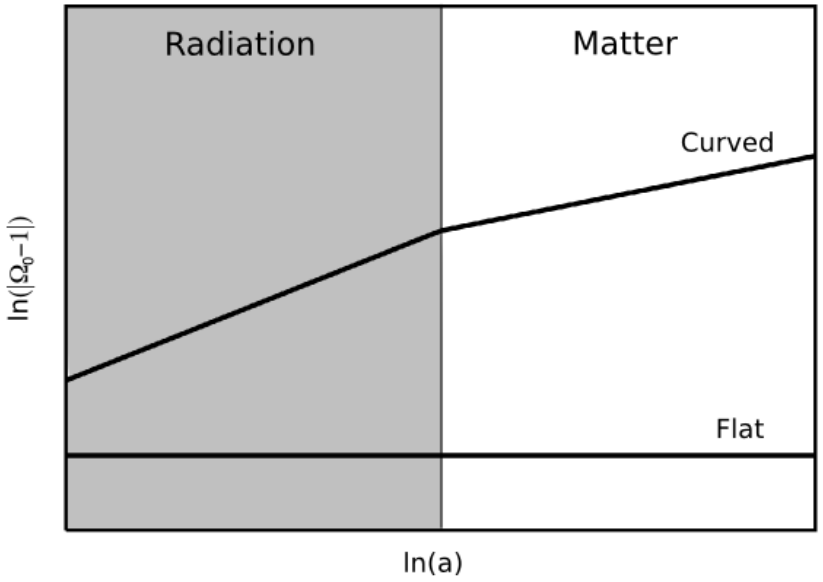

Figure 2.1: Sketch of the evolution of the curvature term through a radiation and a matter dominated period

where the last equality assumes a matter dominated universe from recombination until present day.

This should be compared to the size of the last scattering surface at the time of recombination (assuming a flat geometry):

$$D = \frac{a_{\rm rec}}{a_0} a_0 \int_{t_{\rm rec}}^{t_0} \frac{{\rm d}t}{a(t)} = (1+z_{\rm rec})^{-1} \frac{2}{H_0} \left[1 - (1+z_{\rm rec})^{-1/2}\right] \ . \tag{2.3}$$

Comparing the two results, one finds that the maximum angular distance between two correlated points in the sky to be

$$\theta = \frac{L}{D} \simeq \frac{1}{2}(1+z_{\rm rec})^{-1/2} \approx 1^\circ \ . \tag{2.4}$$

That is to say, any two photons coming from more than 1° apart have never been causally connected, making it quite remarkable that the CMB is so homogeneous. The Horizon Problem is illustrated in figure 2.2 on the next page. The diagram shows clearly that two points on the last scattering surface have past light cones that never overlap. They can therefore not have been in casual connection with one another prior to the photon decoupling epoch.

2.3 A Possible Solution to Both Problems

Alan H. Guth pointed out in 1981 [14] that one could solve both problems by introducing an epoch of accelerated, or inflationary, expansion in the early universe. Though this idea is remarkably simple from a conceptual point of view, it solves the Flatness Problem and the Horizon Problem quite effectively, provided that it goes on for a long enough time.

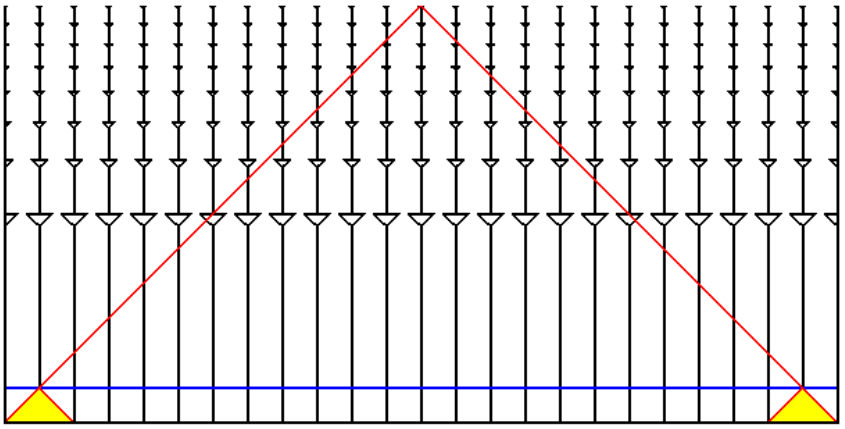

Figure 2.2: Spacetime diagram of the evolution of the Universe with past light cones of two points marked in yellow. Last scattering surface is marked with a blue line. Taken from [13]

In the case of the Flatness Problem the inflationary expansion needs to provide $\Omega(a_{\mathrm{BBN}})-1 \sim 10^{-18}$ at the time of BBN. Since nuclei start to form at around a temperature of $T_{\mathrm{BBN}} \sim 1$ MeV, one can estimate the required time for solving the Flatness Problem by estimating the energy scale of the end of inflation to be around $T_I \sim 10^{15}$ GeV and assuming a radiation dominated universe from the end of inflation to the time of BBN, one gets

$$\Omega_0(a_I) - 1 \sim (\Omega_0(a_{BBN}) - 1) \left[\frac{a_I}{a_{BBN}}\right]^2 \tag{2.5}$$

from eq. 2.1 on page 13. As $T \propto a^{-1}$ one can rewrite this to

$$\Omega_0(a_I) - 1 \sim 10^{-54} \left[\frac{10^{15}\ \mathrm{GeV}}{T_I}\right]^2 . \tag{2.6}$$

Though an initial condition of 10^{-54} may seem impossibly small, this is easily manageable by assuming a nearly exponential growth factor, i.e., an approximate de Sitter solution. In this case the Hubble parameter is nearly constant and one can write

$$\frac{(aH)_f}{(aH)_i} \simeq \frac{a_f}{a_i} = e^{\Delta N}, \tag{2.7}$$

where the number of e-folds ΔN has been introduced. In this case one only needs

$$\Delta N = \frac{1}{2}\ln(10^{54}) \simeq 62 \tag{2.8}$$

to provide a sufficiently flat initial condition to meet the current observational bounds (cf. eq. 2.1 on page 13).

For the Horizon Problem the issue was that any two points more than a degree apart in the sky could not be causally connected. Recasting this problem to one of length scales it means that the physical length $L = a(t)l$ has been larger than the Hubble length H^{-1} previous to recombination. For the largest scales we can observe today ($l \sim (aH)_0^{-1}$), this

means that the ratio between the physical length scale and the Hubble length at the time of BBN was

$$\frac{L_{BBN}}{H_{BBN}^{-1}} = l(aH)_{BBN} = \frac{(aH)_{BBN}}{(aH)_{\text{eq}}}\frac{(aH)_{\text{eq}}}{(aH)_0} \ . \tag{2.9}$$

Again assuming a universe dominated by radiation from the time of BBN to the the time of matter-radiation-equality and matter dominated from then till present day, one gets

$$\frac{L_{BBN}}{H_{BBN}^{-1}} \sim 10^8 \ . \tag{2.10}$$

As aH grows during the inflationary epoch, a sufficient period of inflation will ensure that all observable length scales have at one point been smaller than the Hubble length. Requiring that the largest length scales today have at one point been the size of the Hubble length ($a_* l = H_*^{-1}$), one finds

$$1 = \frac{(aH)_0}{(aH)_*} = \frac{(aH)_{\text{end}}}{(aH)_*}\frac{(aH)_{\text{eq}}}{(aH)_{\text{end}}}\frac{(aH)_0}{(aH)_{\text{eq}}} \tag{2.11}$$

with the assumption of an instant transition from the end of inflation to BBN. Here the subscript *end* marks the end of inflation. If the matter-radiation-equality occurs at a temperature of $T_{\text{eq}} \sim 3$ eV, one can estimate

$$\frac{(aH)_{\text{eq}}}{(aH)_{\text{end}}} = \frac{a_{\text{end}}}{a_{\text{eq}}} = \frac{T_{\text{eq}}}{T_I} = 3 \times 10^{-24}\frac{10^{15}\ \text{GeV}}{T_I} \ . \tag{2.12}$$

Making the same assumption of a nearly exponential growth during inflation, one can find the required number of e-folds, such that the largest observable length scales must have been equal to the Hubble length to be

$$\Delta N \sim 58 + \ln\left(\frac{T_I}{10^{15}\ \text{GeV}}\right) \ . \tag{2.13}$$

Sketching the curvature term as in figure 2.3 on the facing page one can see, how inflation solves the Flatness Problem and the Horizon Problem. By extending the inflationary epoch, one can achieve the initial curvature needed to match the present observational bounds.

2.4 INFLATION AT A GLANCE

To achieve and sustain inflation long enough to solve the Flatness Problem and the Horizon Problem, one needs to set up a scenario in which the Universe accelerates and continues to do so for the required number of e-folds. One can parameterize this acceleration and its stability through the slow-roll parameters, which can be defined by regarding the acceleration requirement

$$0 < \frac{\ddot{a}}{a} = \dot{H} + H^2 \Leftrightarrow \epsilon \equiv -\frac{\dot{H}}{H^2} < 1 \ , \tag{2.14}$$

i.e., one has an accelerated expansion as long as the first slow-roll parameter ϵ is sufficiently small. In order to sustain inflation ϵ should remain small, i.e., the relative change in ϵ

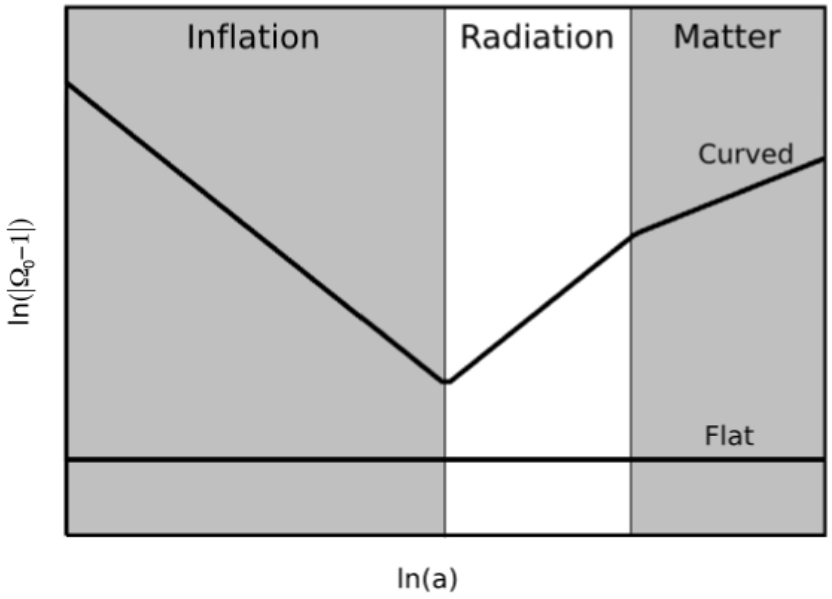

Figure 2.3: Sketch of the evolution of the curvature term through a radiation and a matter dominated period, preceded by a period of inflation

should mostly be small compared to the expansion rate, which yields the definition of the second slow-roll parameter:

$$\eta \equiv \frac{\dot{\epsilon}}{H\epsilon} \ll 1 \ . \tag{2.15}$$

One can estimate an upper bound on the slow-roll parameters, which should be obeyed to achieve the desired number of e-folds:

$$\epsilon = -\frac{\dot{H}}{H^2} = -\frac{H_N}{H} \ , \tag{2.16}$$

where the index N denotes a derivative with respect to the number of e-folds. One can approximate this as $H_N \sim \frac{\Delta H}{\Delta N}$, where the change of the Hubble parameter $-\Delta H < H$. This gives

$$\epsilon < \Delta N^{-1} \sim \frac{1}{60} \ . \tag{2.17}$$

The same argument can be applied to η to find the same bound on the second slow-roll parameter.

Achieving the low values of the slow-roll parameters in the first place is no simple feat, and is highly dependent on the chosen model. In many toy models this reintroduces a level of fine-tuning, and even in more elaborate high energy theories, e.g. string theory, it is not generic that the slow-roll parameters are small. This is sometimes known as the η-problem in string theory, in which suppressed corrections to the model lead to contributions to η of order 1, thus hindering sustained inflation.

The numerical calculations in this work will always assume that both slow-roll parameters are initially small.

Expressing the slow roll condition in terms of the fields involved, it means that the fields driving the cosmological expansion should have a negligible kinetic energy, i.e., their potential should be nearly flat.

At some point inflation ends by breaking slow-roll, i.e. the fields reaches a segment where the kinetic energy of the inflaton becomes comparable to its potential energy. Shortly after that, the inflaton field begins to oscillate around a minimum in the potential. At this point the energy density should be transferred from the inflaton to the matter fields we observe today, a scheme generally referred to as reheating.

This can be achieved in many ways, but is in general described as a two stage process, where the first step (called pre-heating) is an explosive depletion of the energy density of the inflaton to produce an intermediary field χ, followed by a decay of the χ particles to standard model particles and a subsequent or simultaneous thermalisation of the particle products. The original example [15], which will be shortly reviewed here assumes that the inflaton, ϕ, couples to a bosonic field χ and a fermionic field ψ through

$$\mathcal{L}_{\text{int}} = -\frac{1}{2}g^2\phi^2\chi^2 - h\bar{\psi}\psi\phi \ , \tag{2.18}$$

where $h, g \ll 1$. The further details of pre-heating depend on the potential for the inflaton, but in general it is the oscillations of the inflaton fields around the minimum, that excites the bosonic field. In the case of a decay purely to fermionic particles, reheating completes when the decay rate is comparable to the Hubble parameter.

As reheating ends and the radiation dominated period initiates, the last effect of inflation kicks in. The fluctuations of the inflaton field have embedded themselves in the spacetime and afterwards been carried outside the Hubble horizon, due to the expansion of the Universe. As the acceleration stops the horizon starts to expand faster than the Universe, making the fluctuation reappear inside the horizon. These fluctuations acts as perturbation seeds in the self-gravitating fluid, which exists in the Universe.

Expressing the density contrast $\frac{\delta\rho_M}{\rho_M}$ in terms of its Fourier transform

$$\frac{\delta\rho_M}{\rho_M} = \int \mathrm{d}^3\boldsymbol{k}\delta_{\boldsymbol{k}}(t)e^{-i\boldsymbol{k}\cdot\boldsymbol{x}} \ , \tag{2.19}$$

one can write down the evolution of the density contrasts by a Newtonian equation:

$$\ddot{\delta}_{\boldsymbol{k}} + 2H\dot{\delta}_{\boldsymbol{k}} + \left(\frac{\partial p}{\partial\rho_M}\right)^2 \frac{k^2}{a^2}\delta_{\boldsymbol{k}} = 4\pi G\rho_M\delta_{\boldsymbol{k}} \ . \tag{2.20}$$

Solving this for the radiation and matter dominated epochs, one finds $\delta_{\boldsymbol{k}} \propto \ln(a)$ and $\delta_{\boldsymbol{k}} \propto a$, respectively. Thus one will only see a real growth in overdensities during the matter dominated epoch.

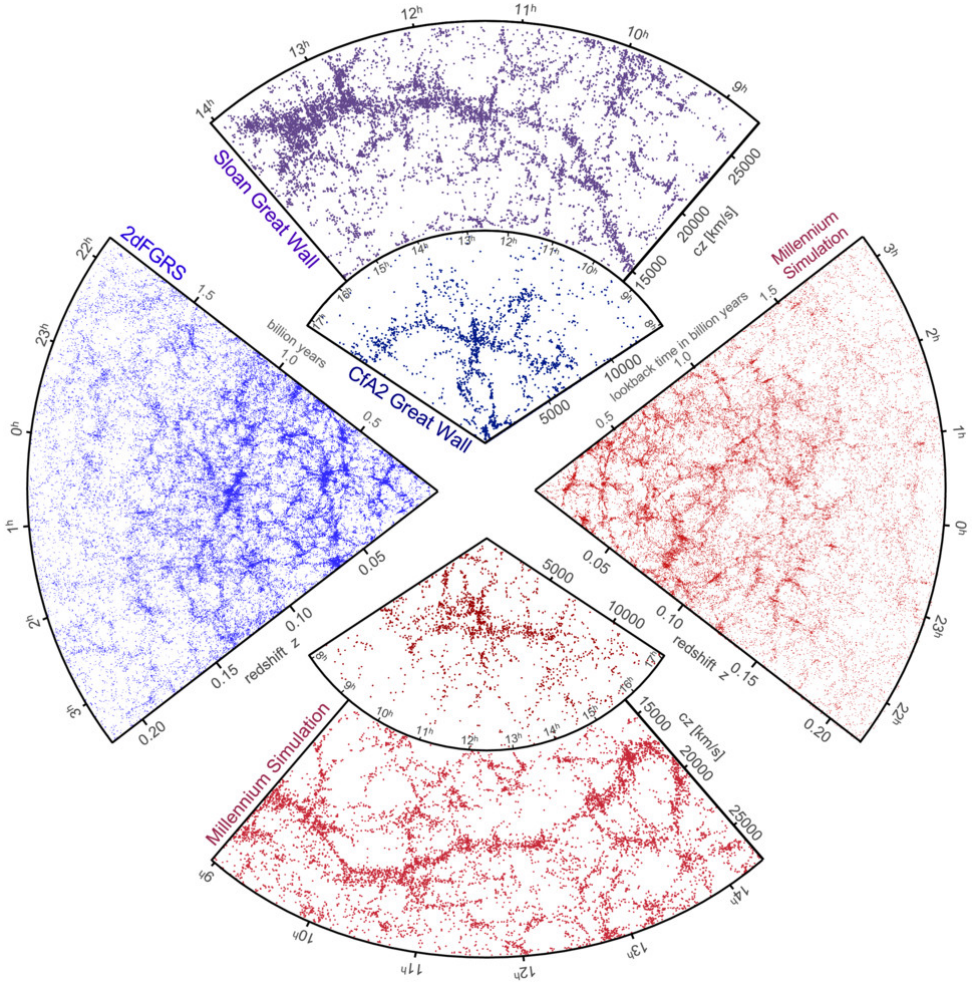

Figure 2.4: Observations of the galactic distribution from 2dFGRS [16] and the SDSS [17], compared to N-body simulation. Figure from [18]

Once the overdensities becomes of order unity, they decouple from the expansion, becoming their own self-gravitating system and begin the process of virial relaxation. These will eventually make up the structure, that we see in our Universe today (see figure 2.4 for a comparison between observation and simulation of large scale structure). This, however, leaves the question of the origin and properties of the initial fluctuations; the scope of this thesis.

3 Statistics and Perturbation Theory

To drive the Universe through an inflationary stage, one usually needs to invoke a high energy quantum field theory or a theory of quantum gravity. As such quantum fluctuations arise as a natural part of inflation.

One therefore needs a framework to understand the effects of these fluctuations on the underlying metric, as well as a definition of the suitable statistics needed to describe the perturbations of the metric and how these statistics are linked to the chosen theory of inflation.

This chapter is dedicated to a review of the necessary statistics and first order perturbation theory. Higher order perturbation theory is deferred to chapter 8. Most of the derivations are inspired by [11].

3.1 Metric Perturbations

Though it might not be evident from the beginning that the quantum fluctuations in the fields driving inflation are tightly linked to the perturbations of the metric, one can construct a simple argument to illustrate this connection qualitatively.

A fluctuating set of fields will, through their contributions to the energy-momentum tensor, introduce a perturbation of the same tensor $\delta T_{\mu\nu}$. This couples to the metric tensor through the Einstein equation:

$$\delta T_{\mu\nu} = \delta \left(R_{\mu\nu} - \frac{1}{2} g_{\mu\nu} R + \Lambda g_{\mu\nu} \right) \propto \delta g_{\mu\nu} \ . \tag{3.1}$$

The reverse effect can also be seen as the metric tensor enters in the equation of motion governing the fields of the theory, e.g., the Dirac or Klein-Gordon equation. Thus a perturbation of the metric tensor will invariably translate into a fluctuation of the fields.

Writing the metric as sum of an unperturbed background and a general perturbation

$$g_{\mu\nu} = g^{(0)}_{\mu\nu} + \delta g_{\mu\nu} \ , \tag{3.2}$$

one usually chooses the background to be the FRW metric (c.f. 1.4 on page 5). The perturbation can be broken down to a combination of scalar modes, vector (or vorticity) modes and tensor (or gravitational wave) modes. The latter occur as a physical degree of freedom in the sense that they can exist independently of the content of the Universe, and even exist in vacuum. The scalar and vector modes will only arise in conjunction with fluctuations of the fields in the Universe.

It can be instructive to commence the discussion about metric perturbation by inventorying the degrees of freedom (DOF) available within each type of mode in a $n+1$ dimensional metric. As the metric must be symmetric, one is left with $\frac{1}{2}(n+2)(n+1)$ DOF in $\delta g_{\mu\nu}$ ($n+1$ from the diagonal and $\frac{1}{2}n(n+1)$ from the off diagonal triangle, picture (a) in figure 3.1). One can now eliminate $n+1$ of these by coordinate transformations and write the remaining as a scalar, a n dimensional vector and a $n \times n$ symmetric tensor (picture (b) in figure 3.1).

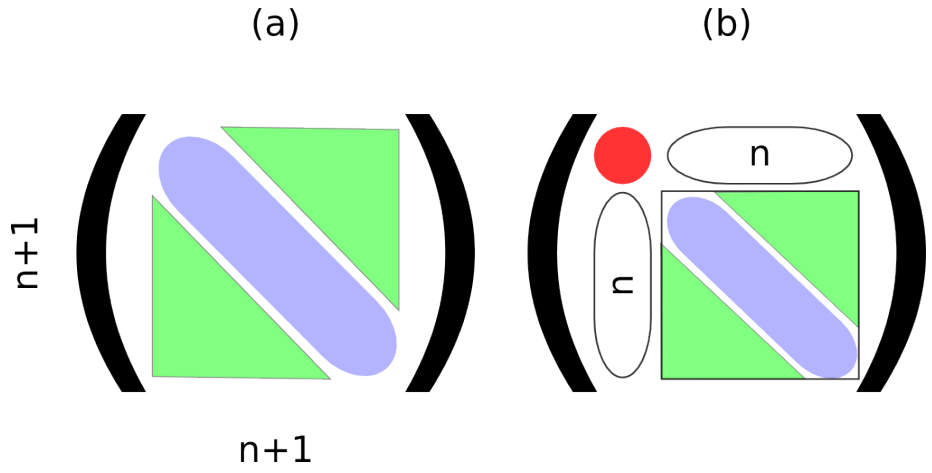

Figure 3.1: Graphical representation of decomposing the metric perturbations

By Helmholtz's theorem one can decompose the vector into a scalar and a divergence free vector ($u_i = \partial_i v + v_i$), leaving $n-1$ vector degrees of freedom due to the divergence condition.

Regarding the tensor modes, one can repeat the above argument to find that the symmetry requirement constrains the DOF to $\frac{1}{2}n(n+1)$. Imposing the additional constraints of the tensor modes being traceless and transverse ($\nabla^i \delta g_{ij} = 0$) removes $n+1$ DOF; one from being traceless and n from requiring it to be transverse. This leaves $\frac{1}{2}(n-2)(n+1)$ tensor DOF.

From this it is now possible to find the total number of scalar DOF to be

$$\underbrace{\frac{1}{2}(n+2)(n+1)}_{\text{Total DOF}} - \underbrace{(n+1)}_{\text{Coordinate transformations}} - \underbrace{(n-1)}_{\text{Vector DOF}} - \underbrace{\frac{1}{2}(n-2)(n+1)}_{\text{Tensor DOF}} = 2 \ . \tag{3.3}$$

The next section will be dedicated to writing down the specific perturbations for the FRW metric.

3.2 PERTURBING THE FRW METRIC

Considering the $3+1$ dimensional flat Friedmann-Robertson-Walker metric

$$ds^2 = -dt^2 + a(t)^2 \eta_{ij} dx^i dx^j \ , \tag{3.4}$$

it is possible to introduce perturbations, by following the classic paper [19]. We limit ourselves to a flat space with only scalar perturbations in the following. The most general

first order scalar perturbation of eq. 3.4 one can write down is

$$ds^2 = -(1+2A)dt^2 + 2\partial_i B dt dx^i + a(t)^2((1+2\psi)\eta_{ij} + D_{ij}E)dx^i dx^j \tag{3.5}$$

with

$$D_{ij} = \partial_i\partial_j - \frac{1}{3}\eta_{ij}\partial^2 \ . \tag{3.6}$$

These perturbations cannot, however, be independent as it was shown above that the total number of scalar degrees of freedom in the system is 2. The two physically relevant perturbations are known as Bardeen's potentials (introduced in [20, 21]). To derive these one can perform a gauge transformation (again regarding solely the scalar contribution)

$$t \to t + \xi \ , \ x^i \to x^i + \partial^i\beta \ , \tag{3.7}$$

and require that the line element, truncated to the first order in this case, is invariant under coordinate transformation. Denoting the perturbation parameters after the coordinate transformation with a tilde, one get

$$\begin{aligned} ds^2 \to &-(1+2(\tilde{A}+\dot{\xi}))dt^2 + 2\partial_i(\tilde{B} - \xi + a^2\dot{\beta})dt dx^i \\ &+ a(t)^2\left[(1+2(\tilde{\psi} + H\xi + \frac{1}{3}\partial^2\beta))\eta_{ij} + D_{ij}(\tilde{E}+2\beta)\right]dx^i dx^j \ . \end{aligned} \tag{3.8}$$

From this one can deduce from eq. 3.5 that

$$\tilde{A} = A - \dot{\xi} \tag{3.9}$$

$$\tilde{B} = B + \xi - a^2\dot{\beta} \tag{3.10}$$

$$\tilde{\psi} = \psi - H\xi - \frac{1}{3}\partial^2\beta \tag{3.11}$$

$$\tilde{E} = E - 2\beta \ . \tag{3.12}$$

From these transformations one can now construct the two Bardeen's potentials (Φ and Ψ):

$$\Phi = A + \frac{\mathrm{d}}{\mathrm{d}t}\left(B - \frac{\dot{E}a^2}{2}\right) \tag{3.13}$$

$$\Psi = \psi + \frac{\partial^2 E}{6} + H\left(B - \frac{\dot{E}a^2}{2}\right) \tag{3.14}$$

The exact expressions for these gauge invariant perturbations are highly dependent on the choice of time coordinate, as different choices correspond to different hypersurfaces of constant time (time slices).

3.3 PERTURBATIONS IN SINGLE FIELD INFLATION

Limiting the discussion for a moment to model with a single scalar field, we introduce three standard gauge choices: The isocurvature gauge, the comoving curvature gauge and the uniform curvature gauge. Each hold its own virtues and will be briefly reviewed.

The discussion requires a knowledge of transformation laws for perturbed scalar quantities. We follow the pedagogical derivation from [11]:

Transforming the coordinate system from $x^\mu \to \tilde{x}^\mu = x^\mu + \delta x^\mu$, one transforms the perturbation of a scalar quantity f as $\delta f(x^\mu) \to \widetilde{\delta f}(\tilde{x}^\mu)$. As

$$\widetilde{\delta f}(\tilde{x}^\mu) = \tilde{f}(\tilde{x}^\mu) - \tilde{f}_0(\tilde{x}^\mu) \ , \tag{3.15}$$

where f_0 is the background quantity, we can rewrite this as

$$\widetilde{\delta f}(\tilde{x}^\mu) = f(x^\mu) - f_0(\tilde{x}^\mu) \ , \tag{3.16}$$

since $f(x^\mu)$ is a physical scalar, i.e. it is independent of the choice of coordinate system. Expanding $f(x^\mu)$ around $\tilde{x}^\mu$ yields

$$\widetilde{\delta f}(\tilde{x}^\mu) = f(\tilde{x}^\mu) - f_0(\tilde{x}^\mu) - \frac{\partial f}{\partial x^\mu}\delta x^\mu = \delta f(\tilde{x}^\mu) - \left.\frac{\partial f}{\partial x^\mu}\right|_{x^\mu=\tilde{x}^\mu} \delta x^\mu \ . \tag{3.17}$$

The curvature referred to in the names of the perturbation choices is the perturbation parameter ψ. This is simply due to, that the intrinsic curvature scalar for the spatial part of the metric is given by

$$\mathcal{R}_3 = -\frac{4}{a^2}\nabla^2\psi \tag{3.18}$$

ISOCURVATURE GAUGE

The isocurvature perturbation distinguishes itself from the other two by having the perturbations solely in the field fluctuations, providing a scheme with nice features for performing slow roll computations, i.e., computations when $\epsilon, \eta \ll 1$.

Requiring the spatial perturbations to vanish, we perform a time translation as was done in eq. 3.7 on the preceding page:

$$\tilde{\psi} = \psi - H\xi = 0 \Rightarrow \xi = \frac{\psi}{H} \ . \tag{3.19}$$

Performing the same time translation on the field fluctuation, gives rise to the Mukhanov-Sasaki variable

$$Q = \delta\phi - \frac{\dot{\phi}}{H}\psi \ , \tag{3.20}$$

which is gauge invariant and identical to $\delta\phi$, when the spatial perturbations go to zero.

COMOVING CURVATURE GAUGE

Observers in the comoving picture will see themselves as free falling, making the expansion seem isotropic, meaning that they do not measure any energy flux ($T_{i0} = 0$). For the canonical single field case, one gets

$$T_{i0} \propto \dot{\phi}\nabla_i\delta\phi \ , \tag{3.21}$$

meaning that the time translation should take $\delta\phi \to 0$. That is

$$\delta\phi \to \delta\phi - \dot{\phi}\xi = 0 \tag{3.22}$$

for the time translation $t \to t + \xi$, meaning that $\xi = \frac{\delta\phi}{\dot{\phi}}$. This transformation gives

$$\psi \to \mathcal{R} \equiv \psi - H\frac{\delta\phi}{\dot{\phi}} \ , \tag{3.23}$$

which is gauge invariant. This quantity $\mathcal{R}$ is the comoving curvature perturbation, which is equal to the gravitational potential, when one transform to hypersurfaces where $\delta\phi = 0$.

UNIFORM DENSITY GAUGE

In single field inflation the choice of $\delta\phi = 0$ implies both comoving curvature perturbations and uniform density perturbations, the definition of the two are however different. For the uniform density perturbations one does a time translation $t \to t + \xi$, such that $\delta\rho \to 0$, i.e.,

$$\delta\rho \to \delta\rho - \dot{\rho}\xi = 0 \ . \tag{3.24}$$

This transformation brings ψ to

$$\psi_{\rm uni} = \psi - H\xi = \psi - H\frac{\delta\rho}{\dot{\rho}} \equiv \zeta \ . \tag{3.25}$$

As we are dealing with a single field, one can write

$$\delta\rho = \dot{\phi}\dot{\delta\phi} + V'(\phi)\delta\phi \ . \tag{3.26}$$

For the general single field slow roll scenario, one can, on superhorizon scales ($k \ll H$), reduce the equation of motion to

$$3H\dot{\phi} + V' \simeq 0 \ , \tag{3.27}$$

giving the first order expression

$$\dot{\delta\phi} \propto (\text{slow roll parameters})H\delta\phi \ , \tag{3.28}$$

which reduces $\delta\rho$ to

$$\delta\rho \simeq V'\delta\phi \ . \tag{3.29}$$

One can now use the fluid equation (eq. 1.7 on page 5) to rewrite

$$\dot{\rho} = -3H(\rho + p) = -3H\dot{\phi}^2 \simeq V'\dot{\phi} \ . \tag{3.30}$$

This totals to

$$\zeta \simeq \psi - H\frac{\delta\phi}{\dot{\phi}} = \mathcal{R} \ . \tag{3.31}$$

One sees that on superhorizon scales the comoving curvature perturbations and the uniform density perturbations reduce to the same quantity.

3.4 STATISTICS IN EXPANDING SPACETIME

As one does not observe the perturbations directly, but more the statistical properties of

the perturbations, one should define the general statistical tools needed to describe the perturbations.

The pivotal ingredient for discussing the properties of a perturbation is the n-point correlation function, written as $\langle \Xi^n \rangle$ for a stochastic variable Ξ, where the brackets denote the vacuum expectation value. This n-point correlation function can in some cases be written in a simple way. In inflation, however, one keeps things simple by distinguishing between such a simple case (Gaussian) and a deviation from this case (non-Gaussian). For the Gaussian case one can write

$$\langle \Xi^n \rangle = \begin{cases} \frac{n!}{2^{n/2}\left(\frac{n}{2}\right)!} \langle \Xi^2 \rangle^{n/2} & \text{for } n \text{ even} \\ 0 & \text{for } n \text{ odd} \end{cases} . \tag{3.32}$$

That there is a one-to-one correspondence between following a Gaussian distribution and obeying eq. 3.32 come from the fact that any distribution is uniquely determined by its moments, i.e., its n-point correlation functions.

One can thus determine if an operator is non-Gaussian by measuring a deviation from eq. 3.32. In the coming we will concern ourselves mainly with the three-point function and the four-point function.

In calculating the n-point function in an expanding spacetime, one is faced with certain difficulties as the vacuum state is not well defined. To work around this issue one formulates the problem in the Heisenberg picture and evolves the vacuum state from a known initial condition. Thus:

$$\begin{aligned} \langle \Xi^n \rangle &= \left\langle \Omega \right| e^{\int \mathrm{d}^4x' \mathcal{H}_I(x')} \Xi_I^n e^{-\int \mathrm{d}^4x' \mathcal{H}_I(x')} \left| \Omega \right\rangle \\ &\simeq \langle \Omega | \, \Xi_I^n \, | \Omega \rangle \\ &\qquad - i \int \mathrm{d}^4x' \, \langle \Omega | \, [\Xi_I^n, \mathcal{H}_I(x')] \, | \Omega \rangle \ . \end{aligned} \tag{3.33}$$

Thus one has a direct influence of the model, through the interaction Hamiltonian, on the n-point correlation function. This makes it possible to compare the observed spectra and theoretical calculations via the relevant correlation functions.

Most of the time, however, one expresses the calculated correlation functions in terms of spectra. First introduced in the field of signal processing, the concept applies nicely to the perturbations that occurs during inflation.

SPECTRA

Starting from the two-point function one defines the power spectrum as the autocorrelation function of the stochastic operator (operators are denoted with capitals, while mode functions are denoted with small case):

$$\begin{aligned} \left\langle \Xi^2 \right\rangle &= \int \mathrm{d}^3\boldsymbol{k} \mathrm{d}^3\boldsymbol{k}' \, \langle \Xi(\boldsymbol{k}) \Xi(\boldsymbol{k}') \rangle \, e^{-i(\boldsymbol{k}+\boldsymbol{k}')\cdot\boldsymbol{x}} \\ &= (2\pi)^3 \int \mathrm{d}^3\boldsymbol{k} |\xi_k|^2 \\ &= 4\pi(2\pi)^3 \int \mathrm{d}k k^2 |\xi_k|^2 \\ &\equiv (2\pi)^6 \int \frac{\mathrm{d}k}{k} \mathcal{P}_\Xi(k) \ . \end{aligned} \tag{3.34}$$

Here we have used the decomposition of the operator into raising and lowering operators

$$\Xi(\boldsymbol{k}) = \xi_k a_{\boldsymbol{k}} + \xi_{-k} a^\dagger_{-\boldsymbol{k}} \tag{3.35}$$

with the normalisation

$$[a_{\boldsymbol{k}}, a_{\boldsymbol{k'}}] = [a^\dagger_{\boldsymbol{k}}, a^\dagger_{\boldsymbol{k'}}] = 0 \ , \ [a_{\boldsymbol{k}}, a^\dagger_{\boldsymbol{k'}}] = (2\pi)^3 \delta^{(3)}(\boldsymbol{k} - \boldsymbol{k'}) \ , \tag{3.36}$$

This gives an equivalent, and for the purposes in this work, more useful definition:

$$\mathcal{P}_\Xi(k) = \frac{k^3}{2\pi^2} |\xi_k|^2 \ . \tag{3.37}$$

As will be shown in eq. 4.22 on page 33, the power spectrum of single field inflation is nearly scale invariant, i.e. independent of k.

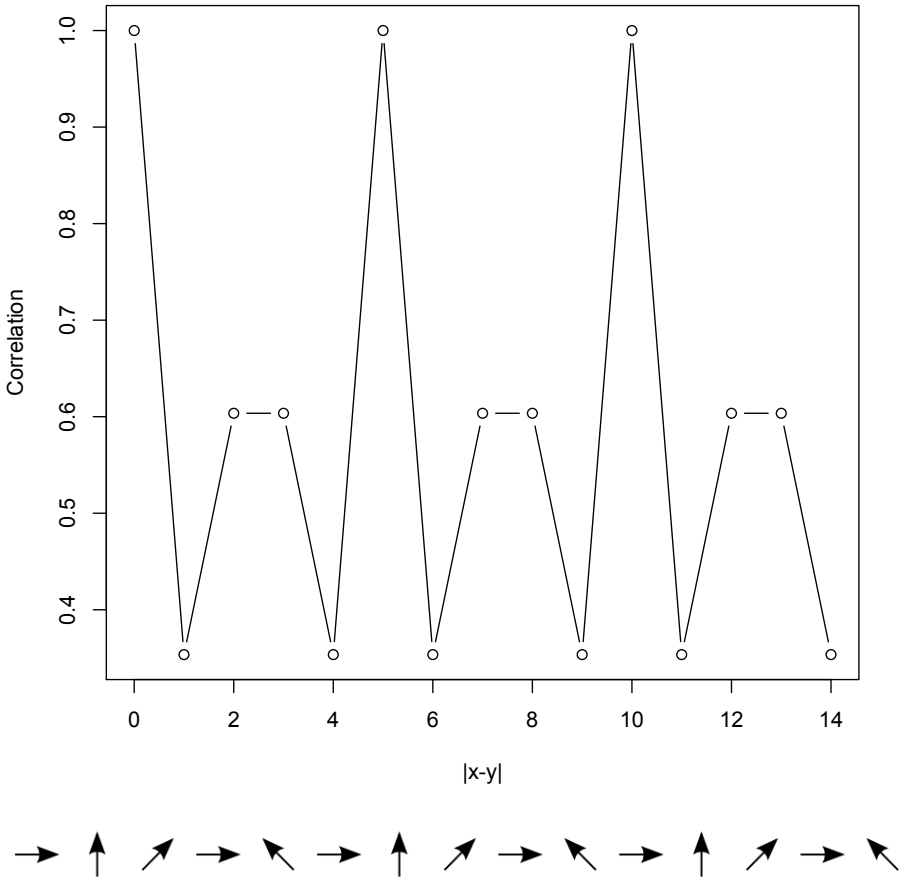

Figure 3.2: Cartoon of correlation function with the "data set" (the arrows) displayed below

From figure 3.2 one can get an impression of the information stored in a two-point correlation function, and through that in the power spectrum. The correlation function in the top frame is drawn as a correlation function of the direction of the arrows in the

bottom frame of figure 3.2. One sees that the correlation function assumes a high value at distances between arrows, where the arrows are in unison, and drops far down when the arrows are out of synchronisation. One can thus use the spectra to probe the scales at which the underlying data shows a recurrence.

Drawing inspiration from the definition eq. 3.34, which can be rewritten as

$$\langle \Xi(\boldsymbol{k})\Xi(\boldsymbol{k}')\rangle = (2\pi)^3\delta^{(3)}(\boldsymbol{k}+\boldsymbol{k}')\frac{2\pi^2}{k^3}\mathcal{P}_\Xi(k)\ , \tag{3.38}$$

one can define the analogue for the three-point function, the bispectrum as

$$\langle \Xi(\boldsymbol{k}_1)\Xi(\boldsymbol{k}_2)\Xi(\boldsymbol{k}_3)\rangle = (2\pi)^3\delta^{(3)}\left(\sum_{i=1}^{3}\boldsymbol{k}_i\right)B_\Xi(\boldsymbol{k}_1,\boldsymbol{k}_2,\boldsymbol{k}_3)\ . \tag{3.39}$$

As one can see things become slightly more complicated with the bispectrum as opposed to the power spectrum. The solution is no longer limited to only depending on the scale of the momenta, but now the shape of the momentum triangle also plays a role. The bispectrum is still independent of the rotation of the momentum triangle due to the cosmological principle. Though the entire range of triangle shapes are interesting, the literature have named three special cases (see figure 3.3 for the labelling of the sides in the triangle):

- **Squeezed**: $k_3 \ll k_1, k_2$
- **Equilateral**: $k_1 = k_2 = k_3$
- **Flattened/Folded**: $k_1 \approx 2k_2 \approx 2k_3$

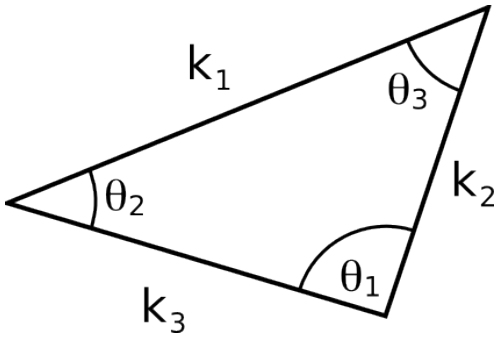

Figure 3.3: Momentum triangle

This principle can of course be expanded to any order of the correlation function, it will suffice for the present to merely define the trispectrum

$$\langle \Xi(\boldsymbol{k}_1)\Xi(\boldsymbol{k}_2)\Xi(\boldsymbol{k}_3)\Xi(\boldsymbol{k}_4)\rangle = (2\pi)^3\delta^{(3)}\left(\sum_{i=1}^{4}\boldsymbol{k}_i\right)T_\Xi(\boldsymbol{k}_1,\boldsymbol{k}_2,\boldsymbol{k}_3,\boldsymbol{k}_4)\ . \tag{3.40}$$

This discussion of the added complications of the dependence of the momentum vector is slightly more intricate for the trispectrum, and we will defer that to chapter 8. We will

instead turn the attention to quantifying the deviation from a Gaussian distribution.

NON-LINEARITY PARAMETERS

The spectra are, overall, an elegant description of the properties of the perturbation statistics, but they are not directly a quantification of the level of non-Gaussianities as the even order correlation functions will still have contributions from a Gaussian distribution.

To get a more practical quantification of the deviation from the Gaussian distribution, one tends to expand the stochastic variable around a Gaussian stochastic variable with the same mean [22]:

$$\zeta = \zeta_g - \frac{3}{5} f_{\rm NL} \zeta_g^2 \ . \tag{3.41}$$

We here focus on the perturbation parameter in the uniform density gauge (eq. 3.25 on page 25) as the numerical factor depends on the gauge transformation to the chosen variable.

Inserting the expansion into the three point function of ζ, one can relate the non-linearity parameter $f_{\rm NL}$ to the bispectrum as

$$B_\zeta(\boldsymbol{k}_1, \boldsymbol{k}_2, \boldsymbol{k}_3) = \frac{6}{5} f_{\rm NL} \left[\left(\frac{2\pi^2}{k_1^3} \mathcal{P}_\zeta(k_1) \right) \left(\frac{2\pi^2}{k_2^3} \mathcal{P}_\zeta(k_2) \right) + 2 \text{ perm.} \right] \ . \tag{3.42}$$

Through this definition one can translate a measured bispectrum to a value of $f_{\rm NL}$ and thus test a given model of inflation by comparing the observed $f_{\rm NL}$ to the theoretical. Such tests benefits from an ever increasing constraint on the non-linearity parameter ($-10 \lesssim f_{\rm NL}^{\rm local} \lesssim 70$ at 95% CL [8, 23, 24, 25, 26]).

In a similar fashion one can define τ_{NL} as the trispectrum equivalent to $f_{\rm NL}$ as [27, 28, 29, 30]

$$T_\zeta(\boldsymbol{k}_1, \boldsymbol{k}_2, \boldsymbol{k}_3, \boldsymbol{k}_4) = \frac{1}{2} \tau_{NL} \left[\frac{(2\pi^2)^3}{k_1^3 k_2^3 k_{14}^3} \mathcal{P}_\zeta(k_1) \mathcal{P}_\zeta(k_2) \mathcal{P}_\zeta(k_{14}) + 23 \text{ perms.} \right] \tag{3.43}$$

with $k_{ij} = |\boldsymbol{k}_i + \boldsymbol{k}_j|$. This non-linearity parameter is, at present, virtually unconstrained. The outlook, however, is still positive as the upcoming Planck data [31, 32] should constrain $f_{\rm NL} \sim \mathcal{O}(5)$ and put an initial bound on τ_{NL}.

For the most part of this work, we will focus on $f_{\rm NL}$ as this is the most promising quantity for detecting possible deviations from a Gaussian distribution in the near future, when one considers measurements of the CMB anisotropies.

4 Single Field Inflation

For the remainder of this work, we will constrain ourselves to models with a single scalar field. This is by far the simplest class of models, and the most studied, and though it may seem contrived to have a model with only a single scalar field, these models provide an insight into the multifield cases, where one field is profoundly dominating. It can therefore be helpful to study these models to gain a grasp on the properties of inflation.

4.1 Basic Properties of Single Field Inflation

The properties of single field inflation is, for the most part, defined simply through the choice of action. A large class of actions can be written in the form [33, 34, 35, 36, 37, 38]

$$S = \frac{1}{2}\int d^4x\sqrt{-g}\left[R + 2P(X,\phi)\right] \ , \tag{4.1}$$

where $P(X,\phi)$ is a polynomial with

$$X = -\frac{1}{2}\nabla_\mu\phi\nabla^\mu\phi \ . \tag{4.2}$$

This definition encompasses both the well known canonical models ($P = X - V(\phi)$), as well as more exotic models such as Dirac-Born-Infeld (DBI) inflation and k-inflation. Employing the principle of least action, one can derive an equation of motion for the field to be

$$\nabla^\mu P_X\nabla_\mu\phi + P_X\nabla^2\phi + P_X\frac{\nabla^\mu\sqrt{-g}}{\sqrt{-g}}\nabla_\mu\phi + P_\phi = 0 \ . \tag{4.3}$$

Here the index indicates a derivative, i.e., $P_X = \frac{\partial P}{\partial X}$. Assuming a flat FRW universe

$$ds^2 = -dt^2 + a(t)^2\eta_{ij}dx^i dx^j \ , \tag{4.4}$$

the energy-momentum tensor reduces to that of a perfect fluid

$$T^\nu_\mu = \mathrm{diag}(-\rho, p, p, p) \ . \tag{4.5}$$

From the variational definition of the energy-momentum tensor[2]

$$T^{\mu\nu} = \frac{2}{\sqrt{-g}}\frac{\delta(\sqrt{-g}L_M)}{\delta g_{\mu\nu}} \ , \tag{4.6}$$

[2]See for instance [39]

one can now derive the energy-momentum tensor for the system:

$$T^{\mu\nu} = -P_X \nabla^\mu \phi \nabla^\nu \phi + g^{\mu\nu} P. \tag{4.7}$$

This results in a system with

$$\rho = P_X \dot{\phi}^2 - P \ , \ p = P \ , \tag{4.8}$$

as the assumption of the metric forces the scalar field to be homogeneous. For the canonical case this reduces to

$$\rho = \frac{1}{2}\dot{\phi}^2 + V(\phi) \ , \ p = \frac{1}{2}\dot{\phi}^2 - V(\phi) \ . \tag{4.9}$$

Plugging the result from eq. 4.8 into the Friedmann equation (eq. 1.6 on page 5 with $\kappa = 0$)

$$H^2 = \frac{1}{3}(P_X \dot{\phi}^2 - P) \ , \tag{4.10}$$

one can find the evolution of the background metric.

As one starts to include fluctuations, driving the metric away from the simple, flat FRW-metric, things do, however, become more cumbersome, and we will therefore restrict this discussion to the single field canonical case.

4.2 POWER SPECTRUM OF THE FIELD FLUCTUATIONS

To get a sense of the properties of field fluctuations, we commence with studying the fluctuations of a single, massive scalar field in the isocurvature gauge. Perturbing the equation of motion (eq. 4.3) for this kind of model and truncating it to the first order, one is left with

$$\delta\ddot{\phi}_{\boldsymbol{k}} + 3H\delta\dot{\phi}_{\boldsymbol{k}} + \frac{k^2}{a^2}\delta\phi_{\boldsymbol{k}} + V''(\phi)\delta\phi_{\boldsymbol{k}} = 0 \ , \tag{4.11}$$

where we have introduced the Fourier transform of $\delta\phi$:

$$\delta\phi_{\boldsymbol{k}}(t) = \int \frac{\mathrm{d}^3\boldsymbol{x}}{(2\pi)^3}\delta\phi(\boldsymbol{x}, t)e^{i\boldsymbol{k}\cdot\boldsymbol{x}} \ . \tag{4.12}$$

Introducing the field transformation

$$\delta\phi_{\boldsymbol{k}} = \frac{\delta\chi_{\boldsymbol{k}}}{a} \tag{4.13}$$

and switching to conformal time $d\tau = a^{-1}dt$, one can write the equation of motion for the field as

$$\delta\chi''_{\boldsymbol{k}} + \left[k^2 - \tau^{-2}\left(\nu^2 - \frac{1}{4}\right)\right]\delta\chi_{\boldsymbol{k}} = 0 \ . \tag{4.14}$$

Rewriting the equation of motion to this form is done under the assumption that the background is a pure de Sitter space. Though this can never be achieved exactly for a spacetime with a scalar field, the onset of slow roll makes the approximation reasonable. The assumption gives that one can write the conformal time as

$$\tau = -\frac{1}{aH} \ . \tag{4.15}$$

We have denoted a derivative with respect to this quantity with a prime and defined

$$\nu^2 = \frac{9}{4} - \frac{m_\phi^2}{H^2} \ , \tag{4.16}$$

where the mass squared of the field is defined as the usual

$$m_\phi^2 = V''(\phi) \ . \tag{4.17}$$

The solution to eq. 4.14 can be written in terms of the Hankel functions of the first and second kind ($H_\nu^{(1)}$ and $H_\nu^{(2)}$ respectively) as

$$\delta\chi_{\boldsymbol{k}} = \sqrt{-\tau}\left[c_1(k)H_\nu^{(1)}(-k\tau) + c_2(k)H_\nu^{(2)}(-k\tau)\right] \ . \tag{4.18}$$

In order to determine the coefficients one can regard the solution in the ultraviolet limit ($-k\tau \gg 1$). In this limit the Hankel functions reduce to

$$H_\nu^{(1)}(-k\tau) \sim \sqrt{\frac{-2}{\pi k\tau}}e^{-i(k\tau+\frac{\pi}{2}\nu+\frac{\pi}{4})} \ , \ H_\nu^{(2)}(-k\tau) \sim \sqrt{\frac{-2}{\pi k\tau}}e^{i(k\tau+\frac{\pi}{2}\nu+\frac{\pi}{4})} \text{ for } -k\tau \gg 1, \tag{4.19}$$

which should match the solution of the equation of motion in the same limit:

$$\delta\chi_{\boldsymbol{k}} = \frac{e^{-ik\tau}}{\sqrt{2k}} \ . \tag{4.20}$$

This is achieved with

$$c_1(k) = \frac{\sqrt{\pi}}{2}e^{i(\nu+\frac{1}{2})\frac{\pi}{2}} \ , \ c_2(k) = 0 \ . \tag{4.21}$$

Recasting the result to the $\delta\phi$ field, one obtain

$$|\delta\phi_{\boldsymbol{k}}|^2 = \frac{H^2}{2k^3}\left(\frac{k}{aH}\right)^{3-2\nu} \ . \tag{4.22}$$

Expanding the exponent in terms of slow roll parameters, one finds to the first order

$$3 - 2\nu \simeq 4\epsilon - \eta \ , \tag{4.23}$$

leading to the prediction that slow roll inflation produces a nearly scale invariant spectrum. This can be seen from eq. 3.37 on page 27.

This is by no mean surprising, but merely a statement of what inflation was designed to do. The nearly scale invariant spectrum indicates that the fluctuation, that form the seed for structure formation is isotropic and homogeneous, i.e., obeys the cosmological principle.

4.3 First Order Perturbations

One can now rewrite the line element in the Arnowitt-Deser-Misner (ADM) form [40]:

$$ds^2 = -N^2dt^2 + h_{ij}(dx^i + N^idt)(dx^j + N^jdt) \tag{4.24}$$

where N is the lapse function and N^i is the shift vector, which expresses the difference between to two constant time slices.

Ignoring tensor contributions, we can write the spatial metric as

$$h_{ij} = a^2 e^{2\zeta} \eta_{ij} \ , \tag{4.25}$$

which gives an intrinsic curvature scalar of

$$\mathcal{R}_3 = -4\partial^2 \zeta - 2(\partial\zeta)^2 \ . \tag{4.26}$$

In the ADM formalism the Einstein-Hilbert action (eq. 4.1 on page 31) takes the form

$$\begin{aligned} S = \frac{1}{2} \int \mathrm{d}t \mathrm{d}^3 x \sqrt{h} \Big[& N\mathcal{R}_3 - 2NV(\phi) + N^{-1}(E_{ij}E^{ij} - E^2) + N^{-1}(\dot{\phi} - N^i \nabla_i \phi)^2 \\ & - N h^{ij} \nabla_i \phi \nabla_j \phi \Big] \ . \end{aligned} \tag{4.27}$$

The tensor E_{ij} is defined as a linear combination of the time derivative of h_{ij} and the covariant derivative of the shift vector

$$E_{ij} = \frac{1}{2}(\dot{h}_{ij} - \nabla_i N_j - \nabla_j N_i) \ , \tag{4.28}$$

and $E \equiv E^i_i$ is the trace of the tensor E_{ij}.

One is thus left with four scalar degrees of freedom $(N, N^i, \delta\phi, \zeta)$, two of which can be expressed as a function of the others, as it was shown earlier (eq. 3.3 on page 22) that the system in question only has two true scalar degrees of freedom. It is thereafter possible to reduce the number of degrees of freedom to a single by choosing a gauge.

By varying the action with respect to N and N^i, one can write down the equations of motion for the two parameters as

$$\nabla_i \left[N^{-1}(E^i_j - \delta^i_j E) \right] = N^{-1}(\dot{\phi} - N^i \nabla_i \phi) \nabla_j \phi \tag{4.29}$$

for N^i, and

$$\mathcal{R}_3 - 2V - N^{-2}(E_{ij}E^{ij} - E^2) - N^{-2}(\dot{\phi} - N^i \partial_i \phi)^2 - h^{ij} \partial_i \phi \partial_j \phi = 0 \tag{4.30}$$

for N.

Concerning ourselves with only the first order perturbations, we expand N and N^i as

$$N = 1 + \alpha \ , \ N^i = \partial^i \chi + \beta^i \ , \ \partial_i \beta^i = 0 \ , \tag{4.31}$$

and choose a gauge.

UNIFORM DENSITY GAUGE

For the gauge choice of zero field fluctuations, one finds a scenario where all the perturbations are in the metric tensor. We will for this discussion ignore tensor perturbations, leaving as diagonal metric of the form

$$ds^2 = -dt^2 + a(t)^2 e^{2\zeta} \eta_{ij} dx^i dx^j \ . \tag{4.32}$$

In this gauge the solution of eq. 4.29 and eq. 4.30 [22]:

$$\alpha = H^{-1}\dot{\zeta} \ , \ \chi = -\frac{\zeta}{H} + \xi \ , \ \partial^2 \xi = \epsilon \dot{\zeta} \ , \ \beta^i = 0 \ , \tag{4.33}$$

where ϵ is the first slow roll parameter. Inserting this result into the action, one can write down the third order action for the comoving curvature gauge [22]:

$$S = \int \mathrm{d}t\mathrm{d}^3x a^3 \Bigg\{ - H^{-1}\dot{\zeta}(\partial\zeta)^2 - 2H^{-1}\zeta\dot{\zeta}\partial^2\zeta - \zeta(\partial\zeta)^2 - \zeta^2\partial^2\zeta + 3\epsilon\zeta\dot{\zeta}^2 - \epsilon H^{-1}\dot{\zeta}^3 \\ - \frac{\dot{\zeta}}{2H}(\partial_i\partial_j\chi\partial^i\partial^j\chi - \partial^2\chi\partial^2\chi) - 2\partial_j\chi\partial^i\zeta\partial^2\chi \\ + \frac{3}{2}\zeta(\partial_i\partial_j\chi\partial^i\partial^j\chi - \partial^2\chi\partial^2\chi \Bigg\} . \tag{4.34}$$

Though it would at first appear, that this action, an action of an observable quantity, is not suppressed by the slow roll parameters, meaning that the three-point function of ζ could easily be large, i.e., an easily detectable non-Gaussian feature, it can be shown through partial integrations, that the action is indeed suppressed by slow roll parameters [22]:

$$S = \int \mathrm{d}t\mathrm{d}^3x a^3 \left\{ \epsilon^2[\dot{\zeta}^2\zeta + \zeta(\partial\zeta)^2] - 2\epsilon\dot{\zeta}\partial_i\xi\partial^i\zeta - \frac{\epsilon^3}{2}\dot{\zeta}^2\zeta + 2\epsilon\dot{\eta}\dot{\zeta}\zeta^2 + \frac{\epsilon}{2}\zeta\partial_i\partial_j\xi\partial^i\partial^j\xi \right\} \tag{4.35}$$

As ξ is proportional to the first slow roll parameter, it can be seen that the action is suppressed to the second order in the slow roll parameters.

Isocurvature Gauge

Choosing the gauge where the spatial curvature is zero, we can write the line element as a FRW model:

$$ds^2 = -dt^2 + a(t)^2\eta_{ij}dx^i dx^j \tag{4.36}$$

where the tensor modes have been set to zero. In this gauge the field is expanded as a background field and a scalar perturbation

$$\phi(\boldsymbol{x}, t) = \phi_c(t) + \delta\phi(\boldsymbol{x}, t) \ . \tag{4.37}$$

Under these choices one can solve eq. 4.29 and eq. 4.30 for α, β and χ to get [22]

$$\alpha = \frac{\dot{\phi}_c}{2H}\delta\phi \ , \ \chi = -\partial^{-2}\left[\frac{\dot{\phi}_c^2}{2H^2}\frac{d}{dt}\left(\frac{H}{\dot{\phi}}\delta\phi\right)\right] \ , \ \beta_i = 0 \ , \tag{4.38}$$

giving an action of the form [22]

$$S_{\delta\phi^3} = \int \mathrm{d}^3\boldsymbol{x}\mathrm{d}t a^3 \Bigg\{ - \frac{\dot{\phi}_c}{4H}\delta\phi\dot{\delta\phi}^2 - \frac{\dot{\phi}_c}{4H}\delta\phi(\partial\delta\phi)^2 - \dot{\delta\phi}\partial_i\chi\partial^i\delta\phi \\ + \frac{3\dot{\phi}_c^3}{8H}\delta\phi^3 - \frac{5\dot{\phi}_c^5}{16H^3}\delta\phi^3 - \frac{\dot{\phi}_c V''}{4H}\delta\phi^3 - \frac{V'''}{6}\delta\phi^3 + \frac{\dot{\phi}_c^3}{4H^2}\delta\phi^2\dot{\delta\phi} \\ + \frac{\dot{\phi}_c^2}{4H}\delta\phi^2\partial^2\chi + \frac{\dot{\phi}_c}{4H}(-\delta\phi\partial_i\partial_j\chi\partial^i\partial^j\chi + \delta\phi\partial^2\chi\partial^2\chi) \Bigg\} . \tag{4.39}$$

4.4 NON-GAUSSIAN SIGNALS

At first glance it would appear, that the three point correlation function should nearly vanish, as the third order Hamiltonian is heavily suppressed by slow roll parameters. It is however still possible to produce a large non-Gaussian signal by breaking at least one of the following conditions [41]

1. **Single Field** models are by far the simplest implementation of an inflationary scenario. Holding few degrees of freedom single field models leave little possibility for generating large non-Gaussian features through this channel. Adding extra fields to the model can lead to isocurvature perturbations [42, 43, 44]. This mechanism leads to the possibility of generating perturbations without necessarily having the generating field limited by the slow roll criteria, as the generating field can be made to be a light scalar field, which is not the inflaton [45]. One of the more studied multi field models is the curvaton scenario [46, 47, 48, 49].

2. **Slow Roll** requires, in the strictest sense, that all the slow roll parameters (see eq. 2.14 on page 16 and 2.15 on page 17) are close to zero. As can be seen from the action of the comoving curvature perturbations (eq. 4.35 on the preceding page), the slow roll parameters and their derivatives act as coupling constants in the action. A strict requirement of slow roll will therefore heavily constrain the produced non-Gaussian signal. One can however soften the slow roll requirement to only encompass ϵ, which is the criteria for ongoing inflation. One can in this scenario increase the value of η over a short time period, which will produce a large contribution from selected terms in the action. Especially term $\epsilon\dot{\eta}$ will gain from the rapid change of η. This is achieved in the types of model that includes kinks, bumps and oscillations in the potential or its derivatives [50, 51, 52, 53].

3. **Canonical Kinetic Term** has been the predominant description in quantum field theory since the its inception. With the introduction of string theory and branes the choice of kinetic term has become increasingly murky. A choice of a more complicated kinetic term (see amongst other [35, 36]) leads to a sound speed less than the speed of light, as opposed to the case of a canonical kinetic term where the two speeds are identical. This non-canonical kinetic term will also give contributions to the interaction Hamiltonian, which contribute to the generation of non-Gaussianities.

4. **Initial Vacuum State** is normally assumed to be the Bunch-Davies vacuum [54], which is to say that the quantum field was in the preferred adiabatic vacuum state when the perturbations where generated. This statement is equivalent to saying that the Universe has no memory of any events prior to the generation of perturbations. This can be seen as the Bunch-Davies vacuum assumes that the states are invariant under the de Sitter group, i.e. invariant under the coordinate transformation $t \rightarrow t + \delta t$,$x \rightarrow e^{-H\delta t}x$. As the Universe is assumed to be homogeneous and isotropic this translates into a inability to distinguish between two times, thus removing the possibility of any memory in the system. Choosing a different vacuum state translate to introducing a surface term in the governing action and thus and added effect to the non-Gaussian signal [55, 56, 57].

As mentioned in [41] a violation of one of the four conditions will result in unique signatures for specific triangle shapes (see chapter 3 for the definitions of the triangle shapes). Where as a multi-field model gives a strong signal in a squeezed triangle, a model with a non-conformal kinetic term give a strong signal with a equilateral triangle. Starting inflation from an excited state, i.e. different initial conditions than the Bunch-Davies vacuum will be evident in a flattened/folded triangle. Lastly breaking slow roll will show through more complex triangle configurations. Breaking more than one of the conditions will give rise to a linear combination of the shapes (see e.g. [42, 47, 51, 58, 59, 60, 61]). In the following we will focus a type of model that generates a non-Gaussian signal by breaking slow roll.

5 Axion Monodromy Model

As mentioned in the previous chapter one can envision many ways of realising an inflationary model. The motivation and underlying theory may differ vastly, as the models regarded can be anything from a simple toy model to a realisation of a high energy theory. In this chapter we will concern ourselves with the axion monodromy model [52, 62], which is an effective field theory based on a particular type of string compactification. This chapter is based on [63].

5.1 Axion Monodromy Potential

Regarding a string theoretical realization with a D5-brane or a NS5-brane on a two-cycle, we have a potential of the general form [62]

$$V(\phi_a) \propto \sqrt{l^4 + k^2\phi_a^2} \ , \tag{5.1}$$

where l is related to the size of the cycle. In the large field limit, which is valid during inflation, this yield a linear potential for the axion ϕ_a and an axion action of the the form

$$S_{\phi_a} = \int \mathrm{d}^4x\sqrt{g}\left(\frac{1}{2}(\partial\phi_a)^2 - \mu_a^3\phi_a\right) + \text{corrections} \ . \tag{5.2}$$

One can show that in order to obtain 60 e-folds of inflation with the right level of curvature perturbations, one should have [62]

$$\phi_a \sim 11M_{\text{pl}} \tag{5.3}$$
$$\mu_a \sim 6\cdot 10^{-4}M_{\text{pl}} \tag{5.4}$$

as initial conditions. Though the brane-induced inflaton potential described above is the leading effect for breaking shift symmetries in the class of models considered here, there are other effect present as well. Among the more important is production of instantons, which, in this case, give rise to periodic corrections to the potential. One can therefore write down the effective potential containing these two contributions as

$$V_{eff} = \mu_a^3\phi_a(1 + \alpha_1\cos(\phi/2\pi f_a)) + \alpha_2 M_s^4\cos(\phi/2\pi f_a) \ , \tag{5.5}$$

where M_s is the string scale and α_i are dimensionless parameters which are expected to be much smaller than one, $\alpha_i \ll 1$, depending on the details of the string theory compactifications.

We will study the two case $\alpha_1 \ll \alpha_2$ and $\alpha_1 \gg \alpha_2$, leading to the two limiting potentials

$$V_{eff}^{(1)} = \mu_a^3 \phi_a (1 + \alpha_1 \cos(\phi/2\pi f_a)) \qquad (5.5\ ,\ \alpha_1 \gg \alpha_2)$$

where we will assume $\alpha_1 \sim 0.01$, such that effect on the power spectrum is at the percent level and not yet excluded by data. The other case is

$$V_{eff}^{(2)} = \mu_a^3 \phi_a + \Lambda^4 \cos(\phi/2\pi f_a) \qquad (5.5\ ,\ \alpha_1 \ll \alpha_2)$$

where we will assume $\Lambda^4 = \alpha_2 M_s^4$ is such that the effect on the power spectrum is at the percent level.

The scalar power spectrum for the potential in the second model was computed analytically in [64]. We will return to this point later in eq. 5.19 on page 42.

5.2 Isosceles Limit Estimates of the Bispectrum

As discussed in chapter 3, one can write $f_{\rm NL}$ as a combination of the three point function of $\zeta_{\boldsymbol{k}}$ (the Fourier transform of ζ) and the power spectra of the curvature perturbations:

$$f_{\rm NL} = -\frac{10}{3} \frac{(k_1 k_2 k_3)^3}{\mathcal{P}(k_1)\mathcal{P}(k_2)k_3^3 + 2\,\text{perms.}} \frac{\langle \zeta_{\boldsymbol{k}_1} \zeta_{\boldsymbol{k}_2} \zeta_{\boldsymbol{k}_3} \rangle}{(2\pi)^7 \delta^{(3)}(\boldsymbol{k}_1 + \boldsymbol{k}_2 + \boldsymbol{k}_3)}\ , \tag{5.6}$$

where k_i is the magnitude of the momentum $\boldsymbol{k}_i$. For the case of our models the fluctuations in the power spectrum is of the order one per cent. However if one should concern oneself with models with larger fluctuations in the power spectrum, one may benefit from using a similar definition, given by

$$\tilde{f}_{\rm NL} = -\frac{10}{3} \frac{(k_1 k_2 k_3)^3}{\tilde{\mathcal{P}}^2(k_1^3 + k_2^3 + k_3^3)} \frac{\langle \zeta_{\boldsymbol{k}_1} \zeta_{\boldsymbol{k}_2} \zeta_{\boldsymbol{k}_3} \rangle}{(2\pi)^7 \delta^{(3)}(\boldsymbol{k}_1 + \boldsymbol{k}_2 + \boldsymbol{k}_3)}\ , \tag{5.7}$$

where $\tilde{\mathcal{P}}$ is approximately the amplitude of the power spectrum at the k's considered. It should be noted that this definition reduces to the $\frac{\mathcal{G}}{k_1 k_2 k_3}$ presented in [50] in the equilateral limit, but differs in the squeezed limit, where $\frac{\mathcal{G}}{k_1 k_2 k_3}$ grows as $\frac{k_1}{k_3}$ for triangles of the type $k_1 = k_2 \gg k_3$.

We proceed to find an estimate for the case $k_1 = k_2 \geq k_3$. Though such an estimate does not exist in general, we can obtain one by interpolating between the equilateral limit ($k_1 = k_2 = k_3$) and the squeezed limit ($k_1 = k_2 \gg k_3$).

Equilateral Limit

The model is essentially a linear slow-roll potential with a small oscillating perturbation. We can therefore follow the approach of Chen, Easther and Lim [50] and calculate the first order effect of the small oscillating term as a small correction. In this way one has $\epsilon = \epsilon_0 + \epsilon_{osc}$, $\eta = \eta_0 + \eta_{osc}$. As the background solution (subscript 0), one can start from

$$3H\dot{\phi} + \mu^3 = 0 \tag{5.8}$$

to obtain

$$\phi_0 = \frac{1}{2^{2/3}} (-\sqrt{3}\mu^{3/2} t + 2\phi_i^{3/2})^{2/3} \tag{5.9}$$

and

$$\epsilon_0 = \frac{1}{2\phi_0^2} \ , \qquad \eta_0 = \frac{2}{\phi_0^2} \ . \tag{5.10}$$

As argued in [50] one can estimate $f_{\rm NL}$ in the equilateral limit by

$$f_{\rm NL}^{(eq)} \sim -f_A^{(eq)} \sin\left(\frac{\ln K}{\phi f} + \text{phase}\right) \tag{5.11}$$

in the equilateral limit. Here $K = k_1 + k_2 + k_3$. The factor 2 missing, compared to [50], is due to the underlying linear potential here, as opposed to a quadratic in [50]. The resonance amplitude can be estimated as

$$f_A^{(eq)} \sim \frac{10}{9} \frac{\dot\eta_A}{H\sqrt{f\phi}} \ , \tag{5.12}$$

where $\dot\eta_A$ is the amplitude of $\dot\eta_{osc}$, which can be found from

$$\epsilon_{osc} = \frac{\dot H_{osc}}{\dot H_0}\epsilon_0 = \begin{cases} -3\frac{\Lambda^4}{\mu^3}\frac{1}{\phi_0}\cos\left(\frac{\phi_0}{f}\right) & \Lambda^4 \text{ model} \\ -3\alpha\cos\left(\frac{\phi_0}{f}\right) & \alpha \text{ model} \end{cases} \tag{5.13}$$

$$\eta_{osc} = \frac{\dot\epsilon_{osc}}{\dot\epsilon_0}\eta_0 = \begin{cases} -6\frac{\Lambda^4}{\mu^3 f}\sin\left(\frac{\phi_0}{f}\right) & \Lambda^4 \text{ model} \\ -6\frac{\alpha\phi_0}{f}\sin\left(\frac{\phi_0}{f}\right) & \alpha \text{ model} \end{cases} \ . \tag{5.14}$$

We therefore find the resonance amplitude to be

$$f_A^{(eq)} \sim \begin{cases} \frac{10}{9}\frac{\Lambda^4}{\phi\mu^3}\frac{1}{f^{5/2}\phi^{1/2}} & \Lambda^4 \text{ model} \\ \frac{10}{9}\alpha\frac{1}{f^{5/2}\phi^{1/2}} & \alpha \text{ model} \end{cases} \ . \tag{5.15}$$

SQUEEZED LIMIT

Let us now consider the different limit $k_1 = k_2 \gg k_3$ (for simplicity we define $k_1 = k_2 = k$ and $k_3 = m$). In this limit the long wavelength mode of $\zeta_{\boldsymbol{k}_3}$, will act as a constant rescaling of the background of the two shorter wavelength modes. As shown by Maldacena [22], one can thus calculate the three point correlation function in this limit by calculating the correlation of the long wavelength mode with the variation of the two-point function of the short wavelength modes on the background of the long wavelength mode [22, 65]

$$\lim_{k_3\to 0}\langle\zeta_{\boldsymbol{k}_1}\zeta_{\boldsymbol{k}_2}\zeta_{\boldsymbol{k}_3}\rangle = \langle\zeta_{\boldsymbol{k}_3}\langle\zeta_{\boldsymbol{k}_1}\zeta_{\boldsymbol{k}_2}\rangle_B\rangle \ . \tag{5.16}$$

Then by a Taylor expansion of $\langle\zeta_{\boldsymbol{k}_1}\zeta_{\boldsymbol{k}_2}\rangle_B$ on the unperturbed background, and using $\partial/\partial\zeta \to k\partial/\partial k$ (since the effect of ζ is to take $k \to k - k\zeta$), one finds [22, 65]

$$\begin{aligned}\lim_{k_3\to 0}\langle\zeta_{\boldsymbol{k}_1}\zeta_{\boldsymbol{k}_2}\zeta_{\boldsymbol{k}_3}\rangle &= -(2\pi)^3\delta^3(\boldsymbol{k}_1+\boldsymbol{k}_2+\boldsymbol{k}_3)P_\zeta(m)\frac{2\pi^2}{k^3}\frac{d}{d\ln(k)}\mathcal{P}_\zeta(k) \\ &= -(n_s-1)(2\pi)^3\delta^3(\boldsymbol{k}_1+\boldsymbol{k}_2+\boldsymbol{k}_3)P_\zeta(m)P_\zeta(k)\end{aligned} \tag{5.17}$$

with

$$P(k) \equiv \frac{2\pi^2}{k^3}\mathcal{P}_\zeta(k) \ . \tag{5.18}$$

This can be compared to eq. 3.42 on page 29, and one can read off $f_{\rm NL}^{(sq)} = (5/12)(n_s - 1)$. Here n_s is the spectral index.

As it was shown in [64] the scalar power spectrum for the potential in the second model can be written in the form

$$\mathcal{P}_\zeta(k) = \mathcal{P}_\zeta(k_*)\left(\frac{k}{k_*}\right)^{\tilde{n}_s - 1}\left[1 + \delta n_s \cos\left(\frac{\phi_k}{f}\right)\right] \ . \tag{5.19}$$

with the short hand notation of [64]:

$$\delta n_s = \begin{cases} \frac{12\Lambda^4}{f\mu^3}\frac{\sqrt{\frac{\pi}{8}\coth\left(\frac{\pi}{2f\phi_*}\right)f\phi_*}}{\sqrt{1+(3f\phi_*)^2}} & \Lambda^4 \text{ model} \\ \frac{12\alpha\phi_*}{f}\frac{\sqrt{\frac{\pi}{8}\coth\left(\frac{\pi}{2f\phi_*}\right)f\phi_*}}{\sqrt{1+(3f\phi_*)^2}} & \alpha \text{ model} \end{cases} \ . \tag{5.20}$$

The ϕ_k is the field value, when the momentum k crosses the horizon.

$$\phi_k = \sqrt{\phi_*^2 - 2\ln\left(\frac{k}{k_*}\right)} \simeq \phi_* - \frac{\ln\left(\frac{k}{k_*}\right)}{\phi_*} \ . \tag{5.21}$$

The starred quantities are merely an arbitrarily chosen fix point, where k_* is the momentum that crosses the horizon at $\phi = \phi_*$. Though complicated, the expression for δn_s reduces to

$$\delta n_s \approx \begin{cases} 6\frac{\sqrt{\frac{\pi}{2}}\Lambda^4\phi_*^{1/2}}{f^{1/2}\mu^3} & \Lambda^4 \text{ model} \\ 6\frac{\sqrt{\frac{\pi}{2}}\alpha\phi_*^{3/2}}{f^{1/2}} & \alpha \text{ model} \end{cases} \tag{5.22}$$

for $f \ll 1$.

As $\delta n_s \ll 1$ we find

$$n_s - 1 = \tilde{n}_s - 1 + \frac{\delta n_s}{f\phi_*}\sin\left(\frac{\phi_k}{f}\right) \tag{5.23}$$

to the first order in δn_s. With this one can find an expression for $f_{\rm NL}$ in the squeezed limit:

$$f_{\rm NL}^{(sq)} \sim f_A^{(sq)}\sin\left(\frac{\phi_k}{f}\right) \ , \ f_A^{(sq)} \equiv \frac{5}{12}\frac{\delta n_s}{f\phi_*} \tag{5.24}$$

to the first order in δn_s for $k_1 = k_2 \gg k_3$.

This result can now be combined with eq. 5.11 to form a general estimate for isosceles momentum triangles ($k_1 = k_2 \geq k_3$):

$$f_{\rm NL} \sim \frac{5}{12}(\tilde{n}_s - 1) + \left[f_A^{(sq)} + (f_A^{(eq)} - f_A^{(sq)})\frac{m}{k}\right]\sin\left(\frac{\ln K}{\phi f} + \text{phase}\right) \ , \tag{5.25}$$

where for completeness we have included the slow roll contribution from the underlying linear potential, as the first term.

5.3 SEMICLASSICAL ESTIMATES OF THE TRISPECTRUM

If the bispectrum can become large in a given model, one might be interested in the size of higher order correlation functions as well. While it is beyond the scope of this paper to study the trispectrum in details, we can still make some generic semiclassical estimates in certain limits. Most obviously we can study the trispectrum in the squeezed limit [27, 66], but it is also possible to estimate a particular contribution to the non-Gassianity in the counter-collinear limit [67].

SQUEEZED LIMIT

One can imagine to make a definition of τ_{NL} analogous to the definition of $f_{\rm NL}$ in eq. 5.6, relating it to the four-point function as

$$\tau_{NL} \sim \frac{1}{\tilde{\mathcal{P}}^3(2\pi)^9}\frac{(k_1k_2k_3k_4)^3}{\sum_i k_i^3}\frac{\langle\zeta(\boldsymbol{k}_1)\zeta(\boldsymbol{k}_2)\zeta(\boldsymbol{k}_3)\zeta(\boldsymbol{k}_4)\rangle}{\delta^{(3)}\left(\sum_i \boldsymbol{k}_j\right)} \tag{5.26}$$

By repeating the above calculation for $k \equiv k_1 = k_2 = k_3 \gg k_4$ under the same assumptions, one can get an estimate of the behaviour of the trispectrum in the squeezed limit

$$\lim_{k_4\to 0}\langle\zeta_{\boldsymbol{k}_1}\zeta_{\boldsymbol{k}_2}\zeta_{\boldsymbol{k}_3}\zeta_{\boldsymbol{k}_4}\rangle = -(2\pi)^3\delta^3(\boldsymbol{k}_1+\boldsymbol{k}_2+\boldsymbol{k}_3+\boldsymbol{k}_4)P_\zeta(k_4)\frac{1}{k^6}\frac{d}{d\ln(k)}\left(k^6 B_\zeta(k)\right)\ . \tag{5.27}$$

In order to evaluate this expression approximately, we can insert the estimate for the equilateral bispectrum obtained in eq. 5.11 to find

$$\tau_{NL} \sim \frac{3}{20}f_{\rm NL}^{(eq)}\frac{\mathcal{P}(k)^2\mathcal{P}(k_4)}{\tilde{\mathcal{P}}^3}\left[2(n_s-1)+\frac{\tan\left(\frac{\ln(3k)}{f\phi_*}+\Phi\right)}{f\phi_*}\right]\ . \tag{5.28}$$

However, we can obtain an even simpler estimate of the size of the trispectrum in specific configurations, by considering the double squeezed limit, where $k \equiv k_1 = k_2 >> k_3 >> k_4$. Iteratively, we then obtain

$$\lim_{k_3,k_4\to 0}\langle\zeta_{\boldsymbol{k}_1}\zeta_{\boldsymbol{k}_2}\zeta_{\boldsymbol{k}_3}\zeta_{\boldsymbol{k}_4}\rangle \sim (n_s-1)^2(2\pi)^3\delta^3(\boldsymbol{k}_1+\boldsymbol{k}_2+\boldsymbol{k}_3+\boldsymbol{k}_4)P_\zeta(k_3)P_\zeta(k_4)P_\zeta(k)\ . \tag{5.29}$$

This implies that in this limit $\tau_{NL} \sim \left(f_{\rm NL}^{(sq)}\right)^2$.

COUNTER-COLLINEAR LIMIT

Let us consider the contribution to the four-point function from the exchange of a scalar mode between two pairs of external scalar modes. In the counter collinear limit where the momentum of the exchanged mode goes to zero $\boldsymbol{k}_1 + \boldsymbol{k}_2 \to 0$, the contribution to the four-point function from the exchange process can be expressed as the correlation of a pair of two-point functions $\langle\zeta_{\boldsymbol{k}_1}\zeta_{\boldsymbol{k}_2}\rangle$, $\langle\zeta_{\boldsymbol{k}_3}\zeta_{\boldsymbol{k}_4}\rangle$ due to the presence of the long wavelength scalar mode [67]

$$\lim_{\boldsymbol{k}_1+\boldsymbol{k}_2\to 0}\langle\zeta_{\boldsymbol{k}_1}\zeta_{\boldsymbol{k}_2}\zeta_{\boldsymbol{k}_3}\zeta_{\boldsymbol{k}_4}\rangle = \langle\langle\zeta_{\boldsymbol{k}_1}\zeta_{\boldsymbol{k}_2}\rangle_B\langle\zeta_{\boldsymbol{k}_3}\zeta_{\boldsymbol{k}_4}\rangle_B\rangle$$
$$= (n_s-1)^2(2\pi)^3\delta^3(\boldsymbol{k}_1+\boldsymbol{k}_2+\boldsymbol{k}_3+\boldsymbol{k}_4)P_\zeta(k_{12})P_\zeta(k_1)P_\zeta(k_3)\ , \tag{5.30}$$

with $k_{12}\equiv|\boldsymbol{k}_1+\boldsymbol{k}_2|$.

Again from this contribution clearly $\tau_{NL}\sim\left(f_{\mathrm{NL}}^{(sq)}\right)^2$. Thus if $f_{\mathrm{NL}}^{(sq)}\sim 50$, the find that there are large contributions to the trispectrum of order $\tau_{NL}\sim 2500$, which are also in an interesting range for Planck, that should be sensitive to a $\tau_{NL}\gtrsim 560$ [68].

5.4 NUMERICAL COMPUTATIONS

For the actual matter of numerical calculations, the ζ variable is actually less than optimal. Using it blatantly would produce spurious effects, if one does not take surface terms of the action (eq. 4.35 on page 35) into account. Instead one tends to use a quantity related closer to the field fluctuation in the isocurvature gauge than the metric perturbation in the uniform density curvature gauge. This quantity, ζ_n, is, however, still identical to the metric perturbation to the lowest order.

To derive ζ_n one does a time translation to change from the isocurvature gauge to the uniform density gauge:

$$\phi(t+T)\simeq\phi(t)+\dot\phi T=\phi_c\Rightarrow T=-\frac{\delta\phi}{\dot\phi}\ . \tag{5.31}$$

Applying the same transformation to the spatial metric, one finds to the first order:

$$\zeta=-H\frac{\delta\phi}{\dot\phi}\equiv\zeta_n\ . \tag{5.32}$$

One can now proceed to calculate the interaction Hamiltonian

$$H_I(\tau)=-\int\mathrm{d}^3x\Bigg\{a\epsilon^2\zeta_n\zeta_n'^2+a\epsilon^2\zeta_n\partial_i\zeta_n\partial_i\zeta_n-2\epsilon\zeta_n'\partial_i\zeta_n\partial_i\chi+a\frac{\epsilon\eta'}{2}\zeta_n^2\zeta_n'$$
$$+\frac{\epsilon}{2a}\partial_i\zeta_n\partial_i\chi\partial_j\partial_j\chi+\frac{\epsilon}{4a}\partial_i\partial_i\zeta_n\partial_j\chi\partial_j\chi\Bigg\}\ , \tag{5.33}$$

where we have switched to conformal time and written the partial derivatives out as covariant vectors. A sum over repeated indices is still implied. Under these transformations the perturbation parameter for the shift vector becomes $\chi=a\epsilon\partial^{-2}\zeta_n$, where $\partial^{-2}\partial_i\partial_i=\partial_i\partial_i\partial^{-2}=\mathbf{1}$.

Calculating the three-point function from a well-defined vacuum state at τ_0

$$\langle\zeta_n(\boldsymbol{k}_1)\zeta_n(\boldsymbol{k}_2)\zeta_n(\boldsymbol{k}_3)\rangle=-i\int_{\tau_0}^{\tau}\mathrm{d}\tilde\tau a\left\langle[\zeta_n^I(\boldsymbol{k}_1)\zeta_n^I(\boldsymbol{k}_2)\zeta_n^I(\boldsymbol{k}_3),H_I(\tilde\tau)]\right\rangle\ , \tag{5.34}$$

one expands ζ_n in a linear combination of raising and lowering operators:

$$\zeta_n^I(\boldsymbol{k})=u_k a_{\boldsymbol{k}}+u_{-k}^* a_{-\boldsymbol{k}}^\dagger\ . \tag{5.35}$$

The operators are normalised such that

$$[a_{\boldsymbol{k}}, a_{\boldsymbol{k}'}] = [a^\dagger_{\boldsymbol{k}}, a^\dagger_{\boldsymbol{k}'}] = 0 \ , \ [a_{\boldsymbol{k}}, a^\dagger_{\boldsymbol{k}'}] = (2\pi)^3 \delta^{(3)}(\boldsymbol{k} - \boldsymbol{k}') \ , \tag{5.36}$$

which yield six integrals, which must be calculated to find the three-point function for ζ_n:

$$\begin{aligned} I_1 = \quad & 2i(2\pi)^3 \left(\prod_{i=1}^{3} u_{k_i}(\tau_e) \right) \delta^{(3)}(\boldsymbol{k_1} + \boldsymbol{k_2} + \boldsymbol{k_3}) \\ & \times \int_{\tau_0}^{\tau_e} \mathrm{d}\tau a^2 \epsilon^2 (u^*_{k_1}(\tau) u^{*\,\prime}_{k_2}(\tau) u^{*\,\prime}_{k_3}(\tau) + 2 \text{ perm.}) + \text{c.c.} \end{aligned} \tag{5.37}$$

$$\begin{aligned} I_2 = - \, & 2i(2\pi)^3 \left(\prod_{i=1}^{3} u_{k_i}(\tau_e) \right) \delta^{(3)}(\boldsymbol{k_1} + \boldsymbol{k_2} + \boldsymbol{k_3}) \\ & \times \int_{\tau_0}^{\tau_e} \mathrm{d}\tau a^2 \epsilon^2 \prod_{i=1}^{3} u^*_{k_i} (\boldsymbol{k}_1 \cdot \boldsymbol{k}_2 + 2 \text{ perm.}) + \text{c.c.} \end{aligned} \tag{5.38}$$

$$\begin{aligned} I_3 = - \, & 2i(2\pi)^3 \left(\prod_{i=1}^{3} u_{k_i}(\tau_e) \right) \delta^{(3)}(\boldsymbol{k_1} + \boldsymbol{k_2} + \boldsymbol{k_3}) \\ & \times \int_{\tau_0}^{\tau_e} \mathrm{d}\tau a^2 \epsilon^2 \left(u^*_{k_1}(\tau) u^{*\,\prime}_{k_2}(\tau) u^{*\,\prime}_{k_3}(\tau) \frac{\boldsymbol{k}_1 \cdot \boldsymbol{k}_2}{k_2^2} + 5 \text{ perm.} \right) + \text{c.c.} \end{aligned} \tag{5.39}$$

$$\begin{aligned} I_4 = \quad & i(2\pi)^3 \left(\prod_{i=1}^{3} u_{k_i}(\tau_e) \right) \delta^{(3)}(\boldsymbol{k_1} + \boldsymbol{k_2} + \boldsymbol{k_3}) \\ & \times \int_{\tau_0}^{\tau_e} \mathrm{d}\tau a^2 \epsilon \eta' (u^*_{k_1}(\tau) u^*_{k_2}(\tau) u^{*\,\prime}_{k_3}(\tau) + 2 \text{ perm.}) + \text{c.c.} \end{aligned} \tag{5.40}$$

$$\begin{aligned} I_5 = \quad & \frac{i}{2}(2\pi)^3 \left(\prod_{i=1}^{3} u_{k_i}(\tau_e) \right) \delta^{(3)}(\boldsymbol{k_1} + \boldsymbol{k_2} + \boldsymbol{k_3}) \\ & \times \int_{\tau_0}^{\tau_e} \mathrm{d}\tau a^2 \epsilon^3 \left(u^*_{k_1}(\tau) u^{*\,\prime}_{k_2}(\tau) u^{*\,\prime}_{k_3}(\tau) \frac{\boldsymbol{k}_1 \cdot \boldsymbol{k}_2}{k_2^2} + 5 \text{ perm.} \right) + \text{c.c.} \end{aligned} \tag{5.41}$$

$$\begin{aligned} I_6 = \quad & \frac{i}{2}(2\pi)^3 \left(\prod_{i=1}^{3} u_{k_i}(\tau_e) \right) \delta^{(3)}(\boldsymbol{k_1} + \boldsymbol{k_2} + \boldsymbol{k_3}) \\ & \times \int_{\tau_0}^{\tau_e} \mathrm{d}\tau a^2 \epsilon^3 \left(u^*_{k_1}(\tau) u^{*\,\prime}_{k_2}(\tau) u^{*\,\prime}_{k_3}(\tau) k_1^2 \frac{\boldsymbol{k}_2 \cdot \boldsymbol{k}_3}{k_2^2 k_3^2} + 2 \text{ perm.} \right) + \text{c.c.} \end{aligned} \tag{5.42}$$

Carrying out the actual integration, one needs to take great care as the mode functions u_k tend to oscillate heavily inside the horizon ($-k\tau \gg 1$). To resolve this we follow the approach of [50].

Defining

$$v_k = z u_k \ , \ z = a\sqrt{2\epsilon} \ , \tag{5.43}$$

which has the equation of motion given by

$$v_k'' + k^2 v_k - \frac{z''}{z} v_k = 0 \ , \tag{5.44}$$

one can split the integration range into two subsections $[\tau_0, \tau_s]$ and $[\tau_s, \tau_e]$, where τ_s is chosen to be a time, when all three modes are well inside the horizon. As $\tau_0 \to -\infty$ the

integral over the second interval remains fairly easy to calculate, while the integral over the first interval becomes increasingly difficult. To remedy this one approximate v_k by the WKB approximation:

$$v_k \simeq \frac{1}{\sqrt{2\alpha(k)}} \exp\left[i\int \alpha(k)\mathrm{d}\tau\right] + \text{c.c.}\ ,\ \alpha(k)^2 = k^2 + \frac{z''}{z}\ . \tag{5.45}$$

As τ_s are chosen such that the modes are deep inside the horizon, one can approximate $\alpha \sim k$. This reduces the first part of the integrals to the form

$$I_s = \int_{-\infty}^{\tau_s} \mathrm{d}\tau \frac{\theta(\tau)}{\sqrt{8k_1k_2k_3}} e^{iK(\tau-\tau_s)}\ , \tag{5.46}$$

where $\theta(\tau)$ is a function of the slow roll parameters and momenta, and $K = k_1 + k_2 + k_3$. As this function is proportional with $\frac{a^2}{z^3}$, it will potentially diverge as $\tau \to -\infty$. In the limit of an approximate de Sitter space, this fraction is linear in τ. It would therefore make sense to perform two partial integrations of I_s to eliminate the divergence:

$$I_s = \frac{\left[\frac{-i}{K}\theta(\tau) - \left(\frac{-i}{K}\right)^2 \frac{\mathrm{d}\theta}{\mathrm{d}\tau}\right] e^{iK(\tau-\tau_s)}}{\sqrt{8k_1k_2k_3}}\Bigg|_{-\infty}^{\tau_s} + \int_{-\infty}^{\tau_s} \mathrm{d}\tau \frac{\mathrm{d}^2\theta}{\mathrm{d}\tau^2}\left(\frac{-i}{K}\right)^2 \frac{e^{iK(\tau-\tau_s)}}{\sqrt{8k_1k_2k_3}}\ . \tag{5.47}$$

One could continue to perform several partial integrations, but with the present the integrand should remain finite for the entire integration range. That the constant term is finite can be seen by performing a Wick rotation, by which the contribution from evaluation of the lower limit goes to zero, leaving

$$I_s = [8k_1k_2k_3]^{-1/2}\left[\frac{-i}{K}\theta(\tau_s) - \left(\frac{-i}{K}\right)^2 \frac{\mathrm{d}\theta}{\mathrm{d}\tau}\Big|_{\tau=\tau_s}\right] + \int_{-\infty}^{\tau_s} \mathrm{d}\tau \frac{\mathrm{d}^2\theta}{\mathrm{d}\tau^2}\left(\frac{-i}{K}\right)^2 \frac{e^{iK(\tau-\tau_s)}}{\sqrt{8k_1k_2k_3}}\ . \tag{5.48}$$

With the integrals under control, one can now proceed to evaluate the three-point function by first solving the background equations to find the evolution of the scale factor and the inflaton field, then evolve the mode functions (u_k) and calculate the integrals.

Upon calculating the three-point function for ζ_n, one can find the three-point function for ζ from

$$\langle \zeta_{\boldsymbol{k}_1}\zeta_{\boldsymbol{k}_2}\zeta_{\boldsymbol{k}_3}\rangle = \langle \zeta_n(\boldsymbol{k}_1)\zeta_n(\boldsymbol{k}_2)\zeta_n(\boldsymbol{k}_3)\rangle + \frac{\eta}{2}(2\pi)^3\left\{|u_{k_2}|^2|u_{k_3}|^2 + \text{sym.}\right\}\ . \tag{5.49}$$

The additional term comes from the truncating the full second order gauge transformation to the hold only the terms, which are relevant on superhorizon scales, i.e., terms without derivatives of ζ [22]:

$$\zeta \simeq \zeta_n + \frac{\eta}{4}\zeta_n^2\ . \tag{5.50}$$

Evaluating the four-point function, which arise from this second term, involves applying the inverse Fourier transform, invoking the Wick theorem and finally transforming back to momentum space. One should note, that in doing this a delta function over a single k-mode will appear. Such terms will not contribute to the overall result as a mode with zero momentum is not physically viable.

5.5 NUMERICAL RESULTS

To compare the estimates to the numerical solution in a relevant part of the parameter space, we have chosen parameters that neither are ruled out by observations, nor by theoretical considerations, but still generates an interesting signal. As can be seen in eqs. 5.11 and 5.19, this model has the remarkable property that even though it is a single field model of inflation, it can generate a feature that is readily seen in the bispectrum, but not even with Planck, can be detected in the power spectrum.

In Flauger et al [64] different observational and microphysical bounds of the model have been explored. They find that the non-detection of wiggles in the WMAP data limits $\Lambda^4/\mu^3 \approx \alpha\phi < 10^{-4}$, and that it is difficult to create realistic microphysical models that have $f < 10^{-4}$. We have therefore chosen a range of models, specified in table 5, that are characterised by having a currently non-observable wiggle amplitude power spectrum, but an $f_{\rm NL} > 5$. For the background potential we use $\mu \sim 6 \times 10^{-4} M_{\rm pl}$ and the initial value of $\phi \sim 11 M_{\rm pl}$ found in [62], that gives the correct overall amplitude in the power spectrum, and corresponds to approximately 60 e-folds before the end of inflation in the model.

name	**k**-config	$k_{\rm min}$	$k_{\rm max}$	f	α	Λ	$f_{\rm A}$	δn_s
α_1	equilateral	1	2	3×10^{-3}	1×10^{-5}	0	6.50	5.63×10^{-2}
α_2	equilateral	1	2	1×10^{-3}	7×10^{-7}	0	7.16	6.64×10^{-3}
α_3	equilateral	1	2	5×10^{-4}	1×10^{-7}	0	5.82	1.29×10^{-3}
α_4	equilateral	1	2	1×10^{-3}	1×10^{-7}	0	1.02	9.60×10^{-4}
α_5	equilateral	1	2	2×10^{-3}	4×10^{-6}	0	7.15	2.72×10^{-2}
α_6	equilateral	1	1.1	1×10^{-4}	1×10^{-7}	0	326	2.94×10^{-3}
Λ_1	equilateral	1	2	3×10^{-3}	0	4×10^{-4}	6.91	5.95×10^{-2}
Λ_2	equilateral	1	2	1×10^{-3}	0	2×10^{-4}	6.73	6.20×10^{-3}
Λ_3	equilateral	1	2	5×10^{-4}	0	1×10^{-4}	2.38	5.25×10^{-4}
Λ_4	equilateral	1	2	1×10^{-3}	0	1×10^{-4}	0.421	3.69×10^{-4}
Λ_5	equilateral	1	2	2×10^{-3}	0	3×10^{-4}	5.99	2.26×10^{-2}
Λ_6	equilateral	1	1.1	1×10^{-4}	0	1×10^{-4}	131	1.18×10^{-3}
$\alpha_{\rm s}$-model	squeezed with $m = 1$	1	25	3×10^{-3}	1×10^{-5}	0	–	5.63×10^{-2}
$\Lambda_{\rm s}$-model	squeezed with $m = 1$	1	25	3×10^{-3}	0	4×10^{-4}	–	5.95×10^{-2}
$\alpha_{\rm g}$	general model	0.1	1	3×10^{-3}	1×10^{-5}	0	–	5.63×10^{-2}

Table 5.1: Numerically evaluated models. All models have $\mu \sim 6 \times 10^{-4} M_{\rm pl}$, and the comoving wave numbers k are measured in units of $(aH)_0 = (aH)_{\phi=11M_{\rm pl}}$.

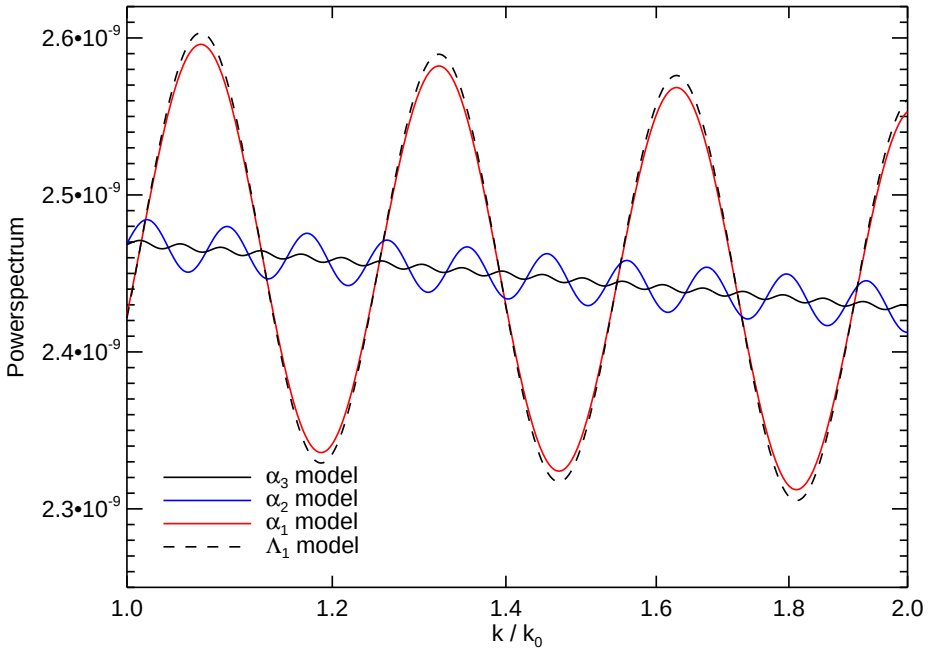

Figure 5.1: The power spectra for the models in table

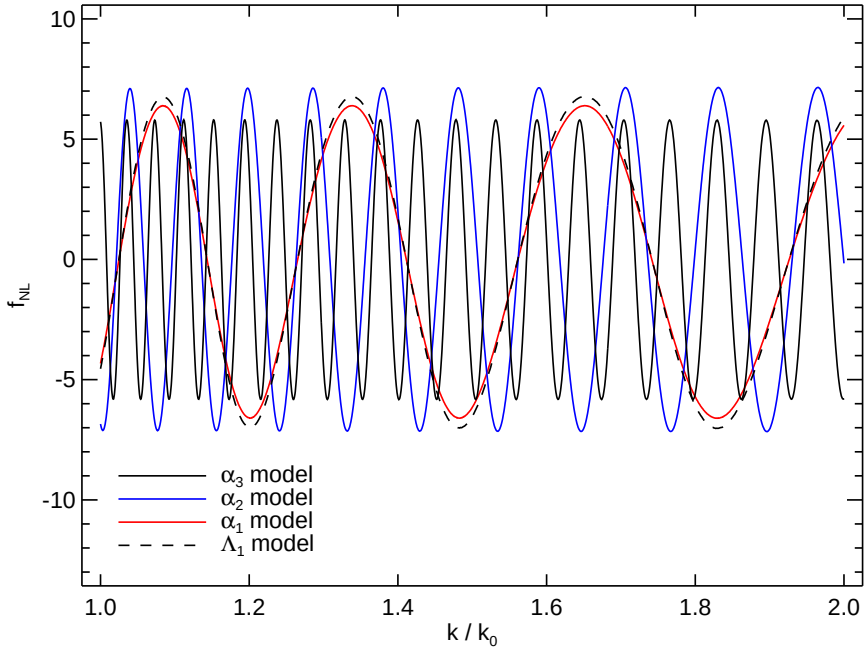

Figure 5.2: The bispectra for the models in table

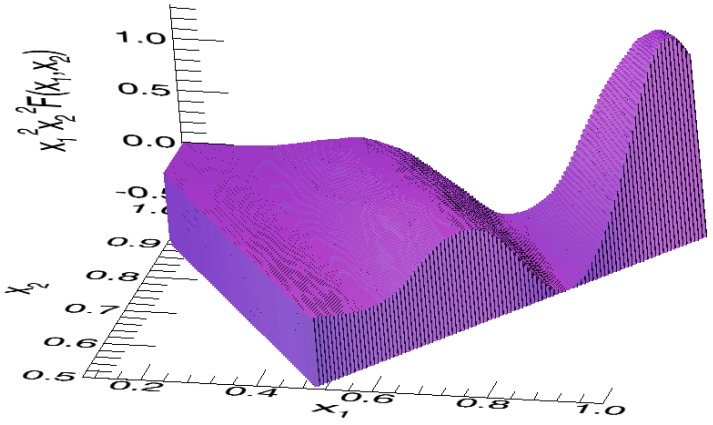

Figure 5.3: The shape function $x_1^2 x_2^2 F(x_1, x_2)$ as defined in eq. 5.52 for the general α_g model. Note that by definition F is normalised to one for the equilateral form $x_1 = x_2 = x_3 = 1$, and that we only plot unique triangles, i.e. triangles with $x_1 > x_2$ have been suppressed in the figure for clarity.

The power spectra of some of the models is shown in figure 5.1, and it can be seen that for the given values the oscillations in P_k are at the per cent to per mill level. For some of the models the wiggles will not even be detected by the Planck satellite [69], while at the same time (see figure 5.2) they have a significant amount of non-gaussianity. Ref. [69] studied the detectability of ripples due to trans-Planckian effects with Planck or a future cosmic variance limited experiment. In order for ripples to be unambiguously detected their frequency must lie within a range such that there is a number of oscillations in the observable k-range *and* their frequency must be lower than the effective width of the experimental window function. With the frequency, ω, defined such that $P(k) \propto \sin(\omega \ln k)$ [69] estimates that $1 \lesssim w \lesssim 50$ for it to be detectable. Even if it falls within this range the amplitude must of course also be sufficiently high. At approximately 1σ the amplitude, A, should be larger than 0.0024 for Planck. Translating to our case we can make the identification $\omega \sim \phi_* f$ and $A \sim \delta n_s$. To take an example with the α-models: $\alpha_3, \alpha_4, \alpha_6$ have too small amplitude to be detected in $P(k)$. α_1 and α_2 may be detectable, but α_5 has $\omega \sim 50$ and may have too fast oscillations for a detection. In conclusion, a number of the models with a measurably large non-Gaussianity would not have measurable wiggles in the power spectrum.

We have used our code to probe a rather large range of parameter space, and in figure 5.5 we show how the analytic estimates for the power spectrum and the bispectrum in the equilateral limit are in excellent agreement with the numerical results. Furthermore, we have also numerically evaluated squeezed triangles (see figure 5.4), and found a simple functional form eq. 5.25 for general isosceles triangles, which agrees at the 5%-level with the numerical result. This result was later calculated analytically by [70] to be

$$f_{\rm NL} = -\frac{5}{4}\frac{\sqrt{2\pi}\Lambda^4}{f^{5/2}\phi_*^{3/2}}\frac{k_1k_2k_3\mathcal{P}(K)}{\mathcal{P}(k_1)\mathcal{P}(k_2)k_3^3 + 2 \text{ perms.}} \times \left[\sin\left(\frac{\ln(K/k_*)}{f\phi_*}\right) + f\phi_* \sum_i \frac{K}{k_i}\cos\left(\frac{\ln(K/k_*)}{f\phi_*}\right) + \mathcal{O}((f\phi_*)^2)\right] . \tag{5.51}$$

As one can see this has the same functional form as the estimate (eq. 5.25 on page 42). Here the second term dominates for squeezed triangles, while it is suppressed for equilateral triangles by $f\phi_*$.

Given that the bispectrum in this model is nearly scale invariant, it makes sense to characterise the signal in terms of the shape function [58]

$$F(x_1 = \frac{k_1}{k_3}, x_2 = \frac{k_2}{k_3}, 1) = f_{\rm NL}(k_1, k_2, k_3)/f_{\rm NL}(k_3, k_3, k_3) \tag{5.52}$$

which measures the relative importance of different geometrical configurations compared to the equilateral configuration.

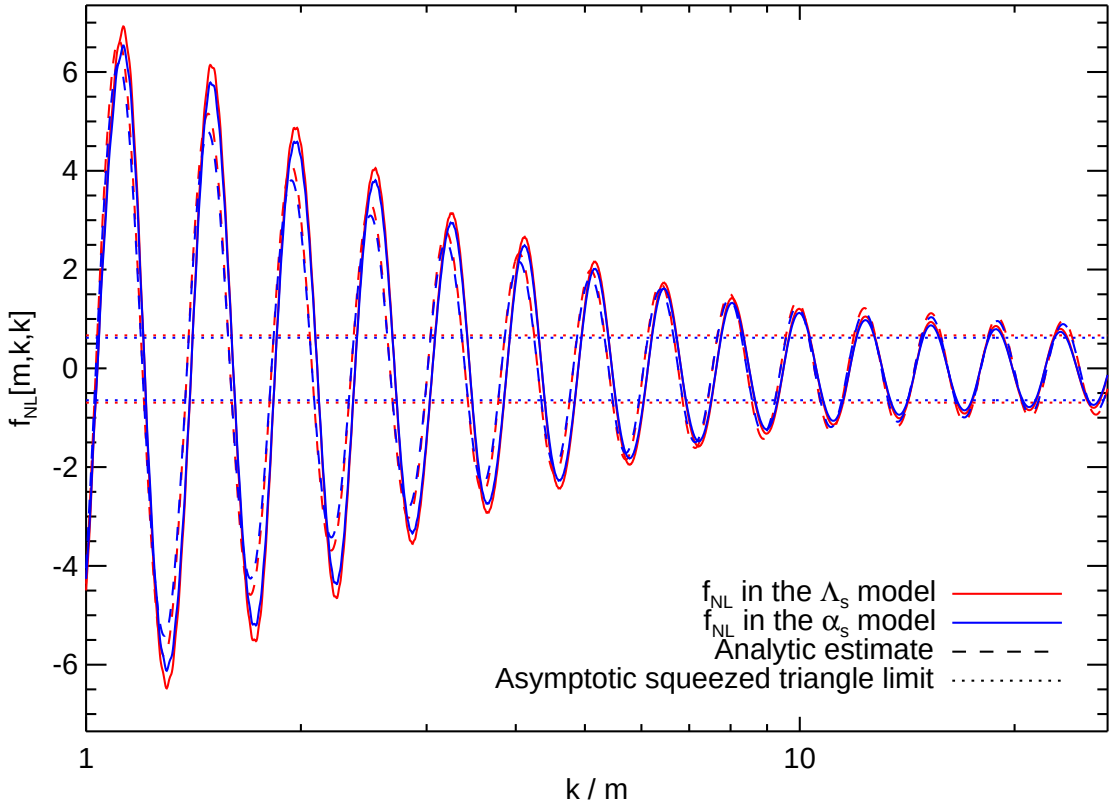

Figure 5.4: The bispectrum for isosceles triangles for the $\alpha_{\rm s}$ and $\Lambda_{\rm s}$ models as a function of side ratio k/m together with the analytic model

In figure 5.3 it can be seen how the squeezed configurations are suppressed compared to the equilateral configuration. This is also observed in higher derivative models, and is in

contrast to local type non-gaussianity from e.g. slow roll inflation, where the squeezed limit is dominating the shape function [58]. But compared to other models in the literature, this models has the distinct feature of oscillations in $f_{\rm NL}$ with an oscillation frequency $\sim \ln K/\phi f$ set by the internal parameters of the theory.

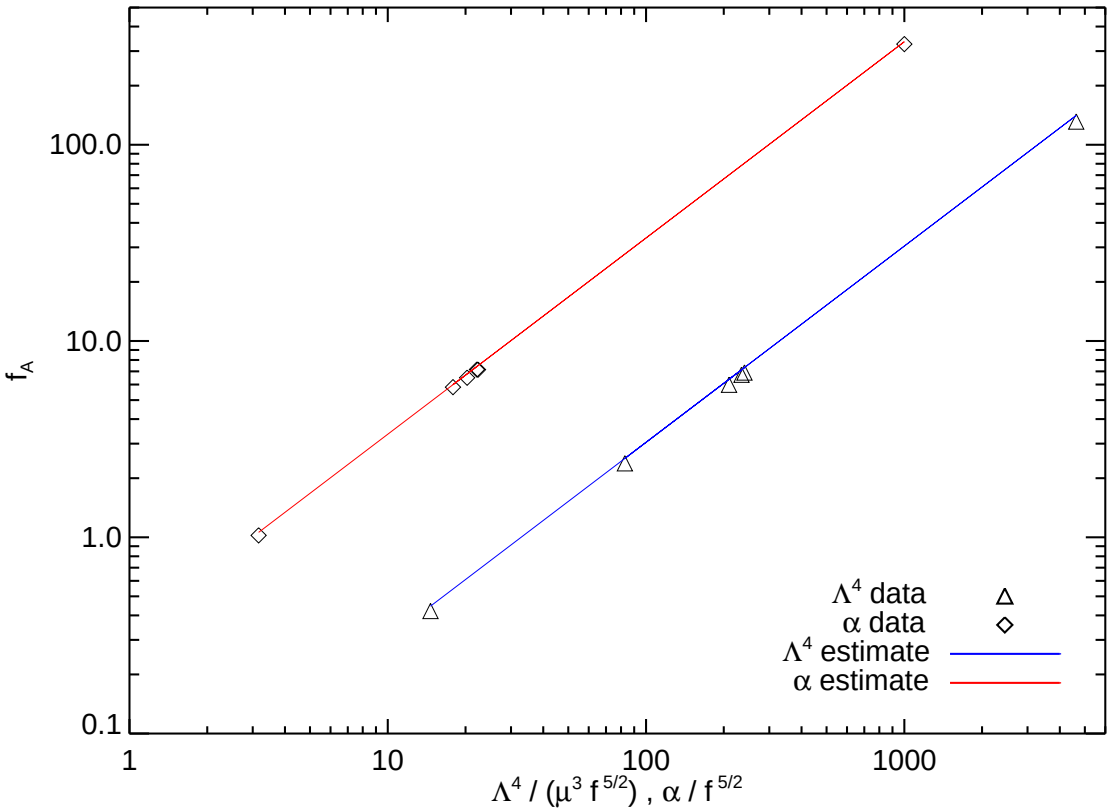

Figure 5.5: Comparison of the analytic estimates of the amplitudes f_A of $f_{\rm NL}$ to the numerical results.

6 Observing CMB Power Spectra

Up to this point the main emphasis has been on the primordial properties of inflation. This is with good reason a highly theoretical discussion as we cannot observe inflation directly. It is, however, still essential to understand how one compares the predictions with observations, and how one infers the parameters describing the primordial spectra. In this chapter we will shortly review what can be learned from observations at present. The following discussions are inspired by [71].

6.1 Angular Power Spectrum

To couple the observed spectra with the primordial ones, one needs to work out a relation between the two. In order to do this, we commence with mapping the temperature fluctuation onto a sphere by decomposing them into spherical harmonics Y_{lm}:

$$\frac{\Delta T}{T}(\hat{\boldsymbol{n}}) = \sum_{lm} a_{lm} Y_{lm}(\hat{\boldsymbol{n}}) \ . \tag{6.1}$$

From the orthonormal relation for the spherical harmonics

$$\int \mathrm{d}\hat{\boldsymbol{n}} Y_{lm}(\hat{\boldsymbol{n}}) Y^*_{l'm'}(\hat{\boldsymbol{n}}) = \delta_{ll'}\delta_{mm'} \ , \tag{6.2}$$

one can invert the decomposition to find

$$a_{lm} = \int \mathrm{d}\hat{\boldsymbol{n}} \frac{\Delta T}{T}(\hat{\boldsymbol{n}}) Y^*_{lm}(\hat{\boldsymbol{n}}) \ . \tag{6.3}$$

One can further expand temperature fluctuations in a series of Legendre polynomials $P_l(\mu)$:

$$\frac{\Delta T}{T}(\hat{\boldsymbol{n}}) = \int \frac{\mathrm{d}^3\boldsymbol{k}}{(2\pi)^3} \sum_{l=0}^{\infty} (-i)^l (2l+1) \mathcal{R}(\boldsymbol{k}) \Delta_l(k) P_l(\hat{\boldsymbol{k}} \cdot \hat{\boldsymbol{n}}) \ . \tag{6.4}$$

Here we have introduced the primordial perturbation, $\mathcal{R}(\boldsymbol{k})$ (see chapter 3 for further details), and the radiation transfer function ($\Delta_l(k)$). Using the spherical harmonic addition theorem

$$P_l(\hat{\boldsymbol{k}} \cdot \hat{\boldsymbol{n}}) = \frac{4\pi}{2l+1} \sum_{m=-l}^{l} Y^*_{lm}(\hat{\boldsymbol{k}}) Y_{lm}(\hat{\boldsymbol{n}}) \ , \tag{6.5}$$

one can write

$$a_{lm} = 4\pi(-i)^l \int \frac{\mathrm{d}^3\boldsymbol{k}}{(2\pi)^3}\mathcal{R}(\boldsymbol{k})\Delta_l(k)Y^*_{lm}(\hat{\boldsymbol{k}}) \tag{6.6}$$

by employing the orthonormality of the spherical harmonics.

From this we can define the rotationally-invariant angular power spectrum as

$$C_l^{TT} = \frac{1}{2l+1}\sum_m \langle a^*_{lm}a_{lm}\rangle \ . \tag{6.7}$$

This has long been the workhorse for inferring constraints on inflation. This is with good reason as it, even at the lowest order, relates the basic properties of the primordial power spectrum.

Combining eqs. 6.6 and 6.7, one can write

$$C_l^{TT} = \frac{2}{\pi}\int k^2\mathrm{d}k\left(\frac{2\pi^2}{k^3}\mathcal{P}(k)\right)\Delta_l(k)^2 \tag{6.8}$$

by carrying out the integral over the delta function (see eq. 3.38 on page 28 for details). This is, in general, not a task for analytical computations as the transfer function ($\Delta_l(k)$) cannot be computed analytically (see [72] for details).

LARGE SCALES

One can, however, simplify matters by only considering large scales (low l-modes). On these scales the perturbations are still well outside the horizon at the time of recombination. This means, first of all, that the perturbations are independent of subhorizon evolution. Secondly the transfer function is, in this regime, approximately a spherical Bessel function [73], reducing the angular power spectrum to

$$C_l^{TT} \simeq \frac{2}{9\pi}\int k^2\mathrm{d}k\left(\frac{2\pi^2}{k^3}\mathcal{P}(k)\right) j_l(k[\tau_0-\tau_{\mathrm{rex}}])^2 \ . \tag{6.9}$$

Here τ_0 is the conformal time today and τ_{rec} is the conformal time at recombination. The spherical Bessel function peaks around $k[\tau_0-\tau_{\mathrm{rec}}]\sim l$. One can therefore write

$$C_l^{TT} \propto \mathcal{P}(k)|_{k\sim l/(\tau_0-\tau_{\mathrm{rec}})}\int \mathrm{d}\ln(x) j_l(x)^2 \ . \tag{6.10}$$

As the integral is proportional to $[l(l+1)]^{-1}$, one has

$$\mathcal{P}(k)|_{k\sim l/(\tau_0-\tau_{\mathrm{rec}})} \propto l(l+1)C_l^{TT} \ . \tag{6.11}$$

To compare observations with theory, one needs to quantify the primordial power spectrum in terms of measurable parameters. Drawing inspiration from the slow roll calculation that led to 4.22 on page 33 and through that

$$\mathcal{P}(k) \propto \left(\frac{k}{aH}\right)^{4\epsilon-\eta} \ , \tag{6.12}$$

one expands the primordial power spectrum in terms of a spectral tilt n_s and a running of the spectral tilt α_s:

$$\mathcal{P}(k) \approx \mathcal{P}(k_*)\left(\frac{k}{k_*}\right)^{n_s-1+\frac{1}{2}\alpha_s\ln(k/k_*)} \ , \tag{6.13}$$

where k_* is an arbitrarily chosen normalisation scale. We use the definitions

$$n_s \equiv \frac{\mathrm{d}\ln(\mathcal{P})}{\mathrm{d}\ln(k)} \ , \ \alpha_s \equiv \frac{\mathrm{d}\ln(n_s)}{\mathrm{d}\ln(k)} \ . \tag{6.14}$$

Here the spectral tilt signifies the overall size of the slow roll parameters, while the running points to their evolution.

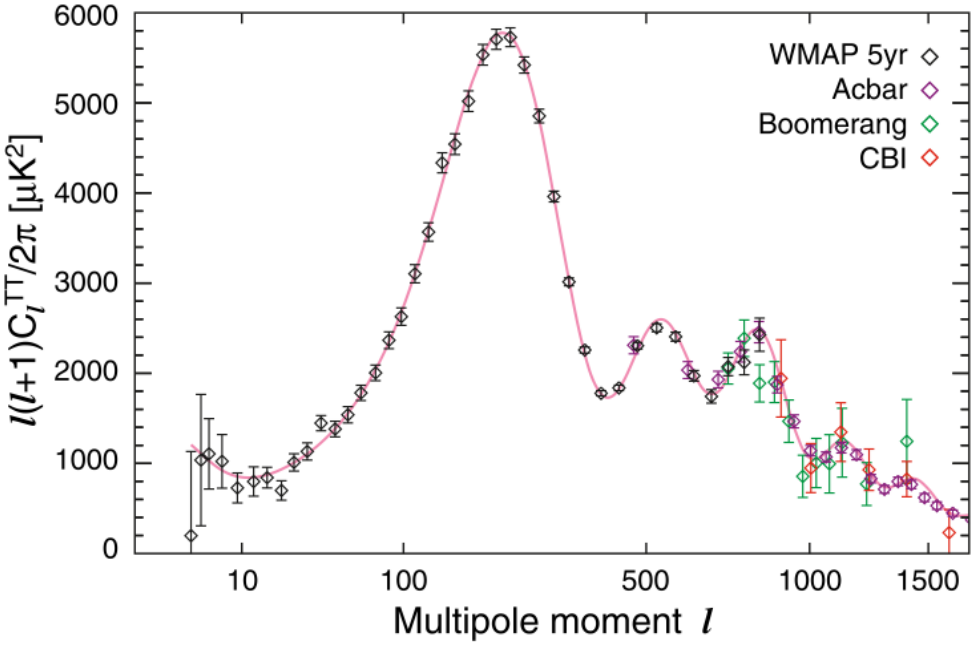

Figure 6.1: Angular CMB power spectrum. From [74]

The spectral tilt is at the same time the underlying tilt of the power spectrum (see figure 6.1).

6.2 POLARISATION

Besides measuring the spectral tilt and its running, the polarisation of the CMB [75] will yield a great additional amount of information when measured accurately. The polarisation is expected to be created through Thomson scattering, due to the velocities of the electron and protons on scales shorter than the photon diffusion scale. When a photon, carrying a quadrupole moment, interacts with an electron, it will receive a net linear polarisation. This mechanism is sensitive to the primordial anisotropies as they are responsible for the velocity field of the particles.

POWER SPECTRA OF SCALAR PERTURBATIONS

Unlike the calculation in the previous section, things become slightly more involved here as the polarisation is a spin-2 field, and not a scalar as was the case for the temperature anisotropies. One therefore defines a 2×2 intensity tensor $I_{ij}(\hat{\boldsymbol{n}})$ for a direction $\hat{\boldsymbol{n}}$ in the sky, and decompose it into orthonormal vectors $\boldsymbol{e}_1$ and $\boldsymbol{e}_2$ orthogonal to $\hat{\boldsymbol{n}}$.

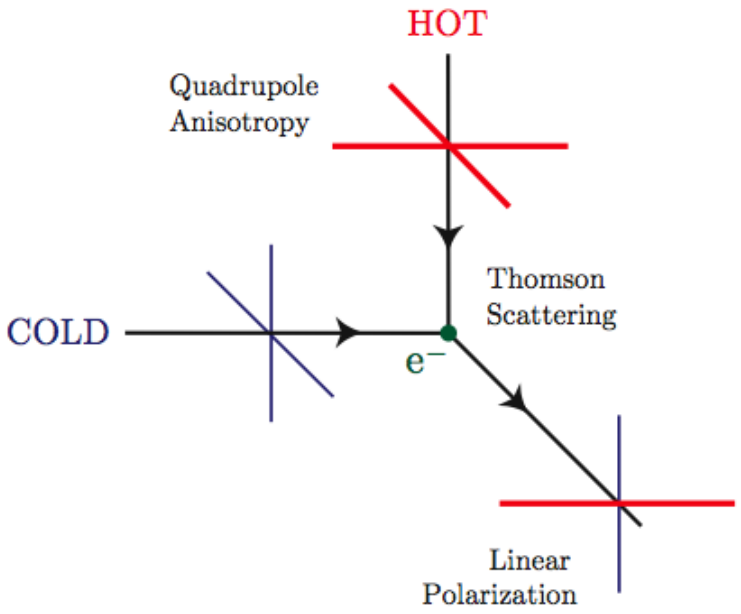

Figure 6.2: Illustration of the formation of linear polarisation from quadrupole moments through Thomson scattering. Taken from [75]

Describing the linear polarisation in terms of the Stokes parameters

$$Q = \frac{1}{4}(I_{11} - I_{22}) \tag{6.15}$$

$$U = \frac{1}{2}I_{12} \ , \tag{6.16}$$

one expands $Q \pm iU$ in tensor spherical harmonics [76, 77]:

$$(Q \pm iU)(\hat{\boldsymbol{n}}) = \sum_{l,m} a_{\pm 2,lm} \, {}_{\pm 2}Y_{lm}(\hat{\boldsymbol{n}}) \ , \tag{6.17}$$

and define the E and B modes as

$$E(\hat{\boldsymbol{n}}) = \sum_{l,m} a_{E,lm} Y_{lm}(\hat{\boldsymbol{n}}) \tag{6.18}$$

$$B(\hat{\boldsymbol{n}}) = \sum_{l,m} a_{B,lm} Y_{lm}(\hat{\boldsymbol{n}}) \tag{6.19}$$

with

$$a_{E,lm} \equiv -\frac{1}{2}(a_{2,lm} + a_{-2,lm}) \tag{6.20}$$

$$a_{B,lm} \equiv -\frac{1}{2i}(a_{2,lm} - a_{-2,lm}) \ . \tag{6.21}$$

One should note that $E(\hat{\boldsymbol{n}})$ and $B(\hat{\boldsymbol{n}})$ transforms as scalars, making them simpler to manipulate than the spin-2 construction $Q \pm iU$. With the addition of these to scalars to

the temperature fluctuations (T-mode), one can now construct four two-point correlation functions, that is the three auto-correlation functions (TT, EE and BB) along with the cross-correlation TE. The remaining modes vanish due to symmetries. From this one can generalise the definition of the angular power spectrum to encompass all four correlation functions:

$$C_l^{XY} = \frac{1}{2l+1} \sum_m \left\langle a^*_{X,lm} a_{Y,lm} \right\rangle \ , \ X, Y = T, E, B \ . \tag{6.22}$$

TENSOR MODES

Though we have not touched upon tensor perturbations in this work so far, they still play an integral part in testing inflationary models. As was mentioned in chapter 3 tensor modes are physical modes and should therefore receive attention, as one can use them to expand the total body of knowledge about inflation. They are particularly interesting as it turns out that different models of inflation produce different amounts of gravitational waves (tensor modes).

Including them in the perturbed metric, one can write the ADM line element

$$ds^2 = -N^2 dt^2 + h_{ij}(dx^i + N^i dt)(dx^j + N^j dt) \tag{6.23}$$

with a change in the spatial metric to include tensor perturbations [22]:

$$h_{ij} = a^2((1 + 2\zeta)\eta_{ij} + \gamma_{ij}) \ . \tag{6.24}$$

Here γ_{ij} is a first order tensor perturbation. One can now decompose this in terms of polarisation tensors [22]:

$$\gamma_{ij} = \int \mathrm{d}^3\boldsymbol{k} \sum_{s=\pm} \epsilon^s_{ij}(k) \gamma^s_{\boldsymbol{k}}(t) e^{-i\boldsymbol{k}\cdot\boldsymbol{x}} \tag{6.25}$$

In a similar fashion to what was done for the scalar perturbations, one can now define the primordial tensor power spectrum as

$$\left\langle \gamma^s_{\boldsymbol{k}} \gamma^{s'}_{\boldsymbol{k}'} \right\rangle = (2\pi)^3 \delta_{ss'} \delta^{(3)}(\boldsymbol{k} + \boldsymbol{k}') \left(\frac{2\pi^2}{k^3} \mathcal{P}_t(k) \right) \ , \tag{6.26}$$

where $\delta_{ss'}$ is the Kroenecker-delta.

Neither power spectrum's amplitude is interesting alone, as they are both subject to normalisation conventions. The ratio between the two, however, is a valuable quantity as it determines the amount of primordial gravitational waves, that is produced during inflation. One usually quantifies this through the tensor-to-scalar ratio:

$$r \equiv \frac{\mathcal{P}_t(k)}{\mathcal{P}(k)} \tag{6.27}$$

This quantity is particularly interesting from an observational point of view as the B-mode power spectrum only receives contributions from vector and tensor modes, i.e., a detection of C_l^{BB} with a primordial origin would constrict the bounds on the tensor-to-scalar ratio and thus the allowed models of inflation. A detection of tensor modes is often quoted a *the*

smoking gun of inflation, as alternatives to inflation seldom produce a detectable amount of tensor modes. Generation of tensor modes from cosmic strings [78, 79, 80] and global phase transitions [81] is possible, but in these cases the signal is usually dominated by the vector modes. In the case of inflation, vector modes are negligible as they decay with the expansion of the Universe.

For single field inflationary models one has a nice consistency relation [82]:

$$n_t = -\frac{r}{8} \tag{6.28}$$

where the spectral tilt of the primordial tensor power spectrum is defined as

$$\mathcal{P}_t(k) = \mathcal{P}_t(k_*)\left(\frac{k}{k_*}\right)^{n_t} . \tag{6.29}$$

6.3 OBSERVATIONAL BOUNDS AND FUTURE POTENTIAL

From the discussion so far we have a total of three parameters describing the primordial power spectrum: n_s, α_s, r; the spectral tilt, the running and the tensor-to-scalar ratio, respectively.

Constraining the parameters solely from the WMAP observations is by no means simple. Though WMAP can give a good constrain on the spectral tilt (on the level of a few per cent), it can only put an upper bound on the tensor-to-scalar ratio. Table 6.1 shows the best fit values of the WMAP 5-year data in combination with the BAO and supernovae data, while confidence intervals for the spectral tilt vs. the tensor-to-scalar ratio is shown in figure 6.3 on the next page

Model	Parameter	Best fit
Power law	n_s	$0.960^{+0.014}_{-0.013}$
Running	n_s	$1.022^{+0.043}_{-0.042}$
	α_s	$-0.032^{+0.021}_{-0.020}$
Tensor	n_s	0.968 ± 0.015
	r	<0.20 (95% CL)
Running+Tensor	n_s	$1.093^{+0.068}_{-0.069}$
	α_s	$-0.055^{+0.027}_{-0.028}$
	r	<0.54 (95% CL)

Table 6.1: Best fit of the primordial power spectrum with error bounds. Definitions in eq. 6.14 on page 55 and eq. 6.27 on the previous page. Table taken from [8]

Though most of the talk is of the TT power spectrum from WMAP, it has been possible to measure other spectra as well, albeit not with the same precision. The measurements of the TE spectrum, however, do deserve mentioning. Showing an anti-correlation (see figure 6.4 on the facing page) at $l = 50-200$ ($1^\circ - 5^\circ$), it testifies to one of the fundamental predictions of inflation; that there should be adiabatic fluctuations present on superhorizon scales at the time of decoupling [83, 84].

To move towards a better determination of the primordial dynamics, one should focus on two directions. The first being to strive to observe the remaining spectra (EE and BB)

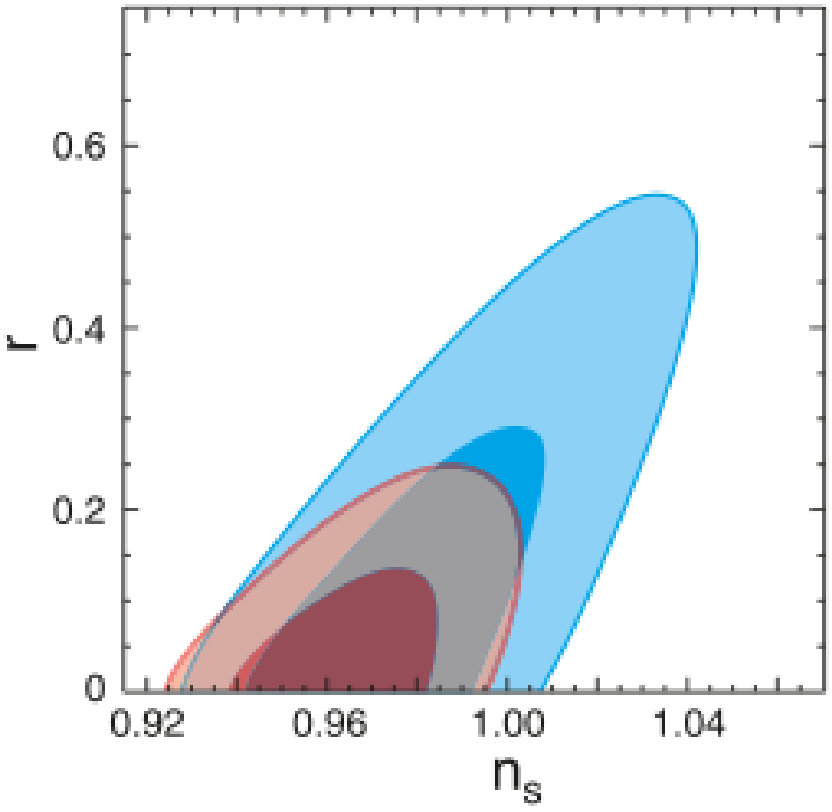

Figure 6.3: Confidence intervals for spectral tilt (n_s) vs. tensor-to-scalar ratio (r). From [8]

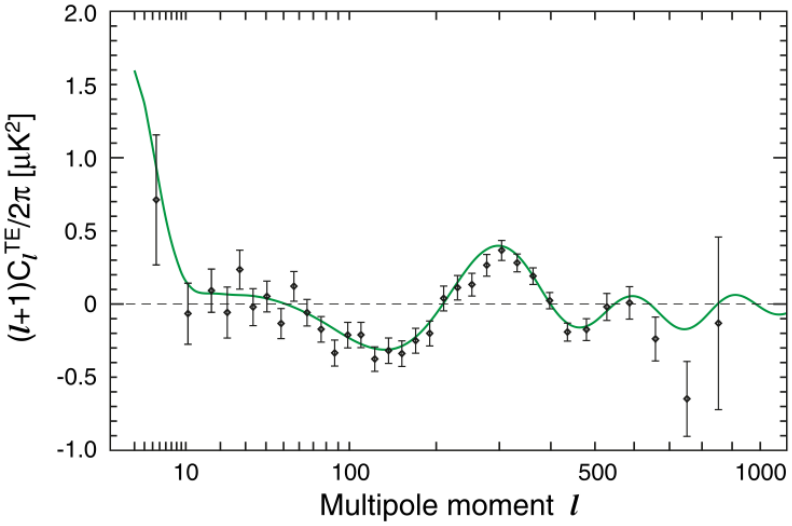

Figure 6.4: TE power spectrum showing anti-correlation at around $l = 50 - 200$. From [74]

to pin down the tensor-to-scalar ratio, and in that way hopefully exclude a vast amount of inflationary models. It has been estimated that the Planck satellite may be able to detect

a tensor-to-scalar ratio, if it is not too far below the present upper bound. If not detected with Planck a next generation CMB polarisation experiment should be able to detect or severely constrain the tensor-to-scalar ratio [85] (see figure 6.5 for the estimated sensitivity for WMAP, Planck and EPIC).

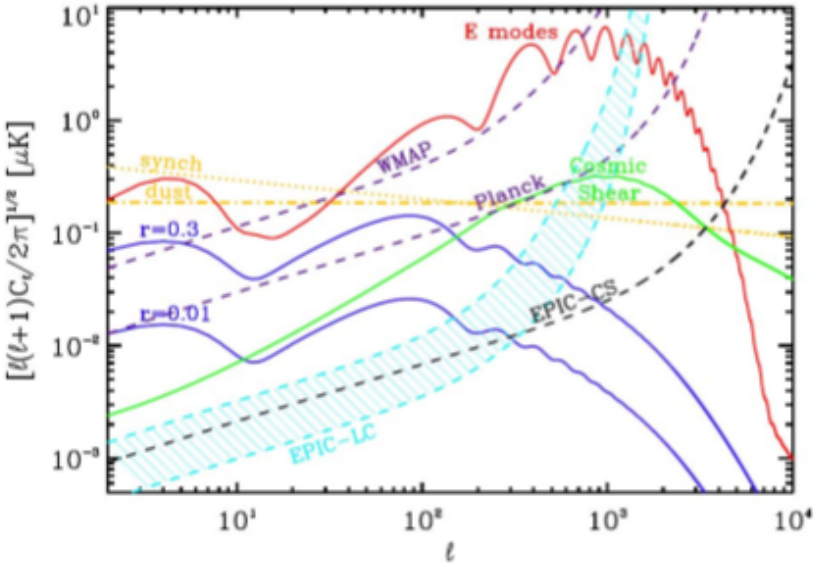

Figure 6.5: Estimated sensitivity for measuring E and B modes for different CMB probes. From [85]

A non-detection of the tensor-to-scalar ratio would favour the single field slow roll scenario as [22]

$$r = 16\epsilon \tag{6.30}$$

in this scenario. Here ϵ is the first slow roll parameter.

The second direction one should follow is observing the higher order spectra. The next chapter will focus on computing the observational bispectrum for the axion monodromy model, that was introduced in chapter 5.

7 The Observational Bispectrum

There is still a long way from the calculated primordial spectra to the observed ones. The primordial perturbations merely provides the initial perturbations of the wavelengths of the CMB photons, they still have to propagate through the Universe as it evolves toward the universe we observe today. During this propagation the content of the Universe will affect the photons and alter the spectra.

This chapter will focus on calculating the observed bispectrum for the axion-monodomy model and remains a work in progress.

7.1 Bispectra in the CMB

Following [86, 87] as the three-point correlation function of a_{lm}, one can insert the expression from eq. 6.6 on page 54 to find

$$\begin{aligned} B^{m_1,m_2,m_3}_{l_1,l_2,l_3} &= \langle a_{l_1m_1} a_{l_2m_2} a_{l_3m_3} \rangle \\ &= (4\pi)^3(-i)^{l_1+l_2+l_3} \int \frac{\mathrm{d}^3\boldsymbol{k}_1}{(2\pi)^3}\frac{\mathrm{d}^3\boldsymbol{k}_2}{(2\pi)^3}\frac{\mathrm{d}^3\boldsymbol{k}_3}{(2\pi)^3} \langle \mathcal{R}(\boldsymbol{k}_1)\mathcal{R}(\boldsymbol{k}_2)\mathcal{R}(\boldsymbol{k}_3)\rangle \\ &\quad \times \Delta_{l_1}(k_1)\Delta_{l_2}(k_2)\Delta_{l_3}(k_3) Y^*_{l_1m_1}(\hat{\boldsymbol{k}}_1) Y^*_{l_2m_2}(\hat{\boldsymbol{k}}_2) Y^*_{l_3m_3}(\hat{\boldsymbol{k}}_3) \ . \end{aligned} \tag{7.1}$$

We can now proceed to write the primordial bispectrum ($\langle \mathcal{R}(\boldsymbol{k}_1)\mathcal{R}(\boldsymbol{k}_2)\mathcal{R}(\boldsymbol{k}_3)\rangle$) in terms of the primordial shape function $F(k_1, k_2, k_3)$, which is defined as

$$\langle \mathcal{R}(\boldsymbol{k}_1)\mathcal{R}(\boldsymbol{k}_2)\mathcal{R}(\boldsymbol{k}_3)\rangle = (2\pi)^3\delta^{(3)}(\boldsymbol{k}_1+\boldsymbol{k}_2+\boldsymbol{k}_3)F(k_1,k_2,k_3). \tag{7.2}$$

Writing the delta function as an integral over the exponential function

$$\delta(\boldsymbol{k}) = \int \frac{\mathrm{d}^3\boldsymbol{x}}{(2\pi)^3} e^{i\boldsymbol{k}\cdot\boldsymbol{x}} \tag{7.3}$$

and replacing the exponential by the Rayleigh expansion

$$e^{i\boldsymbol{k}\cdot\boldsymbol{x}} = 4\pi \sum_l i^l j_l(kx) \sum_m Y_{lm}(\hat{\boldsymbol{k}}) Y^*_{lm}(\hat{\boldsymbol{x}}) \ , \tag{7.4}$$

one can use the orthonormality of the spherical harmonics to integrate out the angular part of the momentum integrals. If one further introduces the Gaunt integral

$$\mathcal{G}^{m_1m_2m_3}_{l_1l_2l_3} = \int \mathrm{d}\Omega Y_{l_1m_1}(\hat{\boldsymbol{x}}) Y_{l_2m_2}(\hat{\boldsymbol{x}}) Y_{l_3m_3}(\hat{\boldsymbol{x}}) \tag{7.5}$$

$$= \sqrt{\frac{(2l_1+1)(2l_2+1)(2l_3+1)}{4\pi}} \begin{pmatrix} l_1 & l_2 & l_3 \\ 0 & 0 & 0 \end{pmatrix} \begin{pmatrix} l_1 & l_2 & l_3 \\ m_1 & m_2 & m_3 \end{pmatrix} \ , \tag{7.6}$$

one can write eq. (refeq:initbispec as

$$B^{m_1,m_2,m_3}_{l_1,l_2,l_3} = \left(\frac{2}{\pi}\right)^3 \mathcal{G}^{m_1m_2m_3}_{l_1l_2l_3} \int x^2 \mathrm{d}x k_1^2 \mathrm{d}k_1 k_2^2 \mathrm{d}k_2 k_3^2 \mathrm{d}k_3 F(k_1,k_2,k_3) \tag{7.7}$$

$$\times \Delta_{l_1}(k_1)\Delta_{l_2}(k_2)\Delta_{l_3}(k_3) j_{l_1}(k_1x) j_{l_2}(k_2x) j_{l_3}(k_3x) \ . \tag{7.8}$$

Assuming statistical isotropy we focus on the angle averaged bispectrum

$$B_{l_1l_2l_3} = \sum_{m_1m_2m_3} \begin{pmatrix} l_1 & l_2 & l_3 \\ m_1 & m_2 & m_3 \end{pmatrix} B^{m_1m_2m_3}_{l_1l_2l_3} \ , \tag{7.9}$$

instead of the one calculated above.

As

$$\sum_{m_1m_2m_3} \begin{pmatrix} l_1 & l_2 & l_3 \\ m_1 & m_2 & m_3 \end{pmatrix}^2 = 1 \ , \tag{7.10}$$

we are left with

$$B_{l_1l_2l_3} = \left(\frac{2}{\pi}\right)^3 \sqrt{\frac{(2l_1+1)(2l_2+1)(2l_3+1)}{4\pi}} \begin{pmatrix} l_1 & l_2 & l_3 \\ 0 & 0 & 0 \end{pmatrix}$$

$$\times \int x^2 \mathrm{d}x k_1^2 \mathrm{d}k_1 k_2^2 \mathrm{d}k_2 k_3^2 \mathrm{d}k_3 F(k_1,k_2,k_3) \tag{7.11}$$

$$\times \Delta_{l_1}(k_1)\Delta_{l_2}(k_2)\Delta_{l_3}(k_3) j_{l_1}(k_1x) j_{l_2}(k_2x) j_{l_3}(k_3x) \ .$$

Two important properties of Wigner-3j function in the frontfactor are, that the l-modes must obey the triangle inequality and the sum of the modes must be equal.

7.2 DELTA FUNCTION INTEGRAL

In order to tackle the integral, we begin with singling out the integral over x:

$$k_1k_2k_3 \int_0^\infty x^2 \mathrm{d}x j_{l_1}(k_1x) j_{l_2}(k_2x) j_{l_3}(k_3x) \ , \tag{7.12}$$

which is scale invariant. This is an inherently difficult numerical integral, as the spherical Bessel functions not only oscillate, but also decrease slowly. It is, however, possible to achieve a semianalytical solution through a recursive scheme. Introducing the function

$$\mathcal{J}_n(z) = z^{n+1} j_n(z) \ , \tag{7.13}$$

we define the integral, which will be central to the scheme:

$$I_{(l_1,l_2,l_3)}(k_1,k_2,k_3) = k_1^{-l_1}k_2^{-l_2}k_3^{-l_3} \int_0^\infty \mathrm{d}x \frac{\mathcal{J}_{l_1}(k_1x)\mathcal{J}_{l_2}(k_2x)\mathcal{J}_{l_3}(k_3x)}{x^{l_1+l_2+l_3+1}} \ . \tag{7.14}$$

This integral is equivalent to the one in eq. 7.12.

RECURSIVE EXPRESSION

From the recursive definition of the spherical Bessel function (see e.g. [88] p. 438)

$$j_n(z) = f_n(z)\sin(z) + (-1)^{n+1} f_{-n-1}(z)\cos(z) \ , \tag{7.15}$$

where f_n is defined as

$$f_{n-1}(z) + f_{n+1}(z) = (2n+1)z^{-1} f_n(z) \ , \ f_0(z) = z^{-1} \ , \ f_1(z) = z^{-2} \ , \tag{7.16}$$

one can write down a recursion formula for $F_n(z)$:

$$\begin{aligned} \mathcal{J}_n(z) &= (2n-1)\mathcal{J}_{n-1}(z) - z^2 \mathcal{J}_{n-2}(z) \\ \mathcal{J}_0(z) &= \sin(z) \ , \ \mathcal{J}_1(z) = \sin(z) - z\cos(z) \ . \end{aligned} \tag{7.17}$$

Due to the Wigner-3j function we are thus left with the following possibilities: The special cases $I(0,0,0)$ and permutations of $I(0,1,1)$, as well as the general integral $I(l_1,l_2,l_3)$, where $l_1,l_2,l_3 \geq 1$ and $\max(l_1,l_2,l_3) \geq 2$.

We now proceed, for the general case, to expand the largest l-mode of the integral $I(l_1,l_2,l_3)$ in terms of the recursion formula above. For the case of $l_3 \geq l_1, l_2$, one get

$$\begin{aligned} I(l_1,l_2,l_3) &= (2l_3-1){k_1}^{-l_1} k_2^{-l_2} k_3^{-l_3} \int_0^\infty \mathrm{d}x \frac{\mathcal{J}_{l_1}(k_1x)\mathcal{J}_{l_2}(k_2x)\mathcal{J}_{l_3-1}(k_3x)}{x^{l_1+l_2+l_3+1}} \\ &\quad - I(l_1,l_2,l_3-2) \ . \end{aligned} \tag{7.18}$$

Performing a partial integration of the integral in the first line, one gets

$$\begin{aligned} \int_0^\infty \mathrm{d}x \quad & \frac{\mathcal{J}_{l_1}(k_1x)\mathcal{J}_{l_2}(k_2x)\mathcal{J}_{l_3-1}(k_3x)}{x^{l_1+l_2+l_3+1}} = \frac{-\mathcal{J}_{l_1}(k_1x)\mathcal{J}_{l_2}(k_2x)\mathcal{J}_{l_3-1}(k_3x)}{(l_1+l_2+l_3)x^{l_1+l_2+l_3}}\Bigg|_0^\infty \\ & + \frac{1}{l_1+l_2+l_3} \int_0^\infty \mathrm{d}x \frac{\frac{\mathrm{d}}{\mathrm{d}x}\left[\mathcal{J}_{l_1}(k_1x)\mathcal{J}_{l_2}(k_2x)\mathcal{J}_{l_3-1}(k_3x)\right]}{x^{l_1+l_2+l_3+1}} \ . \end{aligned} \tag{7.19}$$

The constant term vanishes as

$$\lim_{z\to 0} \mathcal{J}_n(z) \propto z^{2n+1} \ , \ \lim_{z\to\infty} \mathcal{J}_n(z) \propto z^n \ . \tag{7.20}$$

To evaluate the remaining integral, we distinguish between the cases of $l_1,l_2,l_3 \geq 1$ and the squeezed triangle case with one l-mode being 0.

In the first case we use the relation

$$\frac{\mathrm{d}}{\mathrm{d}z}\mathcal{J}_n(z) = z\mathcal{J}_{n-1}(z) \ , \ n \geq 1 \tag{7.21}$$

to obtain

$$\begin{aligned} I_{(l_1,l_2,l_3)}(k_1,k_2,k_3) &= \frac{2l_3-1}{l_1+l_2+l_3}\frac{k_1}{k_3} I_{(l_1-1,l_2,l_3-1)}(k_1,k_2,k_3) \\ &\quad + \frac{2l_3-1}{l_1+l_2+l_3}\frac{k_2}{k_3} I_{(l_1,l_2-1,l_3-1)}(k_1,k_2,k_3) \\ &\quad + \left(\frac{2l_3-1}{l_1+l_2+l_3} - 1\right) I_{(l_1,l_2,l_3-2)}(k_1,k_2,k_3) \ . \end{aligned} \tag{7.22}$$

It should be noted at this point, that if (l_1, l_2, l_3) , $l_1, l_2, l_3 \in \mathbb{N}$ forms a triangle with $l_1, l_2 \leq l_3$ and $l_3 \geq 2$, then $(l_1 - 1, l_2, l_3 - 1)$, $(l_1, l_2 - 1, l_3 - 1)$ and $(l_1, l_2, l_3 - 2)$ will all form triangles as well. This can be seen from the following.

As $l_3 \geq l_1, l_2$ and $l_1, l_2 \geq 1$ then

$$l_1, l_2 < \frac{l_1 + l_2 + l_3}{2} \tag{7.23}$$

from the triangle inequality. Equivalently this means that

$$l_1, l_2 \leq \frac{l_1 + l_2 + l_3}{2} - 1 \ , \tag{7.24}$$

which gives that $(l_1 - 1, l_2, l_3 - 1)$ and $(l_1, l_2 - 1, l_3 - 1)$ obey the triangle inequality as well. The last case holds trivially as triangle inequality gives

$$l_3 \leq \frac{l_1 + l_2 + l_3}{2} \ . \tag{7.25}$$

For the case of one l-mode being 0, the triangles reduce to the form $(0, l, l)$ with $l \geq 2$. In this case we use the special case

$$\frac{\mathrm{d}}{\mathrm{d}z}\mathcal{J}_0(z) = z^{-1}\left[\mathcal{J}_0(z) - \mathcal{J}_1(z)\right] \ . \tag{7.26}$$

This gives

$$I_{(0,l,l)}(k_1, k_2, k_3) = -\frac{k_1}{k_3} I_{(1,l,l-1)}(k_1, k_2, k_3) + \frac{k_2}{k_3} I_{(0,l-1,l-1)}(k_1, k_2, k_3) \ . \tag{7.27}$$

It is easily seen, that if $(0, l, l)$ forms a triangle, then $(1, l, l - 1)$ and $(0, l - 1, l - 1)$ must surely also form triangles.

We are thus left with calculating the two special cases, which can be done analytically:

$$I_{(0,0,0)}(k_1, k_2, k_3) = \frac{\pi}{4} \tag{7.28}$$

$$I_{(0,1,1)}(k_1, k_2, k_3) = \frac{\pi}{8}\left(\frac{k_2}{k_3} + \frac{k_3}{k_2} - \frac{k_1^2}{k_2 k_3}\right) \ . \tag{7.29}$$

From the special cases, as well as the the recursive schemes (eqs. 7.22 and 7.27), one infer two important point concerning the solution. The first being that any solution must be of the form

$$I_{(l_1,l_2,l_3)}(k_1, k_2, k_3) = \sum_{c_1+c_2+c_3=0} a_{c_1,c_2,c_3} k_1^{-c_1} k_2^{-c_2} k_3^{-c_3} \ . \tag{7.30}$$

The second is that the powers are bounded by

$$c_i \leq l_i \ , \ i = 1, 2, 3 \ . \tag{7.31}$$

ANGULAR PARAMETERIZATION

Defining the angles of the momentum triangle as given in fig. 7.1, we rewrite the recursion scheme for $l_3 \geq l_1, l_2$ as

$$\begin{aligned} I_{(l_1,l_2,l_3)}(\theta_1,\theta_2,\theta_3) &= \frac{2l_3-1}{l_1+l_2+l_3}\frac{\sin\theta_1}{\sin\theta_3} I_{(l_1-1,l_2,l_3-1)}(\theta_1,\theta_2,\theta_3) \\ &\quad + \frac{2l_3-1}{l_1+l_2+l_3}\frac{\sin\theta_2}{\sin\theta_3} I_{(l_1,l_2-1,l_3-1)}(\theta_1,\theta_2,\theta_3) \\ &\quad + \left(\frac{2l_3-1}{l_1+l_2+l_3}-1\right) I_{(l_1,l_2,l_3-2)}(\theta_1,\theta_2,\theta_3) \end{aligned} \tag{7.32}$$

$$I_{(0,l,l)}(\theta_1,\theta_2,\theta_3) = -\frac{\sin\theta_1}{\sin\theta_3} I_{1,l,l-1}(\theta_1,\theta_2,\theta_3) + \frac{\sin\theta_2}{\sin\theta_3} I_{(0,l-1,l-1)}(\theta_1,\theta_2,\theta_3) \tag{7.33}$$

$$I_{(0,0,0)}(\theta_1,\theta_2,\theta_3) = \frac{\pi}{4} \tag{7.34}$$

$$I_{(0,1,1)}(\theta_1,\theta_2,\theta_3) = \frac{\pi}{4}\cos\theta_1 \tag{7.35}$$

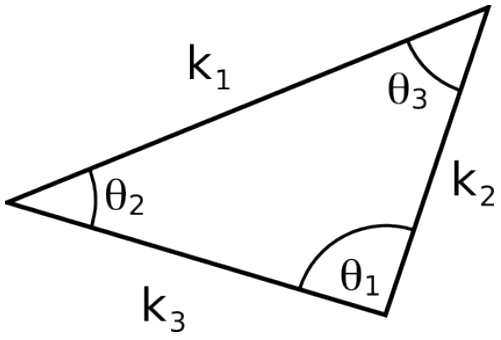

Figure 7.1: Momentum triangle

From the recursive scheme we now compute the first two non-trivial integrals and compute their limits for squeezed and folded triangles. For the triangle $l_1 = l_2 = 1, l_3 = 2$ one gets

$$I_{(1,1,2)}(\theta_1,\theta_2,\theta_3) = \frac{\pi}{32}\frac{3\sin(2\theta_1)+3\sin(2\theta_2)-\sin(2\theta_3)}{\sin(\theta_3)} \ . \tag{7.36}$$

This result can still prove tricky numerically in the cases where $\sin(\theta_3) \to 0$. Using L'Hôpital's rule with the identity

$$\frac{\mathrm{d}\theta_1}{\mathrm{d}\theta_3} + \frac{\mathrm{d}\theta_2}{\mathrm{d}\theta_3} + 1 = 0 \ , \tag{7.37}$$

one can find the limit to be

$$\lim_{\theta_3\to 0} I_{(1,1,2)}(\theta_1,\theta_2,\theta_3) = -\frac{\pi}{16}\left[1+3\cos(2\theta_1)\right] \ . \tag{7.38}$$

One might be concerned with the seemingly lack of symmetry between θ_1 and θ_2. However in the limit $\theta_3 \to 0$, one has $\theta_2 \to \pi - \theta_1$, making the result the same whether one inserts θ_1 or θ_2.

The same technique is applicable for the limit $\theta_3 \to \pi$. As both θ_1 and θ_2 approach zero in this limit, one can evaluate the limit to find

$$\lim_{\theta_3 \to \pi} I_{(1,1,2)}(\theta_1, \theta_2, \theta_3) = \frac{\pi}{4} \ . \tag{7.39}$$

The sign difference between the two limits come from the denominator, when L'Hôpital's rule is applied. The remaining limits are trivially found to be

$$\lim_{\theta_1 \to 0} I_{(1,1,2)}(\theta_1, \theta_2, \theta_3) = \lim_{\theta_2 \to 0} I_{(1,1,2)}(\theta_1, \theta_2, \theta_3) = -\frac{\pi}{4}\cos(\theta_3) \ . \tag{7.40}$$

From this result one can now compute the $I_{(0,2,2)}$-integral:

$$\begin{aligned} I_{(0,2,2)}(\theta_1, \theta_2, \theta_3) = &- \frac{\pi}{32}\frac{3\sin(2\theta_1) + \sin(2\theta_2) + \sin(2\theta_3)}{\sin(\theta_2)\sin(\theta_3)}\sin(\theta_1) \\ &+ \frac{\pi}{8}\frac{\sin^2(\theta_2) + \sin^2(\theta_3)}{\sin(\theta_2)\sin(\theta_3)}\cos(\theta_1) \ . \end{aligned} \tag{7.41}$$

Employing the same principles one can determine the limits for the squeezed triangles for the $I_{(0,2,2)}$:

$$\lim_{\theta_1 \to 0} I_{(0,2,2)} = \frac{\pi}{4} \ . \tag{7.42}$$

Regarding the recursion relations, one can show that this limit is quiet general in the sense that

$$\lim_{\theta_1 \to 0} I_{(0,l,l)} = \frac{\pi}{4} \ . \tag{7.43}$$

To see this one needs to show, one regards eq. 7.33 on the previous page in the limit $\theta_1 \to 0$. As one has $\frac{\sin(\theta_2)}{\sin(\theta_3)} = 1$ for $\theta_1 \to 0$, one only needs to show that $I_{(1,l,l-1)}$ is finite in this limit to obtain

$$I_{(0,l,l)}(\theta_1, \theta_2, \theta_3) = I_{(0,l-1,l-1)}(\theta_1, \theta_2, \theta_3) \ . \tag{7.44}$$

This can be shown recursively by writing the recursive relation eq. 7.32 with l_2 as the largest l-mode. Taking limit $\theta_1 \to 0$ and assuming $\lim_{\theta_1 \to 0} I_{(1,l-1,l-2)} < \infty$, and thereby $\lim_{\theta_1 \to 0} I_{(1,l-2,l-1)} < \infty$ due to the symmetry in θ_2 and θ_3 in the $\theta_1 \to 0$ limit, and $I_{(0,l-1,l-1)} = \frac{\pi}{4}$, one gets

$$\begin{aligned} \lim_{\theta_1 \to 0} I_{(1,l,l-1)}(\theta_1, \theta_2, \theta_3) = &\frac{2l_2 - 1}{l_1 + l_2 + l_3} \lim_{\theta_1 \to 0} I_{(1,l-1,l-2)}(\theta_1, \theta_2, \theta_3)v \\ &+ \left(\frac{2l_2 - 1}{l_1 + l_2 + l_3} - 1\right) \lim_{\theta_1 \to 0} I_{(1,l-2,l-1)}(\theta_1, \theta_2, \theta_3) \\ &< \infty \ . \end{aligned} \tag{7.45}$$

As the basic case ($l = 2$) has already been shown, this concludes the proof by recursion.

For the limit of $\theta_3 \to 0$, or equivalently $\theta_2 \to 0$, one finds, after some arithmetic and use of trigonometric relations, that

$$\lim_{\theta_3 \to 0} I_{(0,2,2)}(\theta_1, \theta_2, \theta_3) = \frac{\pi}{16}\left(2\frac{\sin(2\theta_1)}{\tan(\theta_1)} + 2\cos(2\theta_1) - 2\right) \ . \tag{7.46}$$

To find this solution we used that $\theta_1(\theta_3)$ must be a continuous, bounded function, and it must therefore have a finite first derivative.

The integrals are plotted in figures 7.2 and 7.3, testifying the derived limits.

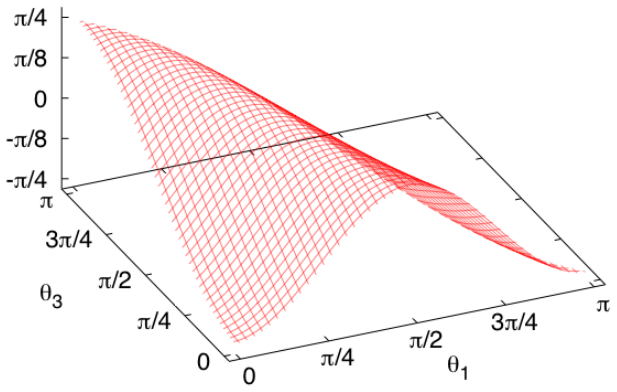

Figure 7.2: The $I_{(1,1,2)}$ integral (eq. 7.36) plotted as a function of θ_1 and θ_3

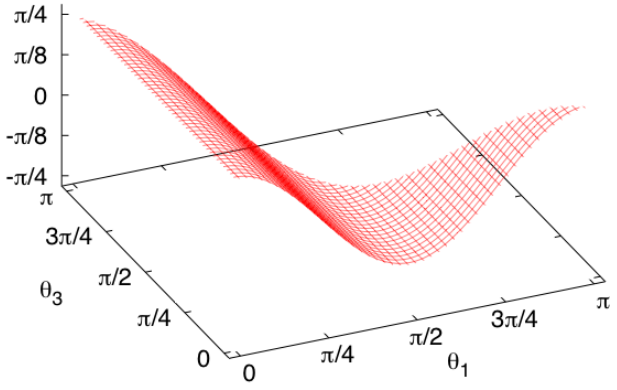

Figure 7.3: The $I_{(1,1,2)}$ integral (eq. 7.41) plotted as a function of θ_1 and θ_3

7.3 SPHERICAL COORDINATES IN THE 1-NORM AND THE SHAPE FUNCTION

For the case of the axion monodromy model, one can find the shape function (eq. 7.2):

$$F(k_1,k_2,k_3) = (2\pi)^4 \quad \frac{3\sqrt{2\pi}\Lambda^4}{8\phi_*^{3/2}f^{5/2}\mu^3}\frac{\mathcal{P}^2(K)}{k_1^2k_2^2k_3^2} \times\left[\sin\left(\frac{\ln(K/k_*)}{f\phi*}\right)+f\phi_*\sum_i\frac{K}{k_i}\cos\left(\frac{\ln(K/k_*)}{f\phi_*}\right)\right] \tag{7.47}$$

with $K = k_1 + k_2 + k_3$. Here the power spectrum is given by [64]

$$\mathcal{P}(k) = \mathcal{P}(k_*)\left(\frac{k}{k_*}\right)^{n_s-1}\left[1+\delta n_s\cos\left(\frac{\phi_k}{f}\right)\right] \ , \tag{7.48}$$

where

$$\delta n_s = \frac{12\Lambda^4}{\mu^3 f}\sqrt{\frac{\frac{\pi}{8}\coth\left(\frac{\pi}{2f\phi_*}\right)f\phi_*}{1+(3f\phi_*)^2}} \tag{7.49}$$

$$\phi_k = \sqrt{\phi_*^2 - 2\ln(k/k_*)} \ . \tag{7.50}$$

Inserting this yields a bispectrum of the form

$$\begin{aligned} B_{l_1l_2l_3} &= \frac{24\pi\Lambda^4}{\phi_*^{3/2}f^{5/2}\mu^3}\sqrt{2(2l_1+1)(2l_2+1)(2l_3+1)}\begin{pmatrix} l_1 & l_2 & l_3 \\ 0 & 0 & 0\end{pmatrix} \\ &\times\int\frac{\mathrm{d}k_1\mathrm{d}k_2\mathrm{d}k_3}{k_1k_2k_3}\mathcal{P}^2(K)\Delta_{l_1}(k_1)\Delta_{l_2}(k_2)\Delta_{l_3}(k_3)I_{(l_1,l_2,l_3)}(k_1,k_2,k_3) \\ &\times\left[\sin\left(\frac{\ln(K/k_*)}{f\phi*}\right)+f\phi_*\sum_i\frac{K}{k_i}\cos\left(\frac{\ln(K/k_*)}{f\phi_*}\right)\right] \ . \end{aligned} \tag{7.51}$$

Performing a transformation from (k_1, k_2, k_3) to (K, Δ), where Δ is a two dimensional shape parameter for the triangle, one can schematically write

$$\frac{\mathrm{d}k_1\mathrm{d}k_2\mathrm{d}k_3}{k_1k_2k_3} = \frac{f(\Delta)}{K}\mathrm{d}K\mathrm{d}^2\Delta \ . \tag{7.52}$$

Dividing the area of integration for Δ into three regions, each defined by having one of the sides in the triangle with unit perimeter being smaller than the other two, we define

$$k_s \leq k_+, k_- \ , \ k_s + k_+ + k_- = K \tag{7.53}$$

for each of the three regions. Expressing the new variables in terms of the two parameters (s, t), such that

$$k_s = Ks \tag{7.54}$$

$$k_+ = K(1-s)a_+ \tag{7.55}$$

$$k_- = K(1-s)a_- \tag{7.56}$$

with $a_+ + a_- = 1$. From the triangle inequality one finds $0 \leq s \leq \frac{1}{2}$ and

$$0 \leq \quad (1-s)a_+ \quad \leq \frac{1}{2} \tag{7.57}$$

$$0 \leq \quad (1-s)a_- \quad \leq \frac{1}{2}\ , \tag{7.58}$$

which translates into a bound on a_+:

$$\frac{1-2s}{2(1-s)} \leq a_+ \leq \frac{1}{2(1-s)}\ . \tag{7.59}$$

Introducing the second parameter $t \in [-\frac{1}{2}, \frac{1}{2}]$, one gets

$$k_s = Ks \tag{7.60}$$

$$k_+ = K\left[\frac{1-s}{2} + st\right] \tag{7.61}$$

$$k_- = K\left[\frac{1-s}{2} - st\right] \tag{7.62}$$

One can now determine the area of integration from eq. 7.53 and write the angular averaged bispectrum as

$$\begin{aligned} B_{l_1 l_2 l_3} = & \frac{24\pi\Lambda^4}{\phi_*^{3/2} f^{5/2}\mu^3}\sqrt{2(2l_1+1)(2l_2+1)(2l_3+1)}\begin{pmatrix} l_1 & l_2 & l_3 \\ 0 & 0 & 0 \end{pmatrix} \\ & \times \int_0^{\frac{1}{3}} \mathrm{d}s \int_{\max\left(\frac{3s-1}{2s}, -\frac{1}{2}\right)}^{\min\left(\frac{1-3s}{2s}, \frac{1}{2}\right)} \frac{\mathrm{d}t}{\left[\frac{1-s}{2}\right]^2 - s^2t^2} \int_0^\infty \frac{\mathrm{d}K}{K}\mathcal{P}^2(K) \\ & \quad \times \left[\sin\left(\frac{\ln(K/k_*)}{f\phi *}\right) + f\phi_* \sum_i \frac{K}{k_i}\cos\left(\frac{\ln(K/k_*)}{f\phi_*}\right)\right] \\ & \quad \times \Big[\Delta_{l_1}(k_s)\Delta_{l_2}(k_+)\Delta_{l_3}(k_-)I_{(l_1,l_2,l_3)}(s,t) \\ & \qquad + \Delta_{l_2}(k_s)\Delta_{l_1}(k_+)\Delta_{l_3}(k_-)I_{(l_2,l_1,l_3)}(s,t) \\ & \qquad + \Delta_{l_3}(k_s)\Delta_{l_2}(k_+)\Delta_{l_1}(k_-)I_{(l_3,l_2,l_1)}(s,t)\Big]\ . \end{aligned} \tag{7.63}$$

In the above we used that a permutation of two momenta $k_i \leftrightarrow k_j$ translates into a permutation in the l-modes $l_i \leftrightarrow l_j$, as well as the symmetry of the integration over t, which makes the labelling of k_+ and k_- indifferent. We have furthermore introduced the shorthand notation

$$I_{(l_1,l_2,l_3)}(s,t) \equiv I_{(l_1,l_2,l_3)}(k_s, k_+, k_-)\ . \tag{7.64}$$

At the time of writing a code is being developed for computing this integral. It is however yet to be fully operational. The integral in eq. 7.63 should be finite over the entire integration volume, as the transfer functions should go to zero faster than linearly in k as k goes to 0. This conjecture is motivated by the discussion from chapter 6, where we used

$$\Delta_l(k) \approx \frac{1}{3}j_l(k) \tag{7.65}$$

for small l, and $j_l(k) \propto k^{2l}$ for $k \to 0$.

8 Beyond the Bispectrum

It might seem slightly esoteric to consider calculating higher order correlation functions, when we are still waiting for an accurate measurement. There are still valuable things to learn from going beyond the bispectrum, as the computation will not only make it possible to calculate the trispectrum, but also loop corrections to the power spectrum. The fact remains that the quality of measurements improve, tightening the bounds on the spectra, and thus makes it necessary to go beyond the lowest order. Finally some models of inflation may give a large trispectrum without having a particularly large contribution to the bispectrum. This chapter is based on [89].

8.1 The Action to Fourth Order in Uniform Density Gauge

Continuing along the line of chapter 4, we write down the Einstein-Hilbert action in the ADM form (c.f. 4.27 on page 34):

$$S = \frac{1}{2}\int \mathrm{d}t\mathrm{d}^3x\sqrt{h}\Big[N\mathcal{R}_3 - 2NV(\phi) + N^{-1}(E_{ij}E^{ij} - E^2) + N^{-1}(\dot{\phi} - N^i\nabla_i\phi)^2 \\ - Nh^{ij}\nabla_i\phi\nabla_j\phi\Big] \ . \tag{8.1}$$

Working in the comoving curvature gauge:

$$\phi = \phi_c(t) \quad h_{ij} = a(t)^2(e^{2\zeta(\boldsymbol{x},t)}\delta_{ij} + \gamma_{ij}) \ , \ \gamma_{ii} = 0 \quad \partial_i\gamma_{ij} = 0 \ , \tag{8.2}$$

we proceed to expand the perturbation parameters N and N^i to the second order, while neglecting any tensor perturbatinos

$$N = 1 + (\alpha^{(1)} + \alpha^{(2)}) \quad N_i = \partial_i(\chi^{(1)} + \chi^{(2)}) + (\beta_i{}^{(1)} + \beta_i{}^{(2)}) \tag{8.3}$$

with the constraint (cf. Helmholtz theorem)

$$\partial^i\beta_i = 0 \ . \tag{8.4}$$

It is now possible to solve the equations of motion for N^i and N, eq. 4.29 and eq. 4.30 on page 34, respectively, order by order for all three perturbation parameters. As it will turn out, we only need to calculate the first and second order perturbation parameters. The fourth order terms only appears in the action multiplied by the equation of motion for the background field, ϕ_c, while the third order terms cancel one another. From eq. 4.29, by taking the divergence and employing eq. 8.4, one solve for α. Inserting this result back

into eq. 4.29 one can solve for β_i.

PERTURBATION PARAMETERS

Recounting the results of chapter 4, the first order parameters are

$$\alpha^{(1)} = H^{-1}\dot{\zeta} \ . \tag{8.5}$$

and

$$\beta_i{}^{(1)} = 0 \ . \tag{8.6}$$

Utilising the same techniques for the second order contributions, we get

$$\begin{aligned}\alpha^{(2)} = \frac{1}{2H}\partial^{-2}\Big\{&\partial^j\left(\partial_j\alpha^{(1)}\partial^2\chi^{(1)} - \partial_i\alpha^{(1)}\partial^i\partial_j\chi^{(1)}\right) - 2\partial_i\partial_j\left(\partial^j\chi^{(1)}\partial^i\zeta\right)\\ &+ \partial^j\left(\partial_l\zeta\partial^l\partial_j\chi^{(1)}\right) + \partial^j\left(\partial_j\zeta\partial^2\chi^{(1)}\right)\Big\}\end{aligned} \tag{8.7}$$

for the scalar part, and

$$\begin{aligned}\beta_j{}^{(2)} = 2\partial^{-2}\Big\{&\partial_j\alpha^{(1)}\partial^2\chi^{(1)} - \partial_i\alpha^{(1)}\partial^i\partial_j\chi^{(1)} + \partial_j\zeta\partial^2\chi^{(1)} - 2H\partial_j\alpha^{(2)}\\ &- \partial_i\left(\partial_j\chi^{(1)}\partial^i\zeta + \partial^i\chi^{(1)}\partial_j\zeta\right) + \partial_l\zeta\partial^l\partial_j\chi^{(1)}\Big\}\end{aligned} \tag{8.8}$$

for the vector perturbation. In the equations above $\chi^{(1)}$ is the first order part of the third perturbation parameter, which will be addressed in a moment. From this we see, that α to the lowest order only describe how the metric changes in time, as could be expected from its role in the metric.

Similarly we can solve eq. 4.30 for the χ parameters, whereby one gets

$$\chi^{(1)} = -\frac{\zeta}{H} + \xi \quad , \quad \partial^2\xi = \frac{H^{-2}}{2}\dot{\phi}^2\dot{\zeta} \tag{8.9}$$

to the first order [22]. Likewise to the second order in χ, we obtain (for readability we refrain from inserting the values of the α and β)

$$\begin{aligned}4H\partial^2\chi^{(2)} = &-2\left(\partial\zeta\right)^2 + 2(\dot{\phi}^2 - 6H^2)\alpha^{(2)} + 4\dot{\zeta}\partial^2\chi^{(1)} + 4\dot{\phi}^2\alpha^{(1)}\zeta\\ &- 4H\partial_l\chi^{(1)}\partial^l\zeta - 3{\alpha^{(1)}}^2\dot{\phi}^2 + \partial^2\chi^{(1)}\partial^2\chi^{(1)} - \partial_i\partial_j\chi^{(1)}\partial^i\partial^j\chi^{(1)}\end{aligned} \tag{8.10}$$

It is seen, that the β and χ parameters of a given order depends on the α parameter of the same order, as opposed to the α that only depends on parameters of lower orders. This translates into a dependence of the lapse function in the shift parameter, which is reasonable as the lapse function is linked to the thickness of the time-slices, and in that way affect the size of the shift.

FOURTH ORDER ACTION

Truncating the action at the fourth order and exploiting the equation of motion for the background field

$$\dot{\phi}^2 - 6H^2 + 2V = 0 \ , \tag{8.11}$$

we write the action in terms of the perturbation parameters, and simplify it by using partial spatial integrations. This gives

$$
\begin{aligned}
S^{(4)} = \frac{1}{2}\int \mathrm{d}t\mathrm{d}^3x a^3 \Bigg\{ & -\frac{1}{3}\zeta^3\partial^2\zeta - 2\alpha^{(1)}(\zeta\partial_i\zeta\partial^i\zeta + \zeta^2\partial^2\zeta) + \dot{\phi}_c^2\alpha^{(1)2}\left[\frac{9}{2}\zeta^2 - 3\zeta\alpha^{(1)} + \alpha^{(1)2}\right] \\
& \left[\frac{1}{2}\zeta^2 + \zeta\alpha^{(1)} + \alpha^{(1)2}\right]\left[\partial_i\partial_j\chi^{(1)}\partial^i\partial^j\chi^{(1)} - \partial^2\chi^{(1)}\partial^2\chi^{(1)}\right] + (6H^2 - \dot{\phi}^2)\alpha^{(2)2} \\
& - 2[\zeta + \alpha^{(1)}]\left[\partial_i\partial_j\chi^{(1)}\partial^i\partial^j\chi^{(2)} - \partial^2\chi^{(1)}\partial^2\chi^{(2)} - 2\partial_i\partial_j\chi^{(1)}\partial^i\chi^{(1)}\partial^j\zeta\right] \\
& - 2\left[2\partial_i\partial_j\chi^{(2)}\partial^i\chi^{(1)}\partial^j\zeta + 2\partial_i\partial_j\chi^{(1)}\partial^i\chi^{(2)}\partial^j\zeta - \partial_j\chi^{(1)}\partial_i\zeta\partial^i\chi^{(1)}\partial^j\zeta\right] \\
& + \frac{1}{2}\partial_i\beta_j{}^{(2)}\partial^i\beta^{j\,(2)} - 2\alpha^{(1)}\partial_i\partial_j\chi^{(1)}\partial^i\beta^{j\,(2)}\Bigg\}
\end{aligned}
\tag{8.12}
$$

Though fairly compact in its presentation, it is not clear from this form that the action in eq. 8.12 does indeed vanish in the slow roll limit. The zeroth order slow-roll terms can however be removed by partial integrations. To make this more evident, it is simpler to expand the gauge transformation (eq. 5.50 on page 46) between the isocurvature gauge and the present gauge, in order to calculate the action by a gauge transformation of the equivalent action in the uniform curvature gauge.

Furthermore one is faced with the same complications as those discussed in chapter 5, if one tries to perform a computation using the version of the action in eq. 8.12. It is therefore prudent to compute the gauge transformation.

8.2 GAUGE TRANSFORMATION

Deriving the gauge transformation in a slightly more rigourous fashion than in chapter 5, we perform a translation in the time coordinate in order to transform between the isocurvature gauge and the comoving gauge. Below we follow a procedure, which is similar to the one in ref. [22]. The uniform curvature gauge is given by

$$
\phi(t,\boldsymbol{x}) = \phi_c(t) + \delta\phi(t,\boldsymbol{x}) \ , \ h_{ij} = a(t)^2\delta_{ij} \ , \tag{8.13}
$$

where we have defined the background field $\phi_c \equiv \langle\phi\rangle$, such that the tadpole condition, $\langle\delta\phi\rangle = 0$, is satisfied.

Choosing the time translation given by the vector $\xi_\mu = (T,0,0,0)$, we can write the transformed field fluctuation [90]

$$
\delta\phi(x_\mu + \xi_\mu) = \delta\phi(x_\mu) + \sum_{n=1}^{\infty}\frac{(\xi_\mu\partial^\mu)^n}{n!}\phi(x_\mu) \ . \tag{8.14}
$$

The sum is nothing more than the Taylor expansion along a vector. Requirering the time translation to bring the coordinates to the comoving gauge, we fix ξ_μ by $\delta\phi(x_\mu + \xi_\mu) = 0$.

Evolving order by order we then get for $\xi_0 = T^{(1)} + T^{(2)} + \dots$.

$$T^{(1)} = -\frac{\delta\phi}{\dot{\phi}_c} \tag{8.15}$$

$$T^{(2)} = \frac{\delta\phi\dot{\delta\phi}}{\dot{\phi}_c^2} - \frac{1}{2}\frac{\ddot{\phi}_c}{\dot{\phi}_c^3}\delta\phi^2 \tag{8.16}$$

$$T^{(3)} = \frac{3}{2}\frac{\ddot{\phi}_c}{\dot{\phi}_c^4}\delta\phi^2\dot{\delta\phi} - \frac{1}{2}\frac{\delta\phi^2}{\dot{\phi}_c^3}\ddot{\delta\phi} - \frac{\delta\phi\dot{\delta\phi}^2}{\dot{\phi}_c^3} - \left(\frac{1}{2}\frac{\ddot{\phi}_c^2}{\dot{\phi}_c^5} - \frac{1}{6}\frac{\dddot{\phi}_c}{\dot{\phi}_c^4}\right)\delta\phi^3 \tag{8.17}$$

As a method for finding the relation between ζ in the comoving gauge and $\delta\phi$ in the uniform curvature gauge, we perform coordinate transformation above in the metric associated with the uniform curvature gauge ($g_{\mu\nu}^{(\mathrm{uc})}$) and equate it with metric in the comoving gauge ($g_{\mu\nu}^{(\mathrm{cm})}$).

The spatial part of the metric gives after the time translation (again ignoring tensor contributions)

$$h_{ij}^{(\mathrm{cm})} = a^2(t+T)\delta_{ij} - N^2\partial_i T\partial_j T + \partial_i T N_j + \partial_j T N_i \ , \tag{8.18}$$

with N and N_i defined as in eq. 8.3. Solving the first order contribution in the above equation gives $\zeta = HT$ or [22]

$$\zeta = -H\frac{\delta\phi}{\dot{\phi}_c} \equiv \zeta_n \ . \tag{8.19}$$

No spatial reparametrization is needed for the first order. To higher orders one must do a transformation $x_i \to x_i + \upsilon_i$, such that

$$-N^2\partial_i T\partial_j T + (\partial_i T N_j + \partial_j T N_i) + \partial_i\upsilon_j + \partial_j\upsilon_i = \exp\left(2\sum_n \iota_n\right) a^2(t)\eta_{ij} \tag{8.20}$$

with ι_n being a parameter of the n'th order. Recalling that $\iota_1 = 0$ and writing $a(t) = e^{\rho(t)}$ like in ref. [22], we can write the equation for ζ up to third order

$$\zeta = \rho(t+T) - \rho(t) + (\iota_2 + \iota_3) \tag{8.21}$$

By taking the trace and $\partial^i\partial^j$ of eq. 8.20, one can solve to second order

$$4\iota_2 = 2\partial^i T^{(1)}\partial_i{\chi_\phi}^{(1)} - 2\partial^{-2}\partial^i\partial^j(\partial_i T^{(1)}\partial_j{\chi_\phi}^{(1)}) - (\partial_i T^{(1)}\partial^i T^{(1)} - \partial^{-2}\partial^i\partial^j(\partial_i T^{(1)}\partial_j T^{(1)})) \tag{8.22}$$

as ${\beta_i}^{(1)} = 0$. Thereby giving [22]

$$\begin{aligned}\zeta = \zeta_n - f_2(\zeta_n) =& \zeta_n + \frac{1}{2}\frac{\ddot{\phi}_c}{\dot{\phi}_c H}\zeta_n^2 + \frac{1}{4}\frac{\dot{\phi}_c^2}{H^2}\zeta_n^2 + \frac{\zeta_n\dot{\zeta}_n}{H} + \frac{1}{2}\partial^i\zeta_n\partial_i{\chi_\phi}^{(1)} - \frac{1}{2}\partial^{-2}\partial^i\partial^j(\partial_i\zeta_n\partial_j{\chi_\phi}^{(1)}) \\ &- \frac{1}{4H^2}\left(\partial_i\zeta_n\partial^i\zeta_n - \partial^{-2}\partial^i\partial^j(\partial_i\zeta_n\partial_j\zeta_n)\right)\end{aligned} \tag{8.23}$$

where we implicitly defined $f_2(\zeta_n)$. We refer to appendix A for the definitions of the functions of the type ${\alpha_\phi}^{(i)}$, ${\chi_\phi}^{(i)}$, and ${\beta_\phi}^{(i)}$. Computing the third order terms in a similar

fashion, we get

$$\begin{aligned}2\iota_3 =&\partial^i T^{(1)}\partial_i {\chi_\phi}^{(2)} + \partial^i T^{(1)}{\beta_{\phi_i}}^{(2)} + \partial^i T^{(2)}\partial_i {\chi_\phi}^{(1)} - \partial^{-2}\partial^i\partial^j(\partial_i T^{(1)}\partial_j {\chi_\phi}^{(2)})\\ &- \partial^{-2}\partial^j(\partial^i\partial_j T^{(1)}{\beta_{\phi_i}}^{(2)}) - \partial^{-2}\partial^i\partial^j(\partial_i T^{(2)}\partial_j {\chi_\phi}^{(1)})\\ &- [\partial_i T^{(1)}\partial^i T^{(2)} - \partial^{-2}\partial^i\partial^j(\partial_i T^{(1)}\partial_j T^{(2)})]\\ &- {\alpha_\phi}^{(1)}[\partial_i T^{(1)}\partial^i T^{(1)} - \partial^{-2}\partial^i\partial^j(\partial_i T^{(1)}\partial_j T^{(1)})]\end{aligned} \tag{8.24}$$

Repeating the calculation leading to eq. 8.23, we arrive at

$$\begin{aligned}\zeta =&\zeta_n - f_2(\zeta_n) - f_3(\zeta_n)\\ =&\zeta_n - f_2(\zeta_n)\\ &+ \frac{5}{6}\frac{\dot\phi_c\ddot\phi_c}{H^3}\zeta_n^3 + \frac{1}{3}\frac{\dddot\phi_c}{\dot\phi_c H^2}\zeta_n^3 + \frac{1}{4}\frac{\dot\phi_c^4}{H^4}\zeta_n^3 + \frac{3}{2}\frac{\ddot\phi_c}{\dot\phi_c H}\zeta_n^2\dot\zeta_n + \frac{\dot\phi_c^2}{H^3}\zeta_n^2\dot\zeta_n + \frac{\zeta_n\dot\zeta_n^2}{H^2}\\ &+ \frac{1}{2}\frac{\zeta_n^2\ddot\zeta_n}{H^2} + \frac{1}{2H}\partial^i\zeta_n\partial_i {\chi_\phi}^{(2)} + \frac{1}{2H}\partial^i\zeta_n{\beta_{\phi_i}}^{(2)}\\ &+ \frac{1}{2}\left[\frac{\ddot\phi_c}{\dot\phi_c H^2}\zeta_n + H^{-1}\dot\zeta_n + \frac{\dot\phi_c^2}{H^2}\zeta_n\right]\left[\frac{\dot\phi_c^2}{2H^2}\partial^i\zeta_n\partial_i\partial^{-2}\dot\zeta_n - H^{-1}\partial^i\zeta_n\partial_i\zeta_n\right]\\ &+ \frac{\zeta_n}{2H^2}\left(\frac{\dot\phi_c^2}{2H^2}\partial^i\dot\zeta_n\partial_i\partial^{-2}\dot\zeta_n - H^{-1}\partial^i\dot\zeta_n\partial_i\zeta_n\right) - \frac{1}{2H}\partial^{-2}\partial^i\partial^j\left(\partial_i\zeta_n\partial_j {\chi_\phi}^{(2)}\right)\\ &- \frac{\partial^{-2}\partial^i\partial^j}{2}\left\{\left[\frac{\ddot\phi_c}{\dot\phi_c H^2}\zeta_n + H^{-1}\dot\zeta_n + \frac{\dot\phi_c^2}{H^2}\zeta_n\right]\left[\frac{\dot\phi_c^2}{2H^2}\partial_i\zeta_n\partial_j\partial^{-2}\dot\zeta_n - H^{-1}\partial_i\zeta_n\partial_j\zeta_n\right]\right\}\\ &- \partial^{-2}\partial^i\partial^j\left[\frac{\zeta_n}{2H^2}\left(\frac{\dot\phi_c^2}{2H^2}\partial_i\dot\zeta_n\partial_j\partial^{-2}\dot\zeta_n - H^{-1}\partial_i\dot\zeta_n\partial_j\zeta_n\right)\right] - \frac{1}{2H}\partial^{-2}\partial^j(\partial^i\partial_j\zeta_n{\beta_{\phi_i}}^{(2)})\\ &+ \frac{\dot\phi_c^2\zeta_n}{4H^4}\left[\partial_i\zeta_n\partial^i\zeta_n - \partial^{-2}\partial^i\partial^j(\partial_i\zeta_n\partial_j\zeta_n)\right]\ ,\end{aligned} \tag{8.25}$$

where we have implicitly defined the third order contribution in terms of $f_3(\zeta_n)$. Again we refer to appendix A for the definition of functions of the type ${\alpha_\phi}^{(i)}$, ${\chi_\phi}^{(i)}$, and ${\beta_\phi}^{(i)}$.

By inverting eq. 8.25 to third order and recalling the definition of ζ_n from eq. 8.19, we are able to calculate the fourth order action of the metric perturbations in the comoving gauge from the action of the inflaton field fluctuations in the uniform curvature gauge. Since the calculation is trivial but tedious, we will not repeat it here in all details. However, from the calculation, one would obtain an action for ζ which is suppressed by only one power of the slow-roll parameter. This can be seen from the gauge transformation above, which contains terms in f_3 of order ζ_n^3, but with no slow-roll suppression. To third order in the gauge transformation we can just replace ζ_n with ζ in f_3, and applied in the second order action for $\delta\phi$ we see immediately that the fourth order action in ζ will receive contributions, which are only suppressed by one slow-roll order. From this one could easily be led to believe, that the trispectrum of the metric perturbation ζ is of the wrong order in the slow-roll parameter ϵ.

However, since all the leading order slow-roll terms comes from using f_3 in the second order action in $\delta\phi$, by partial integrations they can all be rewritten as terms in the action

proportional to the linear equation of motion of perturbations. This complication can be avoided by choosing the gauge of ζ_n, then calculate $\langle\zeta_n^4\rangle$, and afterwards obtaining the super-horizon value of $\langle\zeta^4\rangle$ by virtue of the super-horizon limit of eq. 8.25, analogous to the calculation in ref. [22]. Once the terms proportional to the linear perturbation equation of motion have been eliminated by a change of variables $\zeta \to \zeta_n$, one obtains an action in ζ_n, which is suppressed by two powers of the slow-roll parameter. The full action in the new variable ζ_n has the following form

$$\begin{aligned} S_{\zeta_n} = \int \mathrm{d}t\mathrm{d}^3x a^3 \Bigg\{ & -\frac{\epsilon_H^2}{6}V''''\zeta_n^4 + \frac{1}{2}\partial_i\beta_{\phi_j}{}^{(2)}\partial^i\beta_\phi{}^{j\,(2)} + \epsilon_H^3\partial_i\partial^{-2}\dot\zeta_n\partial_j\partial^{-2}\dot\zeta_n\partial^i\zeta_n\partial^j\zeta_n \\ & - 2\epsilon_H\left[-H\eta_H\zeta_n + \dot\zeta_n\right]\left[\partial_i\chi_\phi{}^{(2)} + \beta_{\phi_i}{}^{(2)}\right]\partial^i\zeta_n \\ & + \alpha_\phi{}^{(2)}\left[-6H^2 + \dot\phi_c^2\right]\left[\epsilon_H^2\zeta_n^2 - \frac{\alpha_\phi{}^{(2)}}{2}\right] \\ & - \epsilon_H^2\zeta_n\Big[\big(\frac{\dot\phi_c}{3H}V''' + 2H^2\eta_H\epsilon_H^2 - H^2\kappa_H\epsilon_H + 3H^2\epsilon_H(\eta_H - \epsilon_H)\big)\zeta_n^3 \\ & + \partial^2\chi_\phi{}^{(2)}\dot\zeta_n + \epsilon_H\zeta_n\partial_i\zeta_n\partial^i\zeta_n - \partial_i\partial_j\chi_\phi{}^{(2)}\partial^i\partial^j\partial^{-2}\dot\zeta_n \\ & - \partial_i\beta_{\phi_j}{}^{(2)}\partial^i\partial^j\partial^{-2}\dot\zeta_n + 2\epsilon_H(2(\epsilon_H - \eta_H)H\zeta_n + \dot\zeta_n)\partial_i\zeta_n\partial^i\partial^{-2}\dot\zeta_n\Big]\Bigg\}\,, \end{aligned} \tag{8.26}$$

where we have introduced the slow roll parameters associated with the Hamilton-Jacobi formalism:

$$\epsilon_H = 2M_{\rm pl}\left(\tfrac{H'(\phi)}{H(\phi)}\right)^2 = \frac{1}{2M_{\rm pl}}\frac{\dot\phi^2}{H^2} \tag{8.27}$$

$$\eta_H = 2M_{\rm pl}\tfrac{H''(\phi)}{H(\phi)} = -\frac{\ddot\phi}{H\dot\phi}\,. \tag{8.28}$$

We have further more added a second order parameter

$$\kappa_H = 2M_{\rm pl}{}^2\frac{H'''(\phi)H'(\phi)}{H(\phi)^2} + \eta_H^2 = \frac{\dddot\phi}{H^2\dot\phi}\,. \tag{8.29}$$

To leading order they are related to the usual slow-roll parameters by $\epsilon_H \approx \epsilon$, $\eta_H \approx \eta - \epsilon$.

8.3 THE DE SITTER LIMIT

Since the curvature perturbation is a pure gauge mode in de Sitter space, the action of the comoving curvature perturbation ζ must be slow-roll suppressed to all orders in perturbations and vanish in the de Sitter limit. However, this does not explain why the third and fourth order action of ζ_n are actually suppressed by the same power of the slow-roll parameter. If we want to estimate the slow-roll order of the n-point function of ζ, we would overestimate it, if we only assumed that the action of ζ has to be slow-roll suppressed.

In fact, the slow-roll order of the action is more easily understood in the uniform curvature gauge. In this gauge, it has been shown that the third order action of the inflaton field fluctuations, $S_3(\delta\phi)$, is suppressed by the square root of the slow-roll parameters [22], while the second, and fourth order actions, $S_2(\delta\phi)$, $S_4(\delta\phi)$, are unsuppressed [27, 91]. Thus, we may wonder what requires the third order action, $S_3(\delta\phi)$, to be slow-roll suppressed, when there is nothing which forces the second and fourth order actions to be slow-roll suppressed.

However, if there are third order terms of $\delta\phi$ in the action, which are unsuppressed and survive in the pure de Sitter limit, they would indicate an instability of the classical de Sitter vacuum. As an example, we will study a toy unsuppressed third order term. In the fourth order action there are unsuppressed terms of the type $\dot{\delta\phi}^2\partial^{-2}(\partial_i\dot{\delta\phi}\partial^i\delta\phi)$ etc. Let us assume for a moment that to third order we have similar unsuppressed terms induced by perturbations of the metric. Then the interaction Hamiltonian for the perturbations will take the form

$$H_I = \int d^3y a^3 \left[\delta\phi(\ddot{\phi}_c + 3H\dot{\phi}_c + V') + gO(\delta\phi^3) + \dots\right] , \tag{8.30}$$

where the unsuppressed $O(\delta\phi^3)$ toy term could be any operator of the type $\delta\phi^3$, $\dot{\delta\phi}^2\delta\phi$, $\dot{\delta\phi}\partial^{-2}(\partial_i\dot{\delta\phi}\partial^i\delta\phi)$, etc. The dots represents any terms to higher order in slow-roll and perturbation theory, and g is a coupling constant.

The term $O(\delta\phi^3)$ will give a contribution to the tadpole diagram in figure 8.1, which will lead to a one-loop correction to the equation of motion of the classical background field. The tadpole condition yields

$$0 = \langle\delta\phi\rangle = \ddot{\phi}_c + 3H\dot{\phi}_c + V' + g\Gamma_t , \tag{8.31}$$

where $g\Gamma_t$ denotes the amputated tadpole contribution, and gives the one-loop correction to the background equation of motion. In the simplest case of a massless scalar field and with $O(\delta\phi^3) = H\delta\phi^3$, the tadpole contribution would become

$$g\Gamma_t = 3gH\left\langle\delta\phi^2\right\rangle = \frac{3g}{4\pi^2}H^4t . \tag{8.32}$$

In this case, the time-independent de Sitter solution is destabilized by the tadpole. If the toy term $O(\delta\phi^3)$ has a more complicated form involving derivatives, the infrared divergency will be absent[3], and the tadpole contribution will not grow indefinitely, but rather approach a constant. However, in the case of a massless scaler field in de Sitter, a time-independent tadpole contribution $g\Gamma_t = const.$ will give an effective linear contribution to the potential of the background term, similar to a source term, which will yield the potential of the massless field unbounded from below. In fact, the solution to eq. 8.31, with $V' = 0$ and $g\Gamma_t = const.$ at late times is

$$\phi_c(t) = -\frac{g\Gamma_t}{3H}t, \tag{8.33}$$

[3]The actual tadpole was calculated to leading order in slow-roll in ref. [92]. Note, that to leading order in slow-roll, the IR divergent terms are not present. The IR divergent contributions to the tadpole, which will dominate the tadpole contribution at late times, appears to higher order in slow-roll, and can be found by taking the appropriate infrared limit in the action as in ref. [91, 93].

which is inconsistent with a time-independent de Sitter solution. Thus, if unsuppressed third order terms were allowed, classical de Sitter space with a massless scalar field would be destabilized.

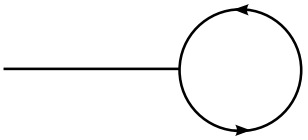

Figure 8.1: Tadpole diagram

Since any unsuppressed odd order terms in the action would lead to a non-vanishing tadpole contribution, we conclude that all odd order terms in the action should be slow-roll suppressed, while even order terms are not slow-roll suppressed. We can then extrapolate our results from $n \leq 4$ to any n, as shown in table 1. Using the extrapolation in table 1, we can calculate the order of magnitude of any n-point correlation function in single field inflation, as shown in table 2. We can also generalize the nonlinearity parameter $f_{\rm NL}$ to n'th order up to a numerical factor of order one

$$\langle \zeta^n \rangle \approx f_{\rm NL}^{(n)} \mathcal{P}_\zeta^{n-1} \ , \tag{8.34}$$

where $\mathcal{P}_\zeta$ is the power-spectrum of comoving curvature perturbations. To second order the generalized nonlinearity parameter coincides with the usual one $f_{\rm NL}^{(3)} = f_{\rm NL}$ for the bi-spectrum, which was initially calculated in ref. [22, 94]. To third order it coincides with the nonlinearity parameter for the tri-spectrum $f_{\rm NL}^{(4)} = \tau_{NL}$, which was calculated in ref. [27].

Order	$S(\delta\phi)$	$S(\zeta_n)$	$S(\zeta)$
2nd	$\mathcal{O}(1)$	$\mathcal{O}(\epsilon)$	$\mathcal{O}(\epsilon)$
3rd	$\mathcal{O}(\epsilon^{1/2})$	$\mathcal{O}(\epsilon^2)$	$\mathcal{O}(\epsilon)$
4rd	$\mathcal{O}(1)$	$\mathcal{O}(\epsilon^2)$	$\mathcal{O}(\epsilon)$
$2n$th	$\mathcal{O}(1)$	$\mathcal{O}(\epsilon^n)$	$\mathcal{O}(\epsilon)$
$(2n+1)$th	$\mathcal{O}(\epsilon^{1/2})$	$\mathcal{O}(\epsilon^{n+1})$	$\mathcal{O}(\epsilon)$

Table 8.1: Slow-roll order of the action to n'th order.

p	$\langle \delta\phi^p \rangle$	$\langle \zeta^p \rangle$	$f_{\rm NL}^{(p)} \approx \langle \zeta^p \rangle / \mathcal{P}_\zeta^{p-1}$
2	$\mathcal{O}(H^2)$	$\mathcal{O}(\epsilon^{-1} H^2)$	$\mathcal{O}(1)$
3	$\mathcal{O}(\epsilon^{1/2} H^4)$	$\mathcal{O}(\epsilon^{-1} H^4)$	$\mathcal{O}(\epsilon)$
4	$\mathcal{O}(H^6)$	$\mathcal{O}(\epsilon^{-2} H^6)$	$\mathcal{O}(\epsilon)$
$2n$	$\mathcal{O}(H^{2p-2})$	$\mathcal{O}(\epsilon^{-p/2} H^{2p-2})$	$\mathcal{O}(\epsilon^{p/2-1})$
$2n+1$	$\mathcal{O}(\epsilon^{1/2} H^{2p-2})$	$\mathcal{O}(\epsilon^{(1-p)/2} H^{2p-2}))$	$\mathcal{O}(\epsilon^{(p-1)/2})$

Table 8.2: Slow-roll order of the n-point functions and generalized nonlinearity parameter.

It is easy to verify that the action $S(\delta\phi)$ to any even order, $2n$, in perturbations will be unsuppressed in the slow-roll parameters, as it will contain contributions from $\alpha^{(2)2n}$,

which is unsuppressed in the slow-roll parameters. Similarly, to odd orders $\alpha^{(2)}$ will always appear in combination with some $\alpha^{(n)}$ or $\chi^{(n)}$ to odd order, say $\alpha^{(1)}$ which is slow-roll suppressed.

As an example we predict that the nonlinearity parameter related to the 5- and 6-point function is $f_{NL}^{(5)} = f_{NL}^{(6)} = \epsilon^2$.

Finally, let us briefly discuss what would be the effect of including gravitational wave modes in the analysis. For gravitational waves the discussion of the de Sitter limit is a little more involved. One can have unsuppressed odd n-terms in the action with gravitational waves, γ_{ij}, of the form $\partial_i\delta\phi\partial_j\delta\phi\gamma^{ij}$, since they will not contribute to the tadpole of the scalar field fluctuation. However, terms like $\delta\phi\dot{\gamma}_{ij}\dot{\gamma}^{ij}$ have to be slow-roll suppressed, because they will contribute to the tadpole with a graviton circulating in the loop. This agrees with the results of ref. [22], where the third order action including gravitational waves has been calculated.

8.4 CHALLENGES OF NUMERICAL COMPUTATION

When one tries to repeat the approach of chapter 5 to calculate the trispectrum numerically, one is faced with an enormous complication in the sheer number of terms needed to be calculated when computing the four-point function from the action in eq. 8.26 on page 76. One can certainly do a fair approximation for fast roll models by only extracting the terms, that contain derivatives of the second slow roll parameter η_H, but this would only be a reasonable description right at the fast roll feature in the potential.

Even if one writes down all the terms for calculation, one has to contemplate the way one represents the quadrangle formed by the momenta of the four-point function. As it turns out it is no longer sufficient to describe the momenta by their lengths once one go beyond the bispectrum.

Regarding n vectors in a D-dimensional momentum space, one has, at first glance, Dn degrees of freedom (DOF). The requirement of momentum conservation discards D of these DOF. The further requirement of isotropy makes it possible to rotate the structure in a suitable way, removing $D-1$ DOF from the first vector, $D-2$ from the second and so forth. This leaves

$$\mathrm{DOF} = D(n-1) - \frac{D(D-1)}{2} + \frac{\max(0, D-n)\left[\max(0, D-n)+1\right]}{2} \tag{8.35}$$

for $n \geq 2$. For four vectors in three dimensions this implies that one needs six parameters to describe the quadrangle.

One realisation of this could be the size of the four momenta, the length of the two diagonals (α and β). See figure 8.2 on the following page. These additional DOF adds a plethora of signature configurations, extending far beyond the three of the momentum triangle. Regarding the quadrangle as two triangles, one can apply the ideas of the three types of triangles to the quadrangle to get a handle of the types. Some of these were discussed in chapter 5. Among these are the squeezed limits $k_1 = k_2 = k_3 \gg k_4$ and $k_1 = k_2 \gg k_3 \gg k_4$, as well as the counter-collinear limit. This last can be expressed having one of the diagonals going to zero.

Finally one can imagine special cases inspired by definition of τ_{NL} (eq. 3.43 on page 29). The equivalent case of the equilateral triangle would be a rhombus twisted in three dimensions, defined by $k_1 = k_2 = k_3 = k_4 = k$. Such a configuration reduces the the number of

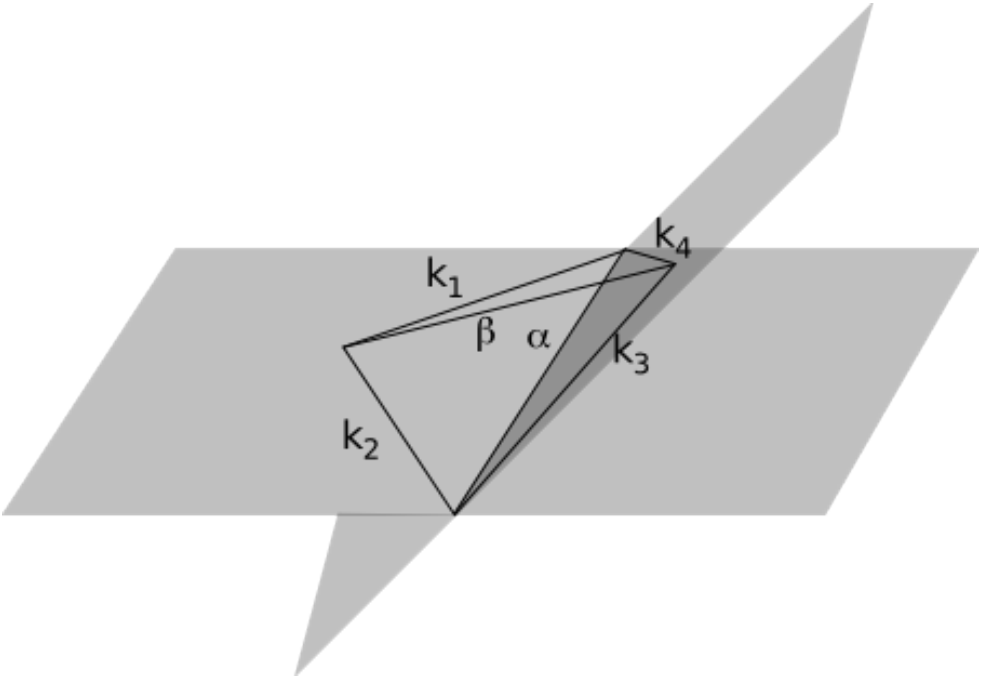

Figure 8.2: Momentum quadrangle parameterized in terms of the lengths and diagonals

terms in the definition of τ_{NL} to two as only the diagonals α and β differ. Another option would be to keep the diagonals equal ($\alpha = \beta$) reducing the number of terms to six. A configuration where the momenta are pair wise orthogonal would reduce the number of terms in the integral, but besides from that such a configuration would not offer any form of simplification.

The combination of the former two cases with $k_1 = k_2 = k_3 = k_4 = \alpha = \beta = k$, forming a regular tetrahedron, reduces all the inner product between momenta to

$$\boldsymbol{k}_i \cdot \boldsymbol{k}_{\boldsymbol{j}} = \pm \frac{k_i k_j}{2} \ , \tag{8.36}$$

reducing complexity of the integrals greatly (see further eq. 8.26 on page 76)

It could be interesting to categorise which quadrangle shapes give a large trispectrum, much like the discussion of triangle shapes and the bispectrum at the end of chapter 4.

9 Concluding Remarks

As inflation is about to enter its fourth decade as a cosmological theory, it has nestled itself firmly as the prominent description of the primordial dynamic of the Universe. Though other scenarios are present [95, 96], inflation is still the preferred choice in the literature. That is not to say, that inflation is without issues at the moment. One still needs to get a detection of a signal that cannot be generated in any other plausible scenario than inflation. A detection of a tensor-to-scalar ratio, and perhaps a non-Gaussian signal, would firmly settle inflation as a great model for the primordial universe, and might even give hint of which direction one should take the search for a theory of inflation. At the moment the success of inflation rests on its simplicity and the ability to solve the Flatness Problem and the Horizon Problem (see chapter 2), as well as producing the nearly scale invariant power spectrum in a very generic way (see chapter 4).

Even if one imagines that the Planck satellite do detect a tell tale signal for inflation, many questions concerning the early universe still need to be resolved. One still has to settle the matters of initiating and ending inflation (discussed towards the end of chapter 1). To trigger the onset of inflation, one needs to deplete the inflaton of its kinetic energy and remain in slow roll for the duration of inflation. Secondly the initial patch that inflates to become our universe may contain initial inhomogeneities that could hinder the accelerated expansion (see e.g. [71, 97] for a further discussion). The matter of ending inflation seems slightly more concrete as it often happens at energies where the current theories are more justified. There is, however, still a large task ahead for anyone trying to work out the exact details of what goes on, when inflation ends. The solution of these two problems is essential for gaining a complete understanding of inflation and testing whether or not it is the correct scenario for the early universe.

Since its emergence in 1981 [14], inflation has matured as a concept. The focus has shifted from merely achieving and sustaining inflation to investigating the perturbations created by the inflaton. Concentrating on creating the required primordial spectrum, models became more elaborate and the body of inflationary models seemed to expand insatiably [37, 38]. Today many of these models have been investigated beyond lowest order. Many types have been classified depending on the kind and amount of non-Gaussian signature they produce.

One such model was investigated in chapter 5. This model, the axion monodromy model, comes from a certain realisation of string theory. The model produces a distinct oscillation in both the power spectrum and the bispectrum, but where the oscillations in the power spectrum is below the detection limit, one would clearly see the signature in the f_{NL} with measurements by the Planck satellite. As part of the axion monodromy work, a

code was developed by Troels Haugbølle to numerically calculate the three-point function for inflationary models with a single scalar field. From the simulations it was seen that this model is capable of producing a value of $f_{\rm NL}$ that could be detected with Planck. Furthermore we derived an empirical formula for the shape of $f_{\rm NL}$ for isosceles triangles. This result was later confirmed by the general derivation of the three-point function for the axion monodromy model in [70].

With the increasing quality of observations one should strive to go beyond simply computing the temperature anisotropy bispectrum, and through that $f_{\rm NL}$, and compute both the trispectrum and the remaining bispectra. The increasing observational sensitivity translates into an added constraint on the power spectrum and trispectrum. To calculate this in single scalar field models, one needs the fourth order action, which was calculated and discussed in chapter 8. This action, along with the accompanying gauge transformation, is necessary to distinguish between models once a detection of $f_{\rm NL}$ has been made. It is possible to produce many different models, that will give the same bispectrum (much like the degeneracy seen with the power spectrum), but each time one adds new type of observed spectrum, the reins are pulled tighter limiting the possibilities within the possible models. Finally it was explained in chapter 8, why one would expect that any even order of the action for field perturbations is not suppressed by slow roll parameters. This arises from the fact that these terms do not contribute to the tadpole's expectation value, which must vanish in the de Sitter limit.

Comparing a calculated primordial $f_{\rm NL}$ to the observed one is by no means an easy feat. One could easily have the impression that once the cumbersome task of calculating a primordial $f_{\rm NL}$ is finished, the process of evolving the result from the end of inflation to present time is straight forward. This is, however, not the case and the computation will, in fact, involve integrals that are numerically difficult to carry out. This was the topic of chapter 7, which summarises a work in progress. Here we developed a recursion scheme for calculating the integral over the spherical Bessel functions, and in that way avoid having to perform a difficult numerical computation. The method was demonstrated on the two triangles with $l_1+l_2+l_3=4$. These triangles, $(1,1,2)$ and $(0,2,2)$, are the first non-trivial triangles one encounters when using the recursive scheme. This demonstration showed that the calculated integrals were well defined for both the squeezed and flattened limits. One would expect that this would hold true for any triangle, but that was only showed, in part, for the triangles of the type $(0,l,l)$. At the time of writing, we still need to completely debug and optimise the code for computing the remaining integrals.

In a time where we are on the verge of obtaining what could be the first positive detection of $f_{\rm NL}$ and quite possibly the shape of it, it is alluring to believe, that it is only a matter of time before one finds the correct model of inflation. One should, however, remember that many models will be able to produce the same signatures, and reconstructing the potential from observations seems discouraging as the inflaton only tracks a small part of the potential during inflation [98, 99, 100]. Though this complicates matters greatly, it does not make the quest futile.

Instead of seeing inflation as the one and only tool for making inference on high energy physics, it should stand as one test among many that any theory of high energy physics must face. In this sense cosmology, and especially inflation, is a great laboratory capable of probing energy ranges that we cannot probe here on Earth. This comes, of course, at the cost of having a considerable less controlled environment and very little to say in the timing of experiments, but history has showed that with audacious study and great

patience these are complications, that we can overcome. Cosmology has emerged as, and will most likely remain, a prolific source for generating and answering the fundamental questions of nature.

There were so many fewer questions,
When stars were still just the holes to Heaven
- Jack Johnson

Acknowledgements

Though these 80-odd pages have been compiled in a few months, they are a the result of four years of work and many more years of living and dreaming. The thesis from cover to cover holds a road map of the paths my life has taken over the last years, a string of memories both good and bad. As one traverses such a landscape of experiences a lot of gratitude accumulates. Mentioning all that deserves a word would double the length of this work, and I will therefore try to limit the specifics.

First of all I would like to thank my supervisor **Steen Hannestad**, who have guided me through the last four years with a philosophy, that allowed me the freedom to explore the ideas, that I found interesting, but at the same time always seemed to be there with careful advice, when it was called for. Under Steen's supervision I have certainly learned to be more independent. This was a lesson he taught me from day one, when he left me in the care of a local television news crew for an afternoon of interviews at selected sites in Aarhus. The next day his only comment was: "I knew you could handle it, and you did fine".

As my second supervisor **Martin S. Sloth** still stands as the one, who got me involved with inflation and those maddening long equations. This turned out to be an interesting process of calculating, recalculating and rethinking, interspersed with trips to Martin's office for yet another discussion on the workings of the Universe. Still it produced two articles that I feel good about having my name on, and through Martin's help I learned many important lessons on Life, The Universe and Everything.

The last of the collaborators, **Troels Haugbølle**, has been a guide deeper into numerical physics. An always patient sparring partner who could both listen, explain and argue, Troels is the source of much of my understanding of the practicalities of inflation. I am going to miss the days of debugging, plotting and writing, followed by late night Thai.

Tina Lund has always been prepared to commit fully to lifting the process and the result to a higher level. Whether it was the case of physics, relaxation, adventure or simply my mistreatment of the English language (in this thesis amongst other), Tina has always weighed in with sound suggestions, that often turned out to be the best solution. She has the ability to put a smile on my face and tell me to just keep swimming.

It is remarkable when you on those rare occasions meet someone, who possesses a vast knowledge and keen insight into a science, while at the same time is able to communicate it in a thoughtful and logical way, without coming off as superior or intimidating. **Jan Hamann** has for me always been such a person. It has been a great joy to discuss with him and learn from him, all the while enjoying his good-natured approach to life, as well as sharing his lust for ice cream. The fact that he took the time to comment on this work has given me great reassurance.

My first day at University of Aarhus brought more than television cameras. It was the same day, that I met a man who would follow me from first to last of this Ph.D. **Jacob Brandbyge** has been a firm part of my everyday for the last four years and he has always been ready with a patient ear, when the rambling overtook me. Always calm, knowledgeable and with a eye on the world with all its sports and politics, Jacob has been a great source of inspiration whenever the world drifted from my awareness. I guess it is time to leave this place and buy that BMW.

I have over the years enjoyed many great moments with the entire **CAPPA** group, both those mentioned above and the rest of the group. Anders Basbøll, Ole Bjælde, Anna Sejersen Riis, Katrine Skovbo and Thomas Tram Bülow have all been part of brightening anything from a coffee break to a late night at the pub. I will miss looking at them apologetic after a fun evening and say: "I have to catch the next train back home, so....".

A constant through my work on inflation has been the **asteroseismology people** that at all times have reminded me, in good spirit, that one should have data to do astrophysics. I am still not quite sure, that I believe them. I suppose the first chapter is partly in their honour. It is as close to data as I will ever get!

Finally, life is much more than work and career. Though too many to be mentioned by name, my deepest gratitude belongs to **family, friends and loved ones**, who have always been there to hold me close or kick me around, to drag me to safe ground or follow me off the deep end, to do what was necessary. Without you I would not have made it through these last four years, let alone this far.

BIBLIOGRAPHY

[1] James B. Hartle. *Gravity - An Introduction to Einstein's General Relativity.* Addison Wesley, 1. edition, 2003.

[2] Barbara Ryden. *Introduction to Cosmology.* Addison Wesley, 1. edition, 2003.

[3] Douglas Clowe et al. A direct empirical proof of the existence of dark matter. *Astrophys. J.*, 648:L109–L113, 2006, astro-ph/0608407.

[4] T. S. van Albada, John N. Bahcall, K. Begeman, and R. Sancisi. THE DISTRIBUTION OF DARK MATTER IN THE SPIRAL GALAXY NGC- 3198. *Astrophys. J.*, 295:305–313, 1985.

[5] D. J. Fixsen et al. The Cosmic Microwave Background Spectrum from the Full COBE/FIRAS Data Set. *Astrophys. J.*, 473:576, 1996, astro-ph/9605054.

[6] WMAP Homepage. http://map.gsfc.nasa.gov/. July 18, 2010.

[7] P. J. E. Peebles and Bharat Ratra. The cosmological constant and dark energy. *Rev. Mod. Phys.*, 75:559–606, 2003, astro-ph/0207347.

[8] E. Komatsu et al. Five-Year Wilkinson Microwave Anisotropy Probe (WMAP) Observations:Cosmological Interpretation. 2008, 0803.0547.

[9] M. Kowalski et al. Improved Cosmological Constraints from New, Old and Combined Supernova Datasets. *Astrophys. J.*, 686:749–778, 2008, 0804.4142.

[10] Daniel J. Eisenstein et al. Detection of the Baryon Acoustic Peak in the Large-Scale Correlation Function of SDSS Luminous Red Galaxies. *Astrophys. J.*, 633:560–574, 2005, astro-ph/0501171.

[11] Antonio Riotto. Inflation and the theory of cosmological perturbations. 2002, hep-ph/0210162.

[12] C. P. Burgess. Lectures on Cosmic Inflation and its Potential Stringy Realizations. *PoS*, P2GC:008, 2006, 0708.2865.

[13] Ned Wright's Cosmological Tutorial. http://www.astro.ucla.edu/∼wright/cosmo_03.htm. July 19, 2010.

[14] Alan H. Guth. The Inflationary Universe: A Possible Solution to the Horizon and Flatness Problems. *Phys. Rev.*, D23:347–356, 1981.

[15] Lev Kofman, Andrei D. Linde, and Alexei A. Starobinsky. Reheating after inflation. *Phys. Rev. Lett.*, 73:3195–3198, 1994, hep-th/9405187.

[16] Matthew Colless et al. The 2dF Galaxy Redshift Survey: Spectra and redshifts. *Mon. Not. Roy. Astron. Soc.*, 328:1039, 2001, astro-ph/0106498.

[17] Donald G. York et al. The Sloan Digital Sky Survey: technical summary. *Astron. J.*, 120:1579–1587, 2000, astro-ph/0006396.

[18] Millennium Simulation MPA Garching. http://www.mpa-garching.mpg.de/millennium/. July 16, 2010.

[19] Hideo Kodama and Misao Sasaki. Cosmological Perturbation Theory. *Prog. Theor. Phys. Suppl.*, 78:1–166, 1984.

[20] James M. Bardeen. Gauge Invariant Cosmological Perturbations. *Phys. Rev.*, D22:1882–1905, 1980.

[21] James M. Bardeen, Paul J. Steinhardt, and Michael S. Turner. Spontaneous Creation of Almost Scale - Free Density Perturbations in an Inflationary Universe. *Phys. Rev.*, D28:679, 1983.

[22] Juan Martin Maldacena. Non-Gaussian features of primordial fluctuations in single field inflationary models. *JHEP*, 05:013, 2003, astro-ph/0210603.

[23] Amit P. S. Yadav and Benjamin D. Wandelt. Evidence of Primordial Non-Gaussianity ($f_{\rm NL}$) in the Wilkinson Microwave Anisotropy Probe 3-Year Data at 2.8σ. *Phys. Rev. Lett.*, 100:181301, 2008, 0712.1148.

[24] Kendrick M. Smith, Leonardo Senatore, and Matias Zaldarriaga. Optimal limits on f_{NL}^{local} from WMAP 5-year data. *JCAP*, 0909:006, 2009, 0901.2572.

[25] Oystein Rudjord et al. An Estimate of the Primordial Non-Gaussianity Parameter f_{NL} Using the Needlet Bispectrum from WMAP. *Astrophys. J.*, 701:369–376, 2009, 0901.3154.

[26] A. Curto, E. Martinez-Gonzalez, and R. B. Barreiro. Improved constraints on primordial non-Gaussianity for the Wilkinson Microwave Anisotropy Probe 5-yr data. *Astrophys. J.*, 706:399–403, 2009, 0902.1523.

[27] David Seery, James E. Lidsey, and Martin S. Sloth. The inflationary trispectrum. *JCAP*, 0701:027, 2007, astro-ph/0610210.

[28] Laila Alabidi and David H. Lyth. Inflation models and observation. *JCAP*, 0605:016, 2006, astro-ph/0510441.

[29] Lotfi Boubekeur and David. H. Lyth. Detecting a small perturbation through its non- Gaussianity. *Phys. Rev.*, D73:021301, 2006, astro-ph/0504046.

[30] David H. Lyth and Yeinzon Rodriguez. The inflationary prediction for primordial non- gaussianity. *Phys. Rev. Lett.*, 95:121302, 2005, astro-ph/0504045.

[31] Kendrick M. Smith and Matias Zaldarriaga. Algorithms for bispectra: forecasting, optimal analysis, and simulation. 2006, astro-ph/0612571.

[32] Eiichiro Komatsu and David N. Spergel. Acoustic signatures in the primary microwave background bispectrum. *Phys. Rev.*, D63:063002, 2001, astro-ph/0005036.

[33] Nima Arkani-Hamed, Hsin-Chia Cheng, Paolo Creminelli, and Lisa Randall. Extranatural inflation. *Phys. Rev. Lett.*, 90:221302, 2003, hep-th/0301218.

[34] Katherine Freese, Joshua A. Frieman, and Angela V. Olinto. Natural inflation with pseudo - Nambu-Goldstone bosons. *Phys. Rev. Lett.*, 65:3233–3236, 1990.

[35] Jaume Garriga and Viatcheslav F. Mukhanov. Perturbations in k-inflation. *Phys. Lett.*, B458:219–225, 1999, hep-th/9904176.

[36] Mohsen Alishahiha, Eva Silverstein, and David Tong. DBI in the sky. *Phys. Rev.*, D70:123505, 2004, hep-th/0404084.

[37] David H. Lyth and Antonio Riotto. Particle physics models of inflation and the cosmological density perturbation. *Phys. Rept.*, 314:1–146, 1999, hep-ph/9807278.

[38] Scott Dodelson, William H. Kinney, and Edward W. Kolb. Cosmic microwave background measurements can discriminate among inflation models. *Phys. Rev.*, D56:3207–3215, 1997, astro-ph/9702166.

[39] Hans Stephani. *Relativity.* Cambridge University Press, 3 edition, 2004.

[40] Richard L. Arnowitt, Stanley Deser, and Charles W. Misner. The dynamics of general relativity. 1962, gr-qc/0405109.

[41] E. Komatsu et al. Non-Gaussianity as a Probe of the Physics of the Primordial Universe and the Astrophysics of the Low Redshift Universe. 2009, 0902.4759.

[42] Andrei D. Linde and Viatcheslav F. Mukhanov. Nongaussian isocurvature perturbations from inflation. *Phys. Rev.*, D56:535–539, 1997, astro-ph/9610219.

[43] David Langlois, Filippo Vernizzi, and David Wands. Non-linear isocurvature perturbations and non- Gaussianities. *JCAP*, 0812:004, 2008, 0809.4646.

[44] David Langlois. Correlated adiabatic and isocurvature perturbations from double inflation. *Phys. Rev.*, D59:123512, 1999, astro-ph/9906080.

[45] G. I. Rigopoulos, E. P. S. Shellard, and B. J. W. van Tent. Large non-Gaussianity in multiple-field inflation. *Phys. Rev.*, D73:083522, 2006, astro-ph/0506704.

[46] N. Bartolo, S. Matarrese, and A. Riotto. On non-Gaussianity in the curvaton scenario. *Phys. Rev.*, D69:043503, 2004, hep-ph/0309033.

[47] David H. Lyth, Carlo Ungarelli, and David Wands. The primordial density perturbation in the curvaton scenario. *Phys. Rev.*, D67:023503, 2003, astro-ph/0208055.

[48] David H. Lyth and David Wands. Generating the curvature perturbation without an inflaton. *Phys. Lett.*, B524:5–14, 2002, hep-ph/0110002.

[49] Martin S. Sloth. Superhorizon curvaton amplitude in inflation and pre-big bang cosmology. *Nucl. Phys.*, B656:239–251, 2003, hep-ph/0208241.

[50] Xingang Chen, Richard Easther, and Eugene A. Lim. Generation and Characterization of Large Non-Gaussianities in Single Field Inflation. *JCAP*, 0804:010, 2008, 0801.3295.

[51] Xingang Chen, Richard Easther, and Eugene A. Lim. Large non-Gaussianities in single field inflation. *JCAP*, 0706:023, 2007, astro-ph/0611645.

[52] Eva Silverstein and Alexander Westphal. Monodromy in the CMB: Gravity Waves and String Inflation. *Phys. Rev.*, D78:106003, 2008, 0803.3085.

[53] Alexei A. Starobinsky. Spectrum of adiabatic perturbations in the universe when there are singularities in the inflation potential. *JETP Lett.*, 55:489–494, 1992.

[54] T. S. Bunch and P. C. W. Davies. Quantum Field Theory in de Sitter Space: Renormalization by Point Splitting. *Proc. Roy. Soc. Lond.*, A360:117–134, 1978.

[55] Brian R. Greene, Koenraad Schalm, Gary Shiu, and Jan Pieter van der Schaar. Decoupling in an expanding universe: Backreaction barely constrains short distance effects in the CMB. *JCAP*, 0502:001, 2005, hep-th/0411217.

[56] Koenraad Schalm, Gary Shiu, and Jan Pieter van der Schaar. Decoupling in an expanding universe: Boundary RG-flow affects initial conditions for inflation. *JHEP*, 04:076, 2004, hep-th/0401164.

[57] F. Nitti, M. Porrati, and J. W. Rombouts. Naturalness in cosmological initial conditions. *Phys. Rev.*, D72:063503, 2005, hep-th/0503247.

[58] Daniel Babich, Paolo Creminelli, and Matias Zaldarriaga. The shape of non-Gaussianities. *JCAP*, 0408:009, 2004, astro-ph/0405356.

[59] Xingang Chen, Min-xin Huang, Shamit Kachru, and Gary Shiu. Observational signatures and non-Gaussianities of general single field inflation. *JCAP*, 0701:002, 2007, hep-th/0605045.

[60] R. Holman and Andrew J. Tolley. Enhanced Non-Gaussianity from Excited Initial States. *JCAP*, 0805:001, 2008, 0710.1302.

[61] David Langlois, Sebastien Renaux-Petel, Daniele A. Steer, and Takahiro Tanaka. Primordial perturbations and non-Gaussianities in DBI and general multi-field inflation. *Phys. Rev.*, D78:063523, 2008, 0806.0336.

[62] Liam McAllister, Eva Silverstein, and Alexander Westphal. Gravity Waves and Linear Inflation from Axion Monodromy. 2008, 0808.0706.

[63] Steen Hannestad, Troels Haugbolle, Philip R. Jarnhus, and Martin S. Sloth. Non-Gaussianity from Axion Monodromy Inflation. *JCAP*, 1006:001, 2010, 0912.3527.

[64] Raphael Flauger, Liam McAllister, Enrico Pajer, Alexander Westphal, and Gang Xu. Oscillations in the CMB from Axion Monodromy Inflation. 2009, 0907.2916.

[65] Paolo Creminelli and Matias Zaldarriaga. Single field consistency relation for the 3-point function. *JCAP*, 0410:006, 2004, astro-ph/0407059.

[66] Xingang Chen, Min-xin Huang, and Gary Shiu. The inflationary trispectrum for models with large non- Gaussianities. *Phys. Rev.*, D74:121301, 2006, hep-th/0610235.

[67] David Seery, Martin S. Sloth, and Filippo Vernizzi. Inflationary trispectrum from graviton exchange. *JCAP*, 0903:018, 2009, 0811.3934.

[68] Noriyuki Kogo and Eiichiro Komatsu. Angular Trispectrum of CMB Temperature Anisotropy from Primordial Non-Gaussianity with the Full Radiation Transfer Function. *Phys. Rev.*, D73:083007, 2006, astro-ph/0602099.

[69] Jan Hamann, Steen Hannestad, Martin S. Sloth, and Yvonne Y. Y. Wong. Observing trans-Planckian ripples in the primordial power spectrum with future large scale structure probes. *JCAP*, 0809:015, 2008, 0807.4528.

[70] Raphael Flauger and Enrico Pajer. Resonant Non-Gaussianity. 2010, 1002.0833.

[71] Daniel Baumann. TASI Lectures on Inflation. 2009, 0907.5424.

[72] Chung-Pei Ma and Edmund Bertschinger. Cosmological perturbation theory in the synchronous and conformal Newtonian gauges. *Astrophys. J.*, 455:7–25, 1995, astro-ph/9506072.

[73] Scott Dodelson. *Modern Cosmology*. Academic Press, 1 edition, March 2003.

[74] M. R. Nolta et al. Five-Year Wilkinson Microwave Anisotropy Probe (WMAP) Observations: Angular Power Spectra. *Astrophys. J. Suppl.*, 180:296–305, 2009, 0803.0593.

[75] Daniel Baumann et al. CMBPol Mission Concept Study: Probing Inflation with CMB Polarization. *AIP Conf. Proc.*, 1141:10–120, 2009, 0811.3919.

[76] Matias Zaldarriaga and Uros Seljak. An All-Sky Analysis of Polarization in the Microwave Background. *Phys. Rev.*, D55:1830–1840, 1997, astro-ph/9609170.

[77] Marc Kamionkowski, Arthur Kosowsky, and Albert Stebbins. Statistics of Cosmic Microwave Background Polarization. *Phys. Rev.*, D55:7368–7388, 1997, astro-ph/9611125.

[78] Thibault Damour and Alexander Vilenkin. Gravitational wave bursts from cusps and kinks on cosmic strings. *Phys. Rev.*, D64:064008, 2001, gr-qc/0104026.

[79] Levon Pogosian, Mark C. Wyman, and Ira Wasserman. Observational constraints on cosmic strings: Bayesian analysis in a three dimensional parameter space. *JCAP*, 0409:008, 2004, astro-ph/0403268.

[80] P. Binetruy, A. Bohe, T. Hertog, and Daniele A. Steer. Gravitational Wave Bursts from Cosmic Superstrings with Y- junctions. *Phys. Rev.*, D80:123510, 2009, 0907.4522.

[81] Katherine Jones-Smith, Lawrence M. Krauss, and Harsh Mathur. A Nearly Scale Invariant Spectrum of Gravitational Radiation from Global Phase Transitions. *Phys. Rev. Lett.*, 100:131302, 2008, 0712.0778.

[82] Andrew R. Liddle and D. H. Lyth. Cosmological inflation and large-scale structure. ISBN-13-9780521828499.

[83] Scott Dodelson. Coherent phase argument for inflation. *AIP Conf. Proc.*, 689:184–196, 2003, hep-ph/0309057.

[84] David N. Spergel and Matias Zaldarriaga. CMB polarization as a direct test of inflation. *Phys. Rev. Lett.*, 79:2180–2183, 1997, astro-ph/9705182.

[85] James Bock et al. The Experimental Probe of Inflationary Cosmology (EPIC): A Mission Concept Study for NASA's Einstein Inflation Probe. 2008, 0805.4207.

[86] J. R. Fergusson and Edward P. S. Shellard. Primordial non-Gaussianity and the CMB bispectrum. *Phys. Rev.*, D76:083523, 2007, astro-ph/0612713.

[87] Li-Min Wang and Marc Kamionkowski. The cosmic microwave background bispectrum and inflation. *Phys. Rev.*, D61:063504, 2000, astro-ph/9907431.

[88] Milton Abramowitz and Irene A. Stegun, editors. *Handbook of Mathematical Functions With Formulas, Graphs, and Mathematical Tables*. National Bureau of Standards, 10 edition, 1973.

[89] Philip R. Jarnhus and Martin S. Sloth. de Sitter limit of inflation and nonlinear perturbation theory. *JCAP*, 0802:013, 2008, 0709.2708.

[90] Marco Bruni, Sabino Matarrese, Silvia Mollerach, and Sebastiano Sonego. Perturbations of spacetime: Gauge transformations and gauge invariance at second order and beyond. *Class. Quant. Grav.*, 14:2585–2606, 1997, gr-qc/9609040.

[91] Martin S. Sloth. On the one loop corrections to inflation and the CMB anisotropies. *Nucl. Phys.*, B748:149–169, 2006, astro-ph/0604488.

[92] David Seery. One-loop corrections to a scalar field during inflation. *JCAP*, 0711:025, 2007, 0707.3377.

[93] Martin S. Sloth. On the one loop corrections to inflation. II: The consistency relation. *Nucl. Phys.*, B775:78–94, 2007, hep-th/0612138.

[94] Viviana Acquaviva, Nicola Bartolo, Sabino Matarrese, and Antonio Riotto. Second-order cosmological perturbations from inflation. *Nucl. Phys.*, B667:119–148, 2003, astro-ph/0209156.

[95] Jean-Luc Lehners. Ekpyrotic and Cyclic Cosmology. *Phys. Rept.*, 465:223–263, 2008, 0806.1245.

[96] Justin Khoury, Burt A. Ovrut, Paul J. Steinhardt, and Neil Turok. The ekpyrotic universe: Colliding branes and the origin of the hot big bang. *Phys. Rev.*, D64:123522, 2001, hep-th/0103239.

[97] Ram Brustein and Paul J. Steinhardt. Challenges for superstring cosmology. *Phys. Lett.*, B302:196–201, 1993, hep-th/9212049.

[98] Kenji Kadota, Scott Dodelson, Wayne Hu, and Ewan D. Stewart. Precision of inflaton potential reconstruction from CMB using the general slow-roll approximation. *Phys. Rev.*, D72:023510, 2005, astro-ph/0505158.

[99] James M. Cline and Loison Hoi. Inflationary potential reconstruction for a WMAP running power spectrum. *JCAP*, 0606:007, 2006, astro-ph/0603403.

[100] Richard Easther and William H. Kinney. Monte Carlo reconstruction of the inflationary potential. *Phys. Rev.*, D67:043511, 2003, astro-ph/0210345.

A Appendix

$$\alpha_{\phi}{}^{(1)} = -\frac{\dot{\phi}_c^2}{2H^2}\zeta_n \tag{A.1}$$

$$\chi_{\phi}{}^{(1)} = \frac{\dot{\phi}_c^2}{2H^2}\partial^{-2}\dot{\zeta}_n \tag{A.2}$$

$$\begin{aligned}\alpha_{\phi}{}^{(2)} = \frac{\dot{\phi}_c^4}{8H^4}\zeta_n^2 - \frac{1}{2H}\partial^{-2}\Bigg(&\frac{\dot{\phi}_c}{H}\partial_i\left[\frac{\dot{\phi}_c\dot{H}}{H^2}\zeta_n - \frac{\ddot{\phi}_c}{H}\zeta_n - \frac{\dot{\phi}_c}{H}\dot{\zeta}_n\right]\partial^i\zeta_n + \frac{\dot{\phi}_c^4}{4H^4}\dot{\zeta}_n\partial^2\zeta_n \\ &+ \frac{\dot{\phi}_c}{H}\left[\frac{\dot{\phi}_c\dot{H}}{H^2}\zeta_n - \frac{\ddot{\phi}_c}{H}\zeta_n - \frac{\dot{\phi}_c}{H}\dot{\zeta}_n\right]\partial^2\zeta_n - \frac{\dot{\phi}_c^4}{4H^4}\partial_i\partial_j\zeta_n\partial^i\partial^j\partial^{-2}\dot{\zeta}_n\Bigg)\end{aligned} \tag{A.3}$$

$$\begin{aligned}4H\partial^2\chi_{\phi}{}^{(2)} = &-\frac{\dot{\phi}_c}{H^2}\partial_i\zeta_n\partial^i\zeta_n - V''\frac{\dot{\phi}_c^2}{H^2}\zeta_n^2 + \frac{\dot{\phi}_c^4}{4H^4}\dot{\zeta}_n^2 - \frac{\dot{\phi}_c^4}{4H^4}\partial_i\partial_j\partial^{-2}\dot{\zeta}_n\partial^i\partial^j\partial^{-2}\dot{\zeta}_n \\ &- \frac{\dot{\phi}_c^4}{H^3}\partial_i\partial^{-2}\dot{\zeta}_n\partial^i\zeta_n - \frac{2\dot{\phi}_c^3}{H^2}\left(\frac{\dot{\phi}_c\dot{H}}{H^2} - \frac{\ddot{\phi}_c}{H}\right)\zeta_n^2 \\ &- (\frac{3\dot{\phi}_c^4}{4H^4}\zeta_n^2 - 2\alpha_{\phi}{}^{(2)})(-6H^2 + \dot{\phi}_c^2) - \left[\frac{\dot{\phi}_c\dot{H}}{H^2}\zeta_n - \frac{\ddot{\phi}_c}{H}\zeta_n - \frac{\dot{\phi}_c}{H}\dot{\zeta}_n\right]^2\end{aligned} \tag{A.4}$$

$$\begin{aligned}\frac{1}{2}\beta_{\phi_i}{}^{(2)} = \partial^{-2}\Bigg(&2H\partial_i\alpha_{\phi}{}^{(2)} - \frac{\dot{\phi}_c^4}{H^3}\zeta_n\partial_i\zeta_n + \frac{\dot{\phi}_c}{H}\left[\frac{\dot{\phi}_c\dot{H}}{H^2}\zeta_n - \frac{\ddot{\phi}_c}{H}\zeta_n - \frac{\dot{\phi}_c}{H}\dot{\zeta}_n\right]\partial_i\zeta_n \\ &+ \frac{\dot{\phi}_c^4}{2H^3}\zeta_n\partial_i\zeta_n + \frac{\dot{\phi}_c^4}{4H^4}\dot{\zeta}_n\partial_i\zeta_n - \frac{\dot{\phi}_c^4}{4H^4}\partial_j\zeta_n\partial_i\partial^j\partial^{-2}\dot{\zeta}_n\Bigg)\end{aligned} \tag{A.5}$$